UNIVERSITA' DEGLI STUDI DI PADOVA

DIPARTIMENTO DI INGEGNERIA CIVILE, EDILE ED AMBIENTALE
Corso di Laurea Magistrale in Ingegneria Civile

TESI DI LAUREA MAGISTRALE

NUMERICAL ANALYSIS OF THE CHEMO-MECHANICAL BEHAVIOUR OF SHALES

Laureando
Jacopo Bontorin

Relatore
Prof. Ing. Lorenzo Sanavia
Correlatore
Dott. Ing. Alessio Ferrari

ANNO ACCADEMICO 2013/2014

Contents

Abstract

This Master Thesis was developed at the *Laboratoire de Mécanique des Sols* at the *École Polytechnique Fédérale de Lausanne* under the supervision of Dr. Alessio Ferrari and with the support of Prof. Lorenzo Sanavia in the period between March 2014 and July 2014.

This work concerns the study and modelling of the mechanical behaviour of a particular shale, Opalinus Clay, when subjected to changes in the chemical composition of the pore liquid. The analysis begins from a series of six oedometric tests run in EPFL LMS laboratory on samples of Opalinus Clay. The tests were conducted with different stress paths, including mechanical loading at a constant osmotic suction and an increasing osmotic suction at a constant mechanical stress. Osmotic suction is the representative variable of the chemical composition of the pore liquid and it is controlled through the ion concentration of sodium chloride in the pore water. The experimental results evidence an influence of osmotic suction on the yield stress value, but no correlation with the oedometric modulus is observed.

A constitutive model developed for a non-swelling illite has been calibrated for this case and simulations corresponding to the experimental test were run: in all cases the numerical results well reproduce the experimental evidences.

Finally, a sensitivity analysis was performed to evaluate the impact of a variation of the input parameters on simulated results.

1. Introduction

Shale is a fine-grained, laminated sedimentary rock consisting of silt- and clay-size particles. Accounting for roughly 70% of sedimentary rock in the crust of earth, it is the most abundant of this rock type.

Several studies were conducted since the half of the last century to determine shales properties because of their essential role in many engineering applications, including nuclear waste disposal, shale gas and wellbore stability.

The nuclear waste disposal concerns the research of repositories suitable for containing nuclear waste. Over the last 10 years argillaceous rocks such as Opalinus Clay have gained acceptance as a potential host formation for geological disposal of nuclear waste [*Corkum et al.*, 2006].

Shale gas, the natural gas trapped within shale formations, has become a major source of fossil energy in the United States, and future growth in use of this source of energy is projected worldwide [*Etminan et al.*, 2013]. Particularly, in the United States shale gas is predicted to become the source of 45% of all gas production by 2035 [*AEO*, 2011], especially considering that other fossil energy resources constitute larger threats for climatic shift, environmental pollution and potential risks for production/exploration. The renewed focus on rock sequences that have hitherto largely been ignored has necessitated the laboratory characterisation of rock properties and the development of methods and interpretation frameworks for characterising shales and understand their mechanical, chemical and thermal properties.

A wellbore or borehole is a hole drilled with the aim of exploring or extracting natural resources such as water, gas or oil where a well may be produced and a resource extracted for a protracted period. The typical structure of a wellbore is represented in figure 1.1.

The stability of tunnels and boreholes is a major problem: instability can lead to a partial or complete collapse of the wellbore or even loss of the well prior to reaching its target and to an increase of drilling costs of up to 15% [*Schmitt et al.*, 1994]. For example, in the oil and gas industry wellbore instability problems cost the industry many millions of dollars annually and it has been estimated that, on a world-wide basis, an excess of US$500 million

is lost each year because of wellbore instability[*Chen et al.*, 1994]. In particular, being the drilled formations made up for over 75% of shales, 80% of borehole instability problems occur in shales [*Schmitt et al.*, 1994]. These problems are mainly caused by the imbalance created between the rock stress and strength when a hole is drilled: the stress-strength imbalance starts as rock is removed from the hole, replaced with drilling fluid, and the drilled formations are exposed to drilling fluids. While drilling, shale becomes unstable when the effective state of the stress near the drilled hole exceeds the strength of the hole. A complicating factor is shale sensitivity to certain drilling constituents. The existence and creation of fissures, fractures and weak bedding planes can also destabilize shale as drilling fluid penetrates them.

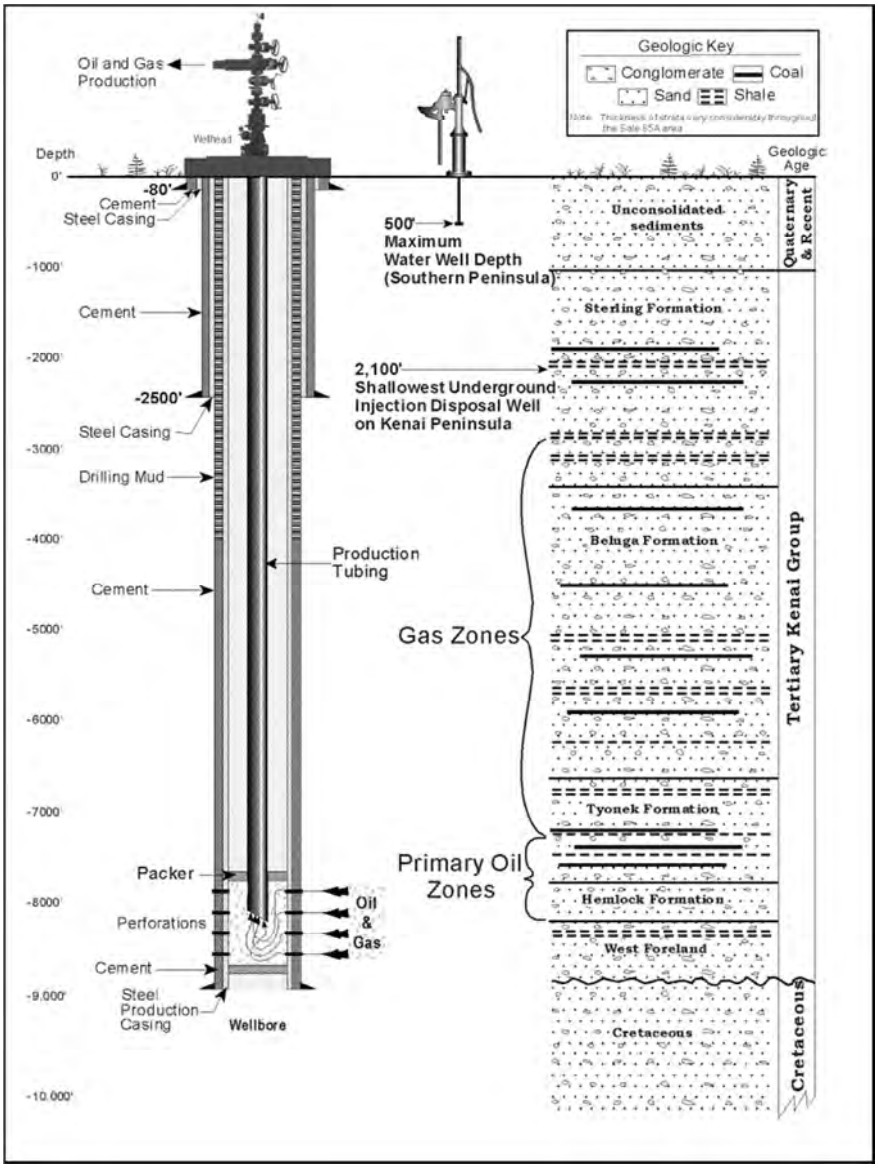

Figure 1.1: A wellbore

Water movement caused by hydraulic gradient is also present but, because of their very low permeability, hydraulic transport is not the dominant form of water movement into the shale sections. Water flow due to a hydraulic gradient can often be several times smaller than the contribution of the chemical and thermal gradients [*Ghassemi et al.*, 2009].

An important stabilization mechanism for boreholes drilled in chemically reactive shale formations with water-based drilling fluids relies on physicochemical interactions between the rock and the mud. In fact the pore pressure in the near-wellbore region can be reduced by an osmotic outflow of pore fluid from the reactive shale, which is triggered by an increased salinity of the drilling fluid [*Sarout et al.*, 2011]. The petroleum industry has been investigating these phenomena since at least the early 1940s with research efforts eventually leading to recommendations for modifying the composition of drilling fluids in order to promote shale stability through oil emulsion and salinity balanced drilling fluids [*Bunger et al.*, 2014].

This thesis work aims to integrate in this field and to reach a better knowledge of behaviour of a particular shale, Opalinus Clay, when subjected to changes in the pore liquid chemistry: particularly, the purpose is to evaluate the variation of the mechanical properties and the one-dimensional consolidation.

2. Mechanics of saturated soils

Soils are generally defined as multi-phase systems composed by a solid phase, a liquid phase and/or a gaseous phase. The liquid and the gas are included into the voids located between the grains constituent the solid frame, as shown in fig. 2.1.

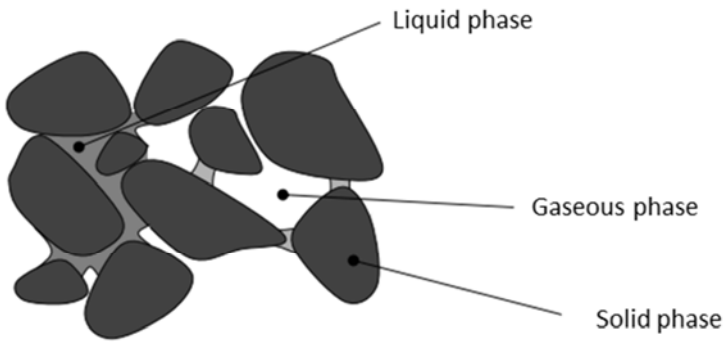

Figure 2.1: Soil representation

Starting from the schematization reported in fig.2.2, we can define:

- Porosity: $n = \frac{V_v}{V}$
- Void ratio: $e = \frac{V_v}{V_s}$
- Water content: $w = \frac{M_l}{M_s}$
- Degree of saturation: $S_r = \frac{V_l}{V_s}$

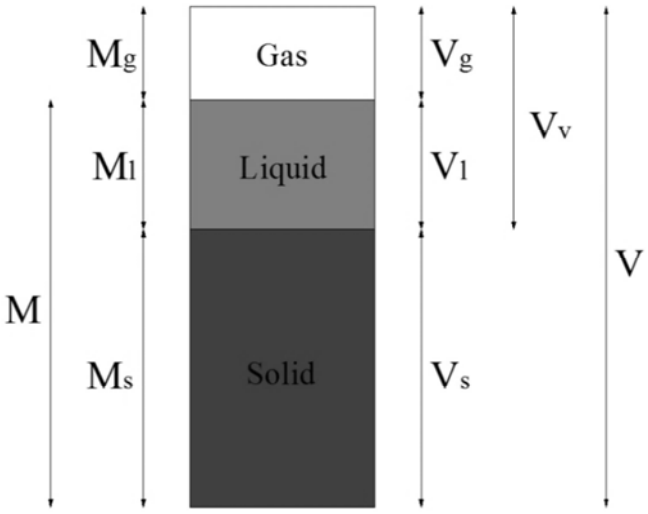

Figure 2.2: Soil schematization

The following relations can be easily verified:

- $n = \frac{e}{1+e}$
- $e = \frac{n}{1-n}$
- $v = 1 + e$

The mass density of the mixture and the unit soil weight are expressed as follows:

- Mass density of the mixture: $\rho = \frac{M}{V}\ \left[\frac{kg}{m^3}\right]$
- Unit soil weight: $\gamma = \frac{Mg}{V}\left[\frac{N}{m^3}\right]$

2.1 Stress and strain

In engineering applications soil is assimilated to three overlapping continuous media which fill the same volume. This assumption implies that the properties of a soil element, infinitesimal or finite, are the same, and that the concepts of stress and strain as defined in the continuum mechanics are valid also for soils.

2.1.1 Stress definition

The stress component σ_{ij} can be introduced:

$$\sigma_{ij} = \lim_{A_i \to 0} \left(\frac{F_j}{A_i}\right)$$

where F_j is the force in the direction j and A_i is the area normal to the direction i.

In three dimension the stress components are organized in a 3x3 tensor:

$$\boldsymbol{\sigma} = \begin{bmatrix} \sigma_{11} & \sigma_{12} & \sigma_{13} \\ \sigma_{21} & \sigma_{22} & \sigma_{23} \\ \sigma_{31} & \sigma_{32} & \sigma_{33} \end{bmatrix}$$

The assumptions for the positive direction are shown in figure 2.3: particularly, the components σ_{ii} are assumed positive when they are compressive.

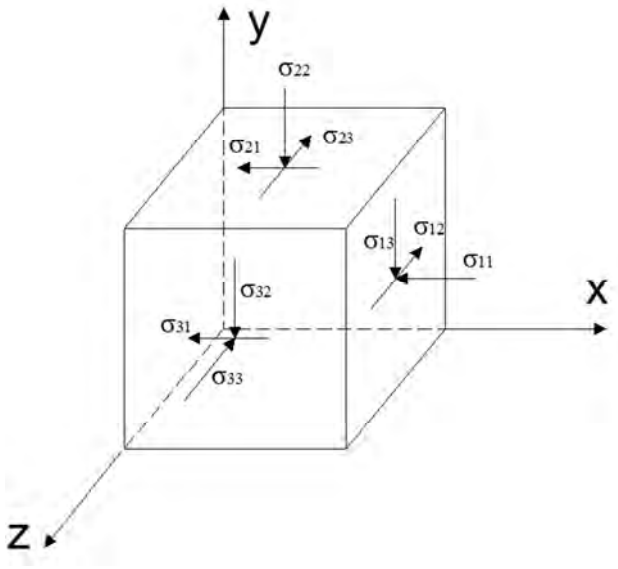

Figure 2.3: Stress assumptions

It can be proved that the stress tensor is symmetric, that is:

$$\sigma_{ij} = \sigma_{ji}$$

The stress tensor has three invariants, quantities which don't depend on the reference system:

$$I_{1\sigma} = \sum_{i=1}^{3} \sigma_{ii} = tr(\boldsymbol{\sigma})$$

$$I_{2\sigma} = \frac{1}{2}\sum_{i=1}^{3}\sum_{j=1}^{3} \sigma_{ij}\sigma_{ji}$$

$$I_{3\sigma} = \frac{1}{3}\sum_{i=1}^{3}\sum_{j=1}^{3}\sum_{k=1}^{3}\sum_{l=1}^{3} \sigma_{ij}\sigma_{kl}\sigma_{li}$$

The *mean stress p*, commonly used in soil mechanics, originates from the first stress invariant:

$$p = \frac{I_{1\sigma}}{3} = \frac{\sigma_{11} + \sigma_{22} + \sigma_{33}}{3}$$

The stress tensor can be decomposed in two different tensors, the deviatoric stress tensor and the hydrostatic stress tensor:

$$\boldsymbol{\sigma} = s_{ij} + \frac{1}{3}\sigma_{kk}\delta_{ij} = \begin{bmatrix} \sigma_{11} - p & \sigma_{12} & \sigma_{13} \\ \sigma_{21} & \sigma_{22} - p & \sigma_{23} \\ \sigma_{31} & \sigma_{32} & \sigma_{33} - p \end{bmatrix} + \begin{bmatrix} p & 0 & 0 \\ 0 & p & 0 \\ 0 & 0 & p \end{bmatrix}$$

where δ_{ij} is the Kronecker's delta:

$$\delta_{ij} = \begin{cases} 0 \; if \; i \neq j \\ 1 \; if \; i = j \end{cases}$$

The *deviatoric stress* q, common in soil mechanics, originates from the second invariant of the deviatoric stress tensor:

$$q = \sqrt{3I_{2s}} = \sqrt{\frac{3s_{ij}s_{ji}}{2}} = \sqrt{\frac{3}{2}\left[\left(\sigma_{ij} - p\delta_{ij}\right)\left(\sigma_{ji} - p\delta_{ji}\right)\right]}$$

The deviatoric stress q becomes:

$$q = \sqrt{[(\sigma_{11} - \sigma_{22})^2 + (\sigma_{11} - \sigma_{33})^2 + (\sigma_{22} - \sigma_{33})^2 + 6({\sigma_{12}}^2 + {\sigma_{13}}^2 + {\sigma_{23}}^2)]}$$

2.1.2 Strain definition

Strains are defined starting from Cauchy's theory: there are *normal strains* and *shear strains*.

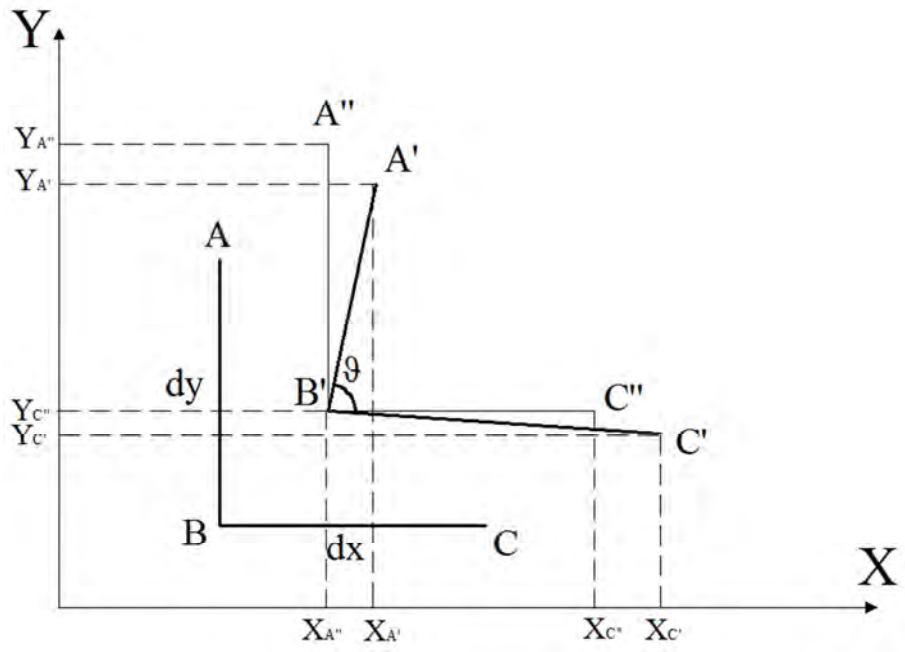

Figure 2.4: Strain definition

Referring to the schematic representation in figure 2.4, let AB and BC be two perpendicular segments, with length *dy* and *dx* respectively, belonging to a body in its original configuration. After the deformation of the body, the new positions of the two segments are $A'B'$ and $B'C'$, while $A''B'$ and $B'C''$ are the corresponding undeformed segments. If the function *f*, which associates to the position of every point of the body its displacement, has

sufficient characteristics of regularity and continuity, strains can be introduced. Let *u* and *v* be the displacements in the *X* and *Y* direction respectively; it is possible to derive:

$$X_{C'} - X_{C''} = \left(\frac{\partial u}{\partial x}\right)_B dx$$

$$X_{A'} - X_{A''} = \left(\frac{\partial u}{\partial y}\right)_B dy$$

$$Y_{C''} - Y_{C'} = \left(\frac{\partial v}{\partial x}\right)_B dx$$

$$Y_{C''} - Y_{C'} = \left(\frac{\partial v}{\partial y}\right)_B dy$$

The specific dilation in the *X* direction is:

$$\frac{dx - \left(dx + \frac{\partial u}{\partial x}dx\right)}{dx} = -\frac{\partial u}{\partial x} = \varepsilon_x$$

that is the normal strain in the *X* direction. In the *Y* direction:

$$\frac{dy - \left(dy + \frac{\partial v}{\partial y}dy\right)}{dy} = -\frac{\partial v}{\partial y} = \varepsilon_y$$

Similarly it is possible to deduce ε_z. These equations consider a reduction of length as a positive strain.

The shear strain γ_{xy} is defined as the change in the angle between AB and BC before and after the deformation process:

$$\frac{\pi}{2} - \vartheta = \frac{\frac{\partial u}{\partial y}dy}{dy} + \frac{\frac{\partial v}{\partial x}dx}{dx} = \gamma_{xy}$$

Similarly γ_{xz} and γ_{yz} are derived.

In three dimensions, the strain state can be represented by a 3x3 tensor:

$$\boldsymbol{\varepsilon} = \begin{bmatrix} \varepsilon_{11} & \frac{1}{2}\gamma_{12} & \frac{1}{2}\gamma_{13} \\ \frac{1}{2}\gamma_{21} & \varepsilon_{22} & \frac{1}{2}\gamma_{23} \\ \frac{1}{2}\gamma_{31} & \frac{1}{2}\gamma_{32} & \varepsilon_{33} \end{bmatrix}$$

It can be proved that the strain tensor is symmetric, that is:

$$\gamma_{ij} = \gamma_{ji}$$

Similarly to the stress tensor, also the strain tensor possesses three invariants:

$$I_{1\varepsilon} = \sum_{i=1}^{3} \varepsilon_{ii} = tr(\boldsymbol{\varepsilon})$$

$$I_{2\varepsilon} = \frac{1}{2}\sum_{i=1}^{3}\sum_{j=1}^{3} \varepsilon_{ij}\varepsilon_{ji}$$

$$I_{3\varepsilon} = \frac{1}{3}\sum_{i=1}^{3}\sum_{j=1}^{3}\sum_{k=1}^{3}\sum_{l=1}^{3} \varepsilon_{ij}\varepsilon_{kl}\varepsilon_{li}$$

The volumetric strain ε_v, commonly used in soil mechanics, is equal to the first invariant:

$$\varepsilon_v = I_{1\varepsilon} = \sum_{i=1}^{3} \varepsilon_{ii} = \varepsilon_{11} + \varepsilon_{22} + \varepsilon_{33}$$

The strain tensor $\boldsymbol{\varepsilon}$ can be divided into two symmetric tensors, the deviatoric strain tensor and the volumetric strain tensor:

$$\boldsymbol{\varepsilon} = e_{ij} + \frac{1}{3}\varepsilon_{kk}\delta_{ij} = \begin{bmatrix} \varepsilon_{11} - \frac{\varepsilon_v}{3} & \frac{1}{2}\gamma_{12} & \frac{1}{2}\gamma_{13} \\ \frac{1}{2}\gamma_{21} & \varepsilon_{22} - \frac{\varepsilon_v}{3} & \frac{1}{2}\gamma_{23} \\ \frac{1}{2}\gamma_{31} & \frac{1}{2}\gamma_{32} & \varepsilon_{33} - \frac{\varepsilon_v}{3} \end{bmatrix} + \begin{bmatrix} \frac{\varepsilon_v}{3} & 0 & 0 \\ 0 & \frac{\varepsilon_v}{3} & 0 \\ 0 & 0 & \frac{\varepsilon_v}{3} \end{bmatrix}$$

The deviatoric strain ε_d is defined from the second invariant of the deviatoric strain tensor:

$$\varepsilon_d = \frac{2\sqrt{3}}{3}\sqrt{I_{2e}} = \frac{\sqrt{6}}{3}\sqrt{e_{ij}e_{ji}}$$

$$= \frac{\sqrt{2}}{3}\sqrt{\left[(\varepsilon_{11} - \varepsilon_{22})^2 + (\varepsilon_{11} - \varepsilon_{22})^2 + (\varepsilon_{11} - \varepsilon_{22})^2 + \frac{3}{2}({\gamma_{12}}^2 + {\gamma_{23}}^2 + {\gamma_{31}}^2)\right]}$$

2.1.3 Triaxial configuration

If the directions of the axis of the coordinate system are principle the stress tensor becomes diagonal (i.e. $\sigma_{ij} = 0$ if $i \neq j$):

$$\boldsymbol{\sigma} = \begin{bmatrix} \sigma_1 & 0 & 0 \\ 0 & \sigma_2 & 0 \\ 0 & 0 & \sigma_3 \end{bmatrix}$$

In typical laboratory tests such as oedometric tests the stress state is triaxial, that is:

$$\sigma_2 = \sigma_3$$

Consequently, the mean stress p and the deviatoric stress q become:

$$p = \frac{\sigma_1 + 2\sigma_3}{3}$$

$$q = \sigma_1 - \sigma_3$$

The triaxial stress configuration is represented in figure 2.5.

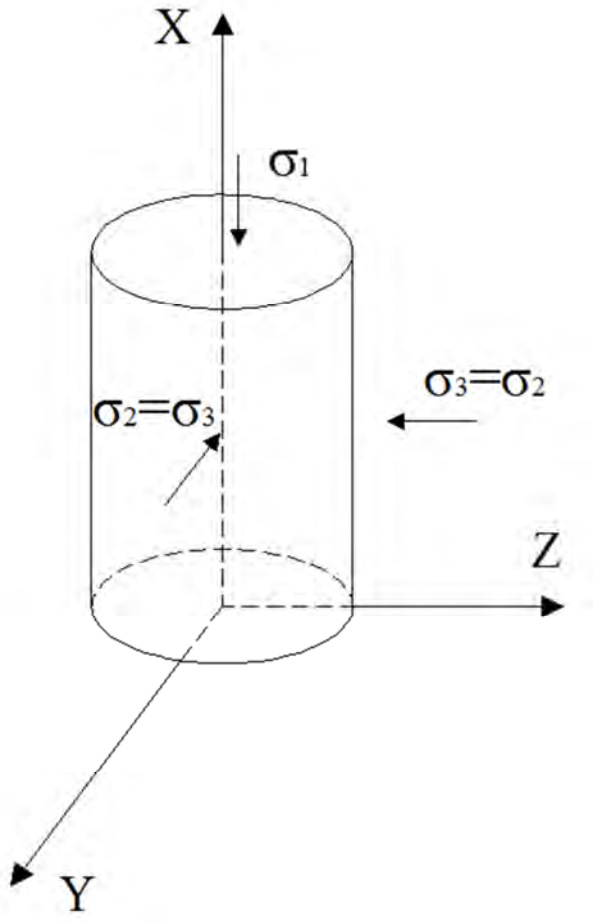

Figure 2.5: Triaxial Stress Configuration

In the principal coordinates, the strain tensor is diagonal, i.e. $\varepsilon_{ij} = 0$ if $i \neq j$:

$$\boldsymbol{\varepsilon} = \begin{bmatrix} \varepsilon_1 & 0 & 0 \\ 0 & \varepsilon_2 & 0 \\ 0 & 0 & \varepsilon_3 \end{bmatrix}$$

Under triaxial configuration, the horizontal stress are equal ($\varepsilon_2 = \varepsilon_3$). It yields:

$$\varepsilon_v = \varepsilon_1 + 2\varepsilon_3$$

$$\varepsilon_d = \frac{2}{3}(\varepsilon_1 - \varepsilon_3)$$

2.2 Terzaghi's principle

Soil in engineering applications is assimilated to three overlapping continuous media which fill the same volume. In saturated conditions the gaseous phase is absent, and all the voids are filled with liquid. In order to apply the stress and strain concepts as previously presented, it is necessary to introduce a law which rules the interactions between the two remaining phases. The *effective stress principle* as stated by K. Terzaghi in 1936 can be introduced:

$$\sigma'_{ij} = \sigma_{ij} - u_w \delta_{ij}$$

where σ'_{ij}, σ_{ij} and u_w represent respectively the *effective stress*, the *total stress* and the *pore pressure*.

Terzaghi's principle attests that it is necessary to refer to two overlapping and mutually interacting continuous media to study the mechanical behaviour of a saturated soil; in every point the *total stress* tensor, the *pore pressure* tensor and, as a difference between them, the *effective stress* tensor are defined. The *effective stress* is presented as a mathematical concept, however a physical interpretation is possible: referring to the saturated soil element represented in figure 2.6, where the vertical direction is the referential one, σ'_{ij} can be seen as the ratio between the sum of the vertical components forces F_i transmitted by the grains separated by a surface which doesn't cut any of them and the surface's area . Mathematically:

$$\sigma' = \frac{\sum_i F_{i,v}}{A_t}$$

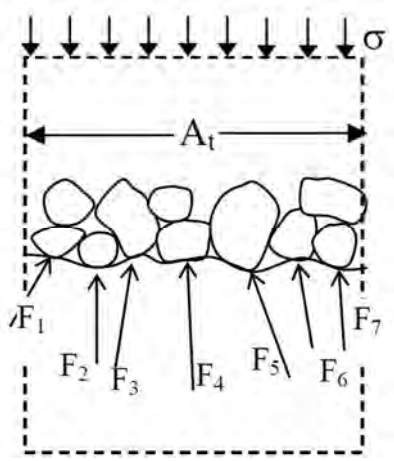

Figure 2.6: Saturated soil element

This definition originates from the equilibrium of the element:

$$F_{t,v} = \sum_i F_{i,v} + u_w(A_t - A_c)$$

where $F_{t,v}$ is the total vertical external force applied to the element, u_w is the pore water pressure and A_c is the area of the intergranular contacts.

Dividing by A_t we have:

$$\sigma = \frac{F_{t,v}}{A_t} = \sigma' + u_w\left(1 - \frac{A_c}{A_t}\right)$$

Being $A_c \ll A_t$:

$$\sigma = \sigma' + u_w$$

that is the effective stress principle for the vertical direction.

The most important implications of Terzaghi's principle are:

- a change in effective stress involves a modification in soil resistance;
- if effective stress is constant soil resistance does not change;
- a volume change always corresponds to a modification in effective stress.

2.3 Oedometric conditions

The compressibility of a soil is usually evaluated in conditions of axial loading and absence of lateral deformation ($\varepsilon_2 = \varepsilon_3 = 0$): these conditions are called *oedometric conditions*. For example, oedometric conditions are present in a soil deposit for lacustrine sedimentation.

It can be derived:

$$\varepsilon_v = \frac{\Delta V}{V_0} = \frac{\Delta H}{H_0} = \varepsilon_a$$

being V_0 and H_0 the initial volume and height of a volume element in the neighbourhood of the considered point P, and ΔV and ΔH the respective variation.

In geotechnical engineering the void ratio e $\left(e = \frac{V_v}{V_s}\right)$ is the variable usually considered to compute volumetric changes:

$$\varepsilon_v = \frac{\Delta V}{V_0} = \frac{\Delta H}{H_0} = \frac{\Delta e}{1 + e_0}$$

where e_0 is the starting void ratio corresponding to an absence of strains.

3.The ACMEG-C constitutive model

3.1 Soil elasto-plasticity

Elasto-plasticity is based on the decomposition of the total strain increment $d\varepsilon_{ij}$ into its two components, the elastic component $d\varepsilon_{ij}^{e}$ and the plastic component $d\varepsilon_{ij}^{p}$. Within the small strain assumptions, it yields:

$$d\varepsilon_{ij} = d\varepsilon_{ij}^{e} + d\varepsilon_{ij}^{p}$$

The elastic part of the strain produced by a given loading is characterised for being fully recoverable through unloading; in contrast, the plastic component remains irrecoverable. In terms of work input per unit volume dW of a material submitted to a strain increment $d\varepsilon_{ij}$:

$$dW = \sigma'_{ij} d\varepsilon_{ij} = \sigma'_{ij} d\varepsilon_{ij}^{e} + \sigma'_{ij} d\varepsilon_{ij}^{p} = dW^{e} + dW^{p}$$

where dW^{e} is the elastic energy recoverable upon unloading while dW^{p} is the irrecoverable plastic work and coincides with the quantity of energy dissipated by the material during loading. The *Prager's condition of irreversibility* (1949) sets that this value must be positive:

$$dW^{p} = \sigma'_{ij} d\varepsilon_{ij}^{p} > 0$$

The *yield criterion*, also called loading surface or yield limit, is the fundamental condition that defines quantitatively the limit of elasticity and the beginning of plastic deformation under any possible combination of stresses. Points within this surface represent stress states which cause only elastic deformations. The limit is expressed in terms of the effective stresses σ'_{ij} and may depend on one or several internal variables π_i. The general form can be expressed as:

$$f(\sigma'_{ij}\, \pi_i) = 0$$

Once the boundary between the elastic and the elasto-plastic domain is established in the stress space, it is necessary to specify the relative magnitude of the various components of the plastic strain when the boundary is reached and their direction (*flow rule*). A plastic potential g must be defined:

$$g(\sigma'_{ij}\,\pi_i) = 0$$

The plastic component of the strain is calculated as:

$$d\varepsilon_{ij}^{p} = \lambda^{p}\frac{\partial g}{\partial \sigma'_{ij}}$$

where λ^p is a non-negative variable, the *plastic multiplier*, which establish the magnitude of the plastic strain, while $\frac{\partial g}{\partial \sigma'_{ij}}$ defines its direction (corresponding to the one along which the potential gradient is maximum). The plastic flow rule is usually *non-associated*, which means that the yield limit *f* and the plastic potential *g* are not the same. In the particular event of the coincidence of the two potentials ($f \equiv g$), the plastic flow rule is called *associated*.

The total strain increment can be re-written:

$$d\varepsilon_{ij} = d\varepsilon_{ij}^{e} + d\varepsilon_{ij}^{p} = E_{ijkl}^{-1} d\sigma'_{kl} + \lambda^{p}\frac{\partial g}{\partial \sigma'_{ij}}$$

where E_{ijkl}^{-1} is the elastic modulus matrix.

It is necessary to verify the uniqueness of the solution of the stress-strain relations: the *uniqueness condition* (Prager, 1950) is automatically verified if the flow rule is associated. In case of non-associated flow rule, the incremental problem can be solved only under certain conditions.

When the stress point reaches the yield limit, plastic strains occur for all stress paths directs towards the exterior of the yield limit. In any other case the material behaviour is elastic. Three possible conditions can be defined:

- Unloading: $f(\sigma'_{ij}\,\pi_i) = 0$ and $\frac{\partial f}{\partial \sigma'_{ij}} d\sigma'_{ij} < 0$
- Neutral loading: $f(\sigma'_{ij}\,\pi_i) = 0$ and $\frac{\partial f}{\partial \sigma'_{ij}} d\sigma'_{ij} = 0$
- Loading: $f(\sigma'_{ij}\,\pi_i) = 0$ and $\frac{\partial f}{\partial \sigma'_{ij}} d\sigma'_{ij} > 0$

This is the *condition of continuity* by Prager (1949).

Being the exterior of the domain unattainable by definition, an evolution of the loading surface must counterbalance the condition $\frac{\partial f}{\partial \sigma'_{ij}} d\sigma'_{ij} > 0$ in order to guaranty the satisfaction of the yield criterion as long as the material is in a plastic state: this is the

condition of consistency (Prager, 1949). The evolution of the yield function f is called hardening and leads to a change in the characteristics of the elastic domain. If an expansion of the elastic domain does not change its shape, its centre and its orientation the hardening is said isotropic.

The evolution of the yield function f is:

$$df = \frac{\partial f}{\partial \sigma'_{ij}} d\sigma'_{ij} + \frac{\partial f}{\partial \pi_i} d\pi_i = 0$$

Following Desai and Siriwardane (1984) '*strain hardening*' hypothesis, it is assumed that the hardening depends on the plastic strain, and so the internal variables:

$$f\left(\sigma'_{ij}\, \pi_i\right) = f\left(\sigma'_{ij}\, \varepsilon^p_{ij}\right)$$

It yields:

$$df = \frac{\partial f}{\partial \sigma'_{ij}} d\sigma'_{ij} + \frac{\partial f}{\partial \varepsilon^p_{ij}} \frac{\partial \varepsilon^p_{ij}}{\partial \lambda^p} \lambda^p = 0$$

Combining this equation with the total strain expression, it is possible to find the value of the plastic multiplier λ^p:

$$\lambda^p = \frac{1}{H} \frac{\partial f}{\partial \sigma'_{ij}} E_{ijkl} d\varepsilon_{kl}$$

where the plastic modulus H is equal to:

$$H = \frac{\partial f}{\partial \sigma'_{ij}} E_{ijkl} \frac{\partial g}{\partial \sigma'_{kl}} - \frac{\partial f}{\partial \varepsilon^p_{ij}} \frac{\partial \varepsilon^p_{ij}}{\partial \lambda^p}$$

3.2 Cam-Clay model

In the field of the elasto-plastic modelling of geomaterials, it is possible to consider the influence of the mean stress imposing that the dimension of the section of the domain perpendicular to the hydrostatic axis ($\sigma_{11} = \sigma_{22} = \sigma_{33}$) becomes greater moving in the direction of compression along the hydrostatic axis. Yield surfaces with this characteristic are those proposed by Drucker and Prager (1952), Drucker and Shield (1955).

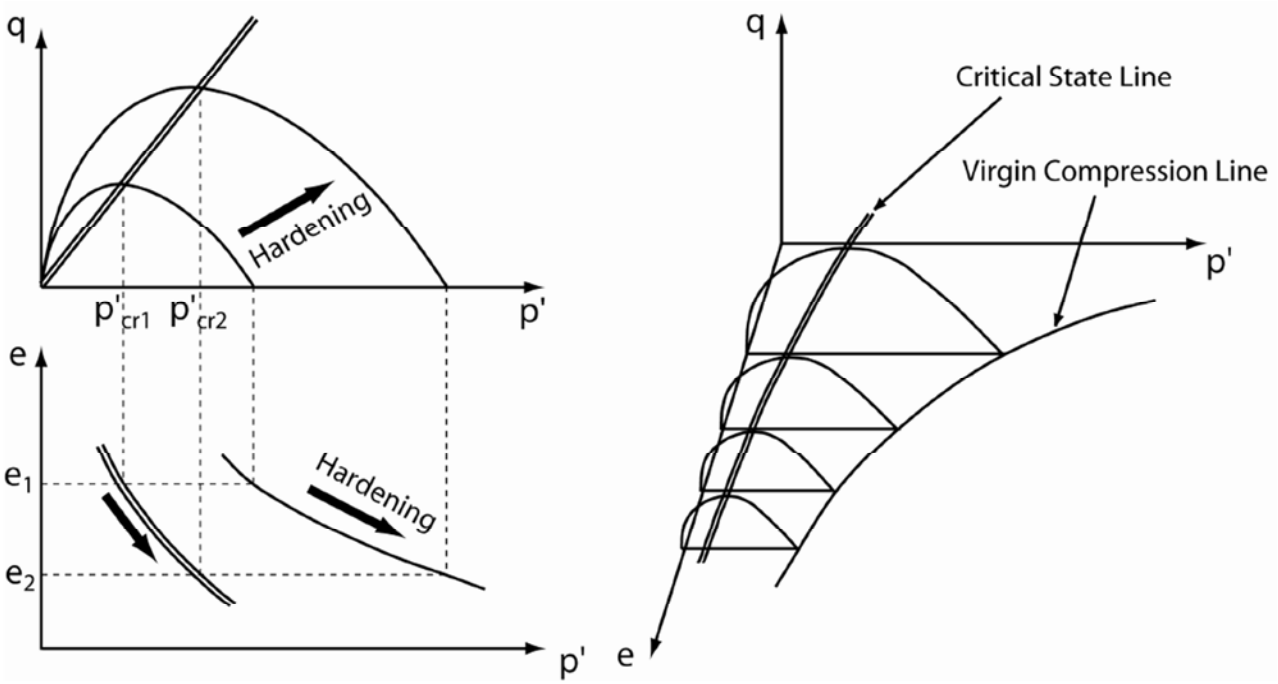

Figure 3.1: Original Cam Clay yield limit (from 'Thermo-Plasticity of Fine-Grained Soils at Various Saturation States: Application to Nuclear Waste Disposal' by B. François, EPFL, 2008)

The Cam-Clay constitutive model for saturated soils was developed in Cambridge in the '60s and is based on the elasto-plasticity concepts previously presented. In this model the yield surface and the critical surface are distinguished for the first time. Two main versions of this model exist, differing from each other in their yield function equation: the *"Original Cam-Clay"* and the *"Modified Cam-Clay"*. The Modified Cam-Clay yield surface is elliptic, while the Original Cam-Clay is almond-shaped. The yield surface depends on void ratio *e* too: any densification of the material leads to a growth of the domain's dimensions. In figure 3.1 the Original Cam-Clay yield limit is represented in the (*p'*, *q*, *e*) space: at any void ratio corresponds a given elastic domain. *P'* is the mean stress *p* corresponding to the effective stress components σ'_{ij}.

In the Cam-Clay model the volumetric response of soil under isotropic loading (oedometric conditions are verified) can be divided into two main parts: the behaviour inside the elastic domain and on the yield limit. The behaviour into the elastic domain is governed by the unloading-reloading curve:

$$e = e_0 - k \ln \frac{p'}{p'_0}$$

being e_0 and p'_0 the starting values of the void ratio and the mean stress and k a material parameter, the *swelling index* (fig.3.2).

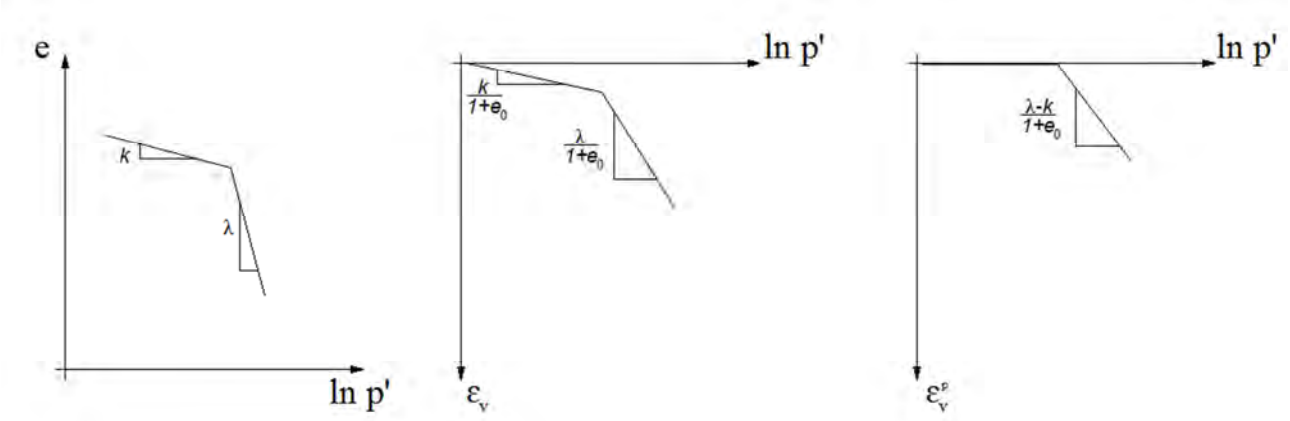

Figure 3.2: Cam Clay model prediction on isotropic compression

The behaviour on the isotropic yield limit, where both plastic and elastic strains are produced, follows this law:

$$e = e_0 - \lambda \ln \frac{p'}{p'_0}$$

where λ is the *compression index*, a material parameter.

As presented in the oedometric conditions, the volumetric strain can be written in terms of void ratio e:

$$\varepsilon_v = \frac{\Delta V}{V_0} = \frac{\Delta H}{H_0} = \frac{e_0 - e}{1 + e_0}$$

The unloading-reloading curve becomes:

$$d\varepsilon_v^e = \frac{dp'}{K_{ref}\left(p'/p'_{ref}\right)}$$

where K_{ref} is the reference *bulk modulus* at the unity mean effective stress p'_{ref}.

$$K_{ref} = \frac{1 + e_0}{k} p'_{ref}$$

In order to calculate the plastic component of the strain during the evolution of the isotropic yield, the swelling index k corresponding to the elastic deformation must be subtracted from the compression index λ. It yields:

$$\beta = \frac{1 + e_0}{\lambda - k}$$

This parameter intervene in the hardening equation, which describes the evolution of the critical pressure p'_{cr} with the generated volumetric plastic strain ε_v^p:

$$p'_{cr} = p'_{cr0} exp(\beta \varepsilon_v^p)$$

As previously disclosed, there are two different Cam-Clay versions: the *Original Cam-Clay* (Schofield and Worth, 1968) and the *Modified Cam Clay* (Roscoe and Burland, 1968).

Original Cam Clay

The yield limit is:

$$f = q - Mp'\left(1 - \ln\frac{p'}{p'_{cr}}\right) = 0$$

where *M* is the slope of the critical state in the (p', q) plane. If the Mohr-Coulomb failure criterion is adopted:

$$M = \frac{6\sin\phi'}{3 - \sin\phi'}$$

The flow rule is the following:

$$d\varepsilon_v^p = \lambda^p \frac{\partial g}{\partial p'} = \lambda^p\left(M - \frac{q}{p'}\right)$$

$$d\varepsilon_d^p = \lambda^p \frac{\partial g}{\partial q} = \lambda^p$$

being $d\varepsilon_d^p$ the increment of the deviatoric plastic strain. The dilatance rule is the following:

$$\frac{d\varepsilon_v^p}{d\varepsilon_d^p} = M - \frac{q}{p'}$$

Modified Cam Clay

The yield limit of the *modified Cam Clay* model is the following:

$$f = q^2 - M^2 p'^2\left(\frac{2p'_{cr}}{p'} - 1\right) = 0$$

The consequent flow rule can be derived:

$$d\varepsilon_v^p = \lambda^p \frac{\partial g}{\partial p'} = \lambda^p\left(M^2 - \left(\frac{q}{p'}\right)^2\right)$$

$$d\varepsilon_d^p = \lambda^p \frac{\partial g}{\partial q} = \lambda^p 2q$$

The corresponding dilatance rule is:

$$\frac{d\varepsilon_v^p}{d\varepsilon_d^p} = \frac{M^2 - \left(\frac{q}{p'}\right)^2}{2\frac{q}{p'}}$$

The expressions for the yield limit and the dilatance rule for both versions are based on two main assumptions:

- Associated flow rule ($g=f$)
- The plastic work is dissipated entirely by friction:

$$dW^p = p'd\varepsilon_v^p + qd\varepsilon_d^p = Mp'd\varepsilon_d^p$$

The two yield functions are represented in figure 3.3.

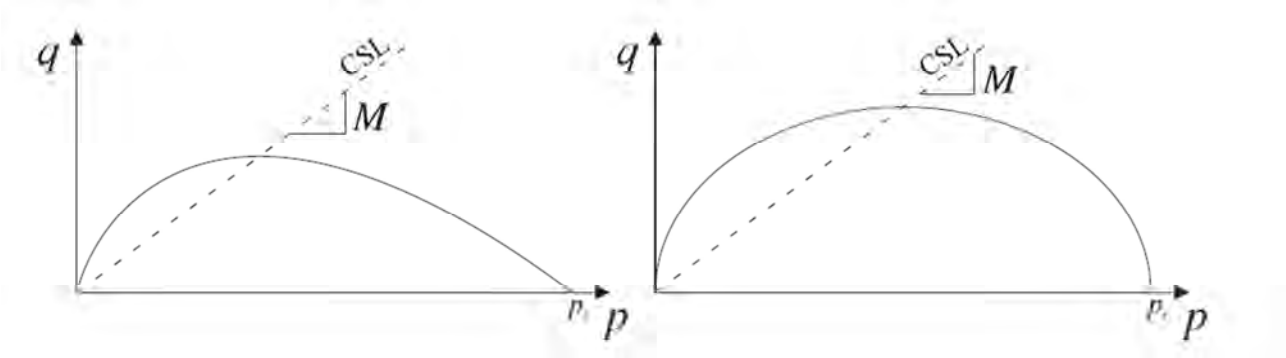

Figure 3.3: Original Cam-Clay and Modified Cam-Clay yield functions

3.3 The ACMEG model

The Cam-Clay model was improved during the years in order to obtain a constitutive tool able to predict soil response upon various mechanical loading. One of the results of these modifications is the ACMEG model, which stands for "Advanced Constitutive Model for Environmental Geomechanics": it is a basic tool, whose improvements are due to several works (Hujeux, 1979; Hajal, 1984; Lassoudière, 1984; Michalski and Rahma, 1989; Piccuezzu, 1991; Modaressi and Laloui, 1997; Laloui and Cekerevac, 2008).

Within the small strain assumptions, the total strain $d\varepsilon$ can be split into the elastic and plastic component:

$$d\varepsilon_{ij} = d\varepsilon_{ij}^e + d\varepsilon_{ij}^p$$

Being the stress and strain tensor symmetric, in the following this notation will be used:

$$\boldsymbol{\varepsilon} = (\varepsilon_{11}\ \varepsilon_{22}\ \varepsilon_{33}\ \gamma_{12}\ \gamma_{13}\ \gamma_{23}\ )^T$$

$$\boldsymbol{\sigma} = (\sigma'_{11}\ \sigma'_{22}\ \sigma'_{33}\ \sigma'_{12}\ \sigma'_{13}\ \sigma'_{23}\ )^T$$

3.3.1 Non linear elasticity

Within the elastic domain the stress-strain relation is, as usual in continuum mechanics:

$$d\varepsilon_{ij}^{e} = E_{ijkl}^{-1} d\sigma'_{kl}$$

where the contraction is assumed positive. E_{ijkl} is the mechanical elastic tensor:

$$\boldsymbol{E} = \begin{bmatrix} K+\frac{4}{3}G & K-\frac{2}{3}G & K-\frac{2}{3}G & 0 & 0 & 0 \\ & K+\frac{4}{3}G & K-\frac{2}{3}G & 0 & 0 & 0 \\ & & K+\frac{4}{3}G & 0 & 0 & 0 \\ & Sym & & G & 0 & 0 \\ & & & & G & 0 \\ & & & & & G \end{bmatrix}$$

where K is the bulk modulus and G is the shear elastic modulus.

Experimental tests evidence that the strains in the elastic domain are strongly non-linear because of a dependence of the elastic modulus on the mean stress. In Cam-Clay model a logarithmic stress-strain relationship of the swelling line is considered; the consequence, as previously illustrated, is a linear dependence of the bulk modulus on the mean stress p':

$$d\varepsilon_{v}^{e} = \frac{dp'}{K_{ref}\left(p'/p'_{ref}\right)} = \frac{dp'}{K}$$

$$K = K_{ref}\left(p'/p'_{ref}\right)$$

$$K_{ref} = \frac{1+e_0}{k} p'_{ref}$$

This expression for the bulk modulus may not be sufficient to reproduce some behaviours of stiff clay. In order to overcome this limitation, an additional exponent n_e is added:

$$K = K_{ref}\left(p'/p'_{ref}\right)^{n_e}$$

As far as the elastic stiffness upon distortional path is concerned, the shear modulus is also affected by the mean effective stress. The same exponent n_e is adopted:

$$G = G_{ref}\left(p'/p'_{ref}\right)^{n_e}$$

where G_{ref} is the shear modulus at the unity mean effective stress p'_{ref}.

The volumetric and deviatoric components of the elastic strain increment are, respectively:

$$d\varepsilon_{v}^{e} = \frac{dp'}{K}$$

$$d\varepsilon_d^e = \frac{dq}{3G}$$

3.3.2 Plastic mechanisms

Isotropic plastic mechanism

The Original Cam-Clay model predicts a deviatoric component of the plastic strain in case of isotropic loading, whereas it should produce only volumetric strains. In the ACMEG model, in agreement with the work of Hujeux (1979), an isotropic yield mechanism is added to the Original Cam Clay deviatoric mechanism:

$$f_{iso} = p' - p'_c r_{iso} = 0$$

where p'_c is the preconsolidation pressure and r_{iso} is the degree of mobilization of the isotropic plastic mechanism ($0 \leq r_{iso} \leq 1$). This parameter is introduced in the model to take in account the progressive mobilization of the plasticity before reaching the yield limit experimentally observed (fig. 3.4).

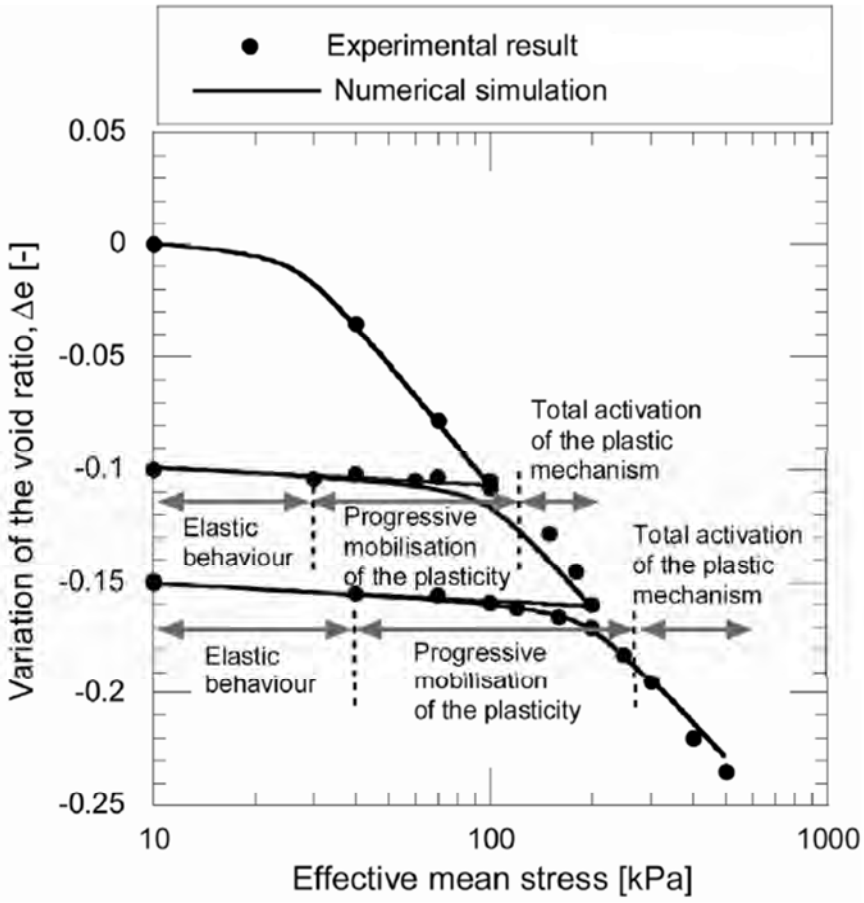

Figure 3.4: Degree of mobilization of the plastic mechanism effect (from 'Thermo-Plasticity of Fine-Grained Soils at Various Saturation States: Application to Nuclear Waste Disposal' by B. François, EPFL, 2008)

During loading, r_{iso} is a hyperbolic function of the volumetric plastic strain induced by the isotropic mechanism:

$$r_{iso} = r_{iso}^{e} + \frac{\varepsilon_v^{p,iso}}{c + \varepsilon_v^{p,iso}}$$

where r_{iso}^{e} is the radius of the isotropic elastic nuclei inside which the strains are fully reversible and *c* is a material parameter.

Its derivate is computed as:

$$dr_{iso} = \frac{(1 - {r_{iso}}^{2})}{c} d\varepsilon_v^{p,iso}$$

During unloading, in order to enable the progressive plasticity upon each isotropic loading, r_{iso} decreases to follow the decrease of effective mean pressure *p'*, while at reloading, r_{iso} is adjusted to keep a constant elastic nuclei (r_{iso}^{e}):

$$r_{iso} = r_{iso}^{e} + \frac{{p'}_{cyc}}{{p'}_{c}} + \frac{\varepsilon_v^{p,cyc,iso}}{c + \varepsilon_v^{p,cyc,iso}}$$

where ${p'}_{cyc}$ is the evolving mean stress, ${p'}_{c}$ is the current preconsolidation pressure and $\varepsilon_v^{p,cyc,iso}$ is the volumetric plastic strain produced by the isotropic mechanism since the change of direction of the solicitation. This mechanism is illustrated in figure 3.5: the unloading takes place elastically and doesn't produce plastic strains. During the unloading A-B, r_{iso} decreases and consequently the position of the isotropic yield function changes.

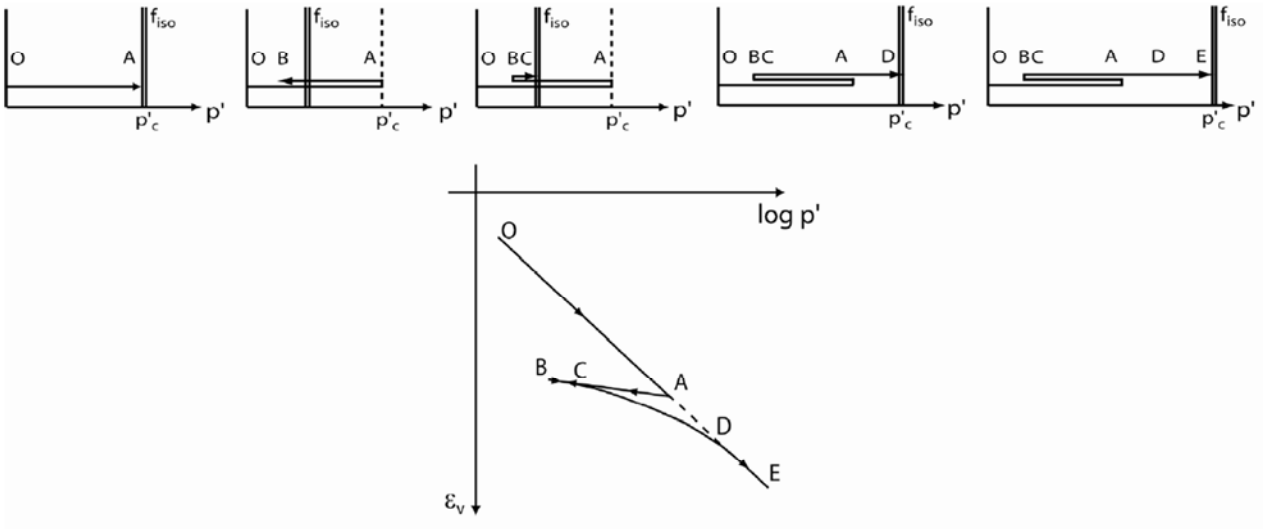

Figure 3.5: Response upon unloading-reloading path (from 'Thermo-Plasticity of Fine-Grained Soils at Various Saturation States: Application to Nuclear Waste Disposal' by B. François, EPFL, 2008)

The reloading is composed by two phases: the first inside the elastic domain (BC) and the second where the yield surface is activated and plastic strains are produced.

The preconsolidation pressure p'_c evolves with the volumetric plastic strain:

$$p'_c = p'_{c0} exp(\beta \varepsilon_v^p)$$

being p'_{c0} the initial preconsolidation pressure and β the plastic compressibility.

Deviatoric plastic mechanism

The expression of the deviatoric yield limit is:

$$f_{dev} = q - Mp' \left(1 - b \ln \frac{dp'}{p'_c}\right) r_{dev} = 0$$

This is the same expression of the Original Cam-Clay model yield limit with the supplement of three parameters: b, d and r_{dev}.

b is a material parameter defining the shape of the yield limit varying from 0 (corresponding to a Mohr-Coulomb model) to 1 (corresponding to original Cam-Clay model). The impact of this parameter on the yield surface is shown in fig. 3.6.

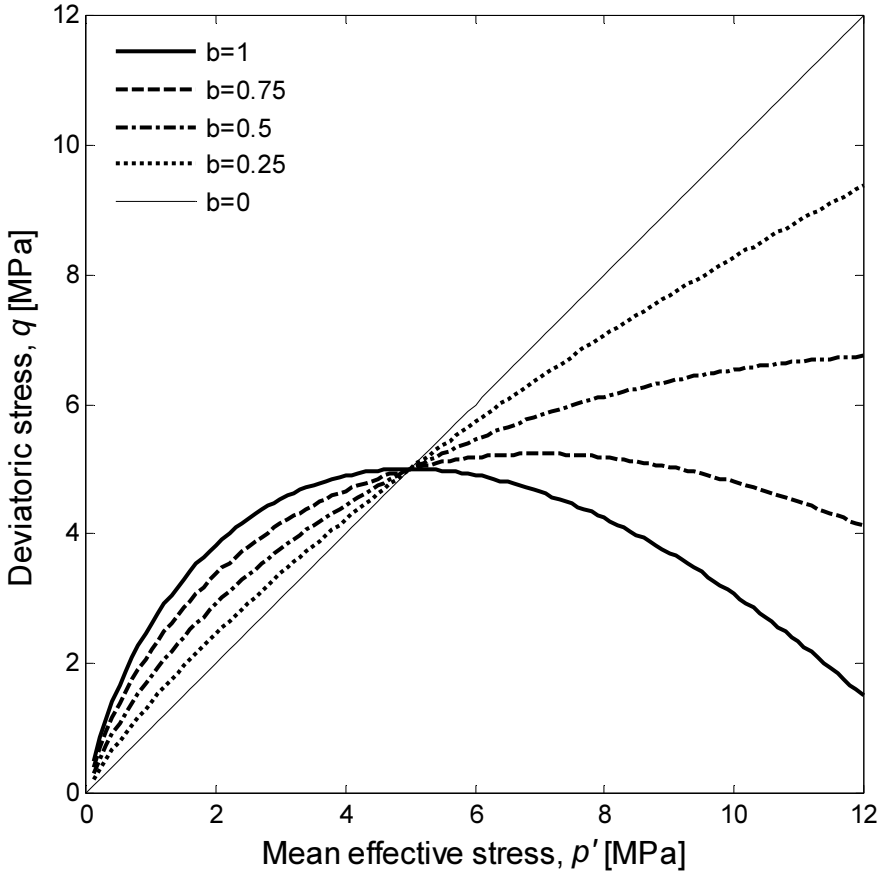

Figure 3.6: Parameter 'b' impact on the yield surface

d is a parameter accounting for the ratio between the preconsolidation pressure p'_c and the critical pressure p'_{cr}:

$$d = \frac{p'_c}{p'_{cr}}$$

d is equal to 2.718 and 2 respectively in the Original Cam-Clay model and in the Modified Cam-Clay model.

r_{dev} is the degree of mobilization of the deviatoric plastic mechanism ($0 \leq r_{dev} \leq 1$). Its evolution is governed by the deviatoric plastic strain ε_d^p:

$$r_{dev} = r_{dev}^e + \frac{\varepsilon_d^p}{a + \varepsilon_d^p}$$

$$dr_{dev} = \frac{(1 - {r_{dev}}^2)}{a} d\varepsilon_d^p$$

where a is a material parameter and r_{dev}^e is the radius of the deviatoric elastic nuclei inside which the strains are fully reversible.

M is the slope of the critical state line in the (p'-q) plane:

$$M = \frac{6 \sin \phi'}{3 - \sin \phi'}$$

In figure 3.7 the elastic domain of the ACMEG model is represented in the (p'-q) plane

3.3.3 Flow rules

The isotropic plastic mechanism, as it is conceived, must produce only volumetric strain, so the plastic potential g_{iso} and the isotropic yield function f_{iso} must be coincident:

$$f_{iso} = g_{iso}$$

The flow rule for the isotropic mechanism is associated:

$$d\varepsilon_{ii}^{p,iso} = \lambda_{iso}^p \frac{\partial g_{iso}}{\partial \sigma'_{ii}} = \frac{\lambda_{iso}^p}{3}$$

$$d\varepsilon_v^{p,iso} = \lambda_{iso}^p \frac{\partial g_{iso}}{\partial p'} = \lambda_{iso}^p$$

If the Original Cam-Clay expression for dilatancy is kept, the consequent g_{dev} expression is different from the ACMEG f_{dev} expression because of the presence of the b parameter: the flow in non-associated.

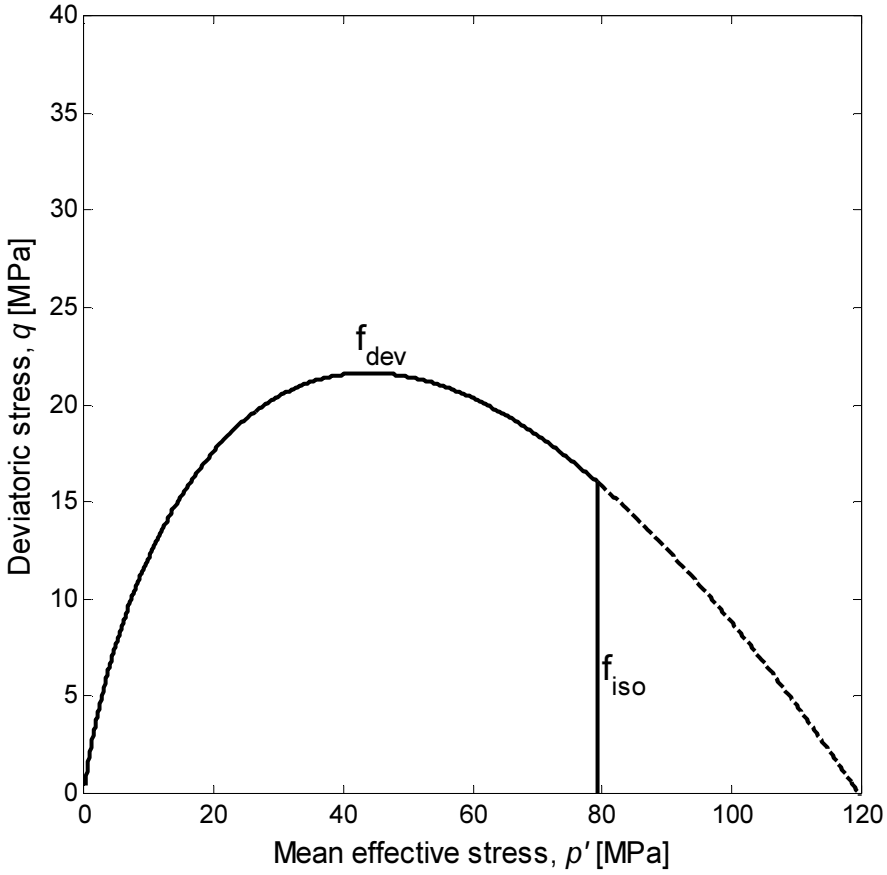

Figure 3.7: ACMEG elastic domain

The Original Cam-Clay plastic potential also fails to predict the volumetric changes during plastic straining: thus, an additional parameter α is introduced in order to catch the various volumetric responses:

$$\frac{d\varepsilon_v^p}{d\varepsilon_d^p} = \alpha\left(M - \frac{q}{p'}\right)$$

The correspondent plastic potential for the deviatoric mechanism is as follows:

$$g_{dev} = q - \frac{\alpha}{\alpha - 1} Mp' \left[1 - \frac{1}{\alpha}\left(\frac{dp'}{p'_c}\right)^{\alpha-1}\right]$$

It can be proved that:

$$\lim_{\alpha\to 1} g_{dev} = \lim_{\alpha\to 1}\left[q - \frac{\alpha}{\alpha - 1} Mp' \left[1 - \frac{1}{\alpha}\left(\frac{dp'}{p'_c}\right)^{\alpha-1}\right]\right] = q - Mp'\left(1 - \ln\frac{dp'}{p'_c}\right)$$

Consequently, if $\alpha = b = 1$ the flow rule is associated; if $\alpha = b = 1$ and $d = 2.71$ the deviatoric mechanism is the same as the Original Cam-Clay model.

The hardening rule is:

$$d\varepsilon_{ii}^{p,dev} = \lambda_{dev}^{p} \frac{\partial g_{dev}}{\partial \sigma'_{ii}} = \lambda_{dev}^{p} \frac{1}{Mp'} \left[\frac{\partial q}{\partial \sigma'_{ij}} + \alpha \left(M - \frac{q}{p'} \right) \frac{1}{3} \delta_{ij} \right]$$

with:

$$\frac{\partial q}{\partial \sigma'_{ij}} = \begin{cases} \frac{3}{2q} (\sigma'_{ii} - p') \; if \; i = j \\ \frac{3\sigma'_{ii}}{q} \qquad\qquad if \; i \neq j \end{cases}$$

The volumetric and deviatoric plastic strains for the deviatoric mechanism are:

$$d\varepsilon_{v}^{p,dev} = \lambda_{dev}^{p} \frac{\partial g_{dev}}{\partial p'} = \lambda_{dev}^{p} \frac{\alpha}{Mp'} \left[M - \frac{q}{p'} \right]$$

$$d\varepsilon_{d}^{p} = \lambda_{dev}^{p} \frac{\partial g_{dev}}{\partial q} = \lambda_{dev}^{p} \frac{1}{Mp'}$$

3.3.4 Coupling between the mechanisms

The isotropic and hardening mechanisms are coupled through the hardening variable ε_v^p: the feature of the ACMEG model is that the total volumetric plastic strain increment is the sum of the volumetric plastic strain due to each mechanism.

$$d\varepsilon_{v}^{p} = d\varepsilon_{v}^{p,iso} + d\varepsilon_{v}^{p,dev} = \lambda_{dev}^{p} \frac{\partial g_{dev}}{\partial p'} + \lambda_{iso}^{p} \frac{\partial g_{iso}}{\partial p'} = \lambda_{dev}^{p} \frac{1}{Mp'} + \lambda_{iso}^{p}$$

The two consistency equations must be verified simultaneously. It yields:

$$\boldsymbol{dF} = \frac{\partial \boldsymbol{F}}{\partial \sigma'} : d\sigma' + \frac{\partial \boldsymbol{F}}{\partial \pi} \frac{\partial \pi}{\partial \lambda^p} \lambda^p = \boldsymbol{j} : d\sigma' - \boldsymbol{H} \cdot \lambda^p \leq 0; \lambda^p \geq 0; \boldsymbol{dF} \cdot \lambda^p \geq 0$$

$$\boldsymbol{dF} = \begin{pmatrix} df_{iso} \\ df_{dev} \end{pmatrix}$$

where $\boldsymbol{\sigma'}$ is the stress vector and $\boldsymbol{\pi}$ the internal variable vector. $\boldsymbol{j}$ is:

$$\boldsymbol{j} = \begin{pmatrix} \frac{\partial f_{iso}}{\partial \sigma'_{11}} & \frac{\partial f_{iso}}{\partial \sigma'_{22}} & \frac{\partial f_{iso}}{\partial \sigma'_{33}} & \frac{\partial f_{iso}}{\partial \sigma'_{12}} & \frac{\partial f_{iso}}{\partial \sigma'_{13}} & \frac{\partial f_{iso}}{\partial \sigma'_{23}} \\ \frac{\partial f_{dev}}{\partial \sigma'_{11}} & \frac{\partial f_{dev}}{\partial \sigma'_{22}} & \frac{\partial f_{dev}}{\partial \sigma'_{33}} & \frac{\partial f_{dev}}{\partial \sigma'_{12}} & \frac{\partial f_{dev}}{\partial \sigma'_{23}} & \frac{\partial f_{dev}}{\partial \sigma'_{13}} \end{pmatrix}$$

$\boldsymbol{\lambda^p}$ is the plastic multiplier vector:

$$\lambda^p = \begin{pmatrix} \lambda_{iso}^{p} \\ \lambda_{dev}^{p} \end{pmatrix}$$

$\boldsymbol{H}$ is the matrix of the hardening moduli:

$$\boldsymbol{H} = \begin{bmatrix} H_{ii} & H_{id} \\ H_{di} & H_{dd} \end{bmatrix}$$

with:

$$\begin{cases} H_{ii} = -\dfrac{\partial f_{iso}}{\partial r_{iso}}\dfrac{\partial r_{iso}}{\partial \lambda^p_{iso}} - \dfrac{\partial f_{iso}}{\partial \varepsilon^p_v}\dfrac{\partial \varepsilon^p_v}{\partial \lambda^p_{iso}} = p'_c \dfrac{(1-r_{iso})^2}{c} + p'_c\, \beta r_{iso} \\ H_{id} = -\dfrac{\partial f_{iso}}{\partial r_{dev}}\dfrac{\partial r_{dev}}{\partial \lambda^p_{dev}} - \dfrac{\partial f_{iso}}{\partial \varepsilon^p_v}\dfrac{\partial \varepsilon^p_v}{\partial \lambda^p_{dev}} = -\dfrac{\partial f_{iso}}{\partial \varepsilon^p_v}\dfrac{\partial \varepsilon^p_v}{\partial \lambda^p_{dev}} = p'_c\, \beta r_{iso}\dfrac{1}{Mp'}\left(M - \dfrac{q}{p'}\right)\alpha \\ H_{di} = -\dfrac{\partial f_{dev}}{\partial r_{iso}}\dfrac{\partial r_{iso}}{\partial \lambda^p_{iso}} - \dfrac{\partial f_{dev}}{\partial \varepsilon^p_v}\dfrac{\partial \varepsilon^p_v}{\partial \lambda^p_{iso}} = -\dfrac{\partial f_{dev}}{\partial \varepsilon^p_v}\dfrac{\partial \varepsilon^p_v}{\partial \lambda^p_{iso}} = Mp' b\beta r_{dev} \\ H_{dd} = -\dfrac{\partial f_{dev}}{\partial r_{dev}}\dfrac{\partial r_{dev}}{\partial \lambda^p_{iso}} - \dfrac{\partial f_{dev}}{\partial \varepsilon^p_v}\dfrac{\partial \varepsilon^p_v}{\partial \lambda^p_{dev}} = -\left(1 - b\ln\dfrac{p'd}{p'_c}\right)\dfrac{(1-r_{dev})^2}{a} - b\beta\left(M - \dfrac{q}{p'}\right)\alpha r_{dev} \end{cases}$$

3.4 The ACMEG-C model

The ACMEG model as previously presented does not take in account the modifications of the material's behaviour due to a change in *osmotic suction*, the representative variable of the chemical composition of the pore liquid.

3.4.1 Total suction and osmotic suction

The *total suction* ψ is the sum of the *matric suction* s and the *osmotic suction* π:

- The *matric suction s* is the term that takes in account the capillary phenomena and adsorption mechanisms. In fact, it is well known that water and air phase form interphases of negligible thickness, which curve to form capillary menisci when in contact with the solid grains. As demonstrated through equilibrium considerations, menisci concave on the air side generate pore water pressures which are lower than the air pressure: the difference between the two pressures is named capillary pressure p_{cap}. This pressure can also be linked to the tensile pull generated along the boundary. The matric suction also groups the suction linked to water adsorption mechanisms, which is particularly important in clayey soils;
- The *osmotic suction* π is due to the presence of dissolved ions in the pore water which cause a variation of pressure caused by osmotic effects (par. 4.1).

As mentioned, the aim of this work is to study the consequence of a variation in the pore liquid composition. Previous studies and tests on this topic [*Witteveen et al.*, 2013] proved

that matric suction can be neglected and, consequently, that the total suction can be assumed coincident with its osmotic component. It can be written:

$$\psi = \pi \text{ [MPa]}$$

3.4.2 The ACMEG-C model

The ACMEG-C model introduces in the previous ACMEG model the *osmotic suction* as representative variable of the chemical composition of the pore liquid: the law which links osmotic suction and the ion concentration for dilute solutions is presented in a following paragraph. The variations introduced in ACMEG-C model are based on studies and experiments on a non-swelling illite carried on at EPFL LMS [*Witteveen et al.*, 2013].

According on experimental results, the reference bulk modulus K_{ref} is assumed to evolve with the osmotic suction following the power function:

$$K_{ref} = K_{ref,0}\left(\frac{\pi}{\pi_0}\right)^{-\delta}$$

being $K_{ref,0}$ the bulk modulus at a reference osmotic suction π_0.

A dependence of the preconsolidation pressure on the osmotic suction value is also observed. The following logarithmic dependence is assumed:

$$p'_c = p'_{c0} exp(\beta \varepsilon_v^p)\left(1 - \gamma_\pi \log\frac{\pi}{\pi_0}\right)$$

being p'_{c0} the preconsolidation stress at a reference osmotic suction π_0, β the plastic compressibility, ε_v^p the total plastic volumetric strain, π the current osmotic suction and γ_π the material parameter defining the variation of the yield limit with respect to the osmotic suction. The plastic compressibility β is also assumed to be influenced by the osmotic suction following a logarithmic dependence:

$$\beta = \beta_0\left(1 + \gamma_\beta \log\frac{\pi}{\pi_0}\right)$$

where γ_β is the chemical evolution factor, π is the current osmotic suction and β_0 is the plastic compressibility at the reference osmotic suction π_0.

The isotropic yield function expression becomes:

$$f_{iso} = p' - p'_c r_{iso} = p' - p'_{c0} exp\left[\left(1 + \gamma_\beta \log\frac{\pi}{\pi_0}\right)\beta_0 \varepsilon_v^p\right] \cdot \left(1 - \gamma_\pi \log\frac{\pi}{\pi_0}\right) r_{iso}$$

where the evolution of the mechanical hardening is expressed by the material parameters β_0 and c (within the r_{iso} expression) and the evolution of the chemical hardening is considered by the parameters γ_π and γ_β.

The new expression for the deviatoric yield function is:

$$f_{dev} = q - Mp' \left[1 - bln \frac{p'd}{p'_{c0} exp\left[\left(1 + \gamma_\beta \log \frac{\pi}{\pi_0} \right) \beta_0 \varepsilon_v^p \right] \cdot \left(1 - \gamma_\pi \log \frac{\pi}{\pi_0} \right) r_{iso}} \right] r_{dev}$$

The isotropic and deviatoric mechanisms are linked through the volumetric plastic stain ε_v^p: their coupling is shown in the following figure 3.8.

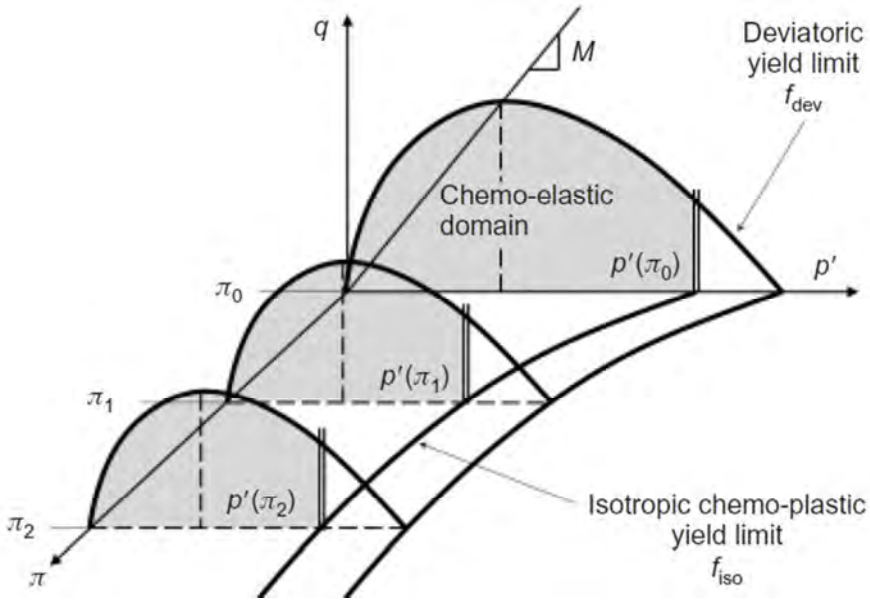

Figure 3.8: Coupling of isotropic and deviatoric mechanisms (from 'An experimental and constitutive investigation on the chemo-mechanical behaviour of a clay', P. Witteveen, A. Ferrari and L. Laloui, Géotechnique, 2013)

Following the experimental results, an increase in osmotic suction entails a decrease of the elastic domain dimensions.

4. Chemo-mechanical oedometric tests on shales

To reach a better knowledge of shales behaviour when subjected to chemical variations similar to those of the drilling fluids, a set of six chemo-mechanical oedometric tests was performed in EPFL LMS laboratory on samples of a particular shale, *Opalinus Clay*. The tests were conducted in saturated and drained conditions: the consequence is the equivalence of the total stress and the effective stress of the material.

4.1 Osmotic processes in shales

Shales behaviour during drilling is attributed to osmotic effects. Osmosis is the transport of water molecules flow from low salinity side of a semi-permeable membrane to the high salinity side to equalize the concentration of the dissolved salts: figure 4.1 shows this phenomenon and allows a better understanding of osmotic suction.

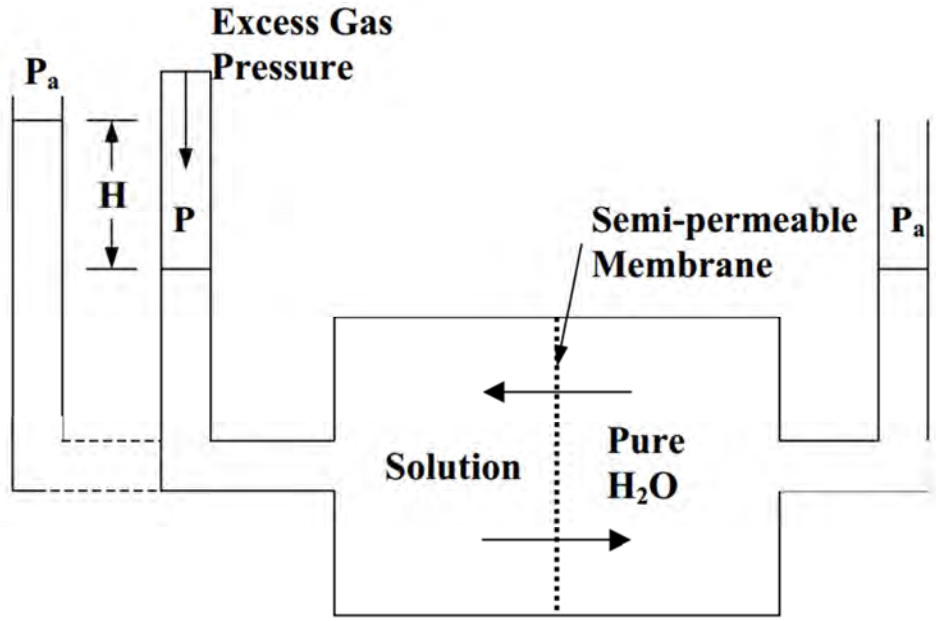

Figure 4.1: The mechanism of osmotic suction

The presence of dissolved ions in the solution triggers the flow of pure water through the semi-permeable membrane. Simultaneously, if an external pressure is applied to the solution, a flow of water through the semi-permeable membrane towards the pure water

begins. When an equilibrium between these two mechanisms is reached, the pressure on the solution is equal to the osmotic suction π.

Because of their wide distribution of the pore range, shales can act as a non-ideal, semi-permeable membrane, which only restricts the passage of some of the solutes in the solvent.

4.2 Chemo-mechanical oedometric tests

A previous laboratory programme on a non-swelling illite carried on at EPFL LMS showed that, for this kind of experiments, the matric suction is negligible and that total suction can be assumed coincident with its osmotic component [*Witteveen et al.*, 2013]. Moreover, a marginal influence of water content was observed in the experimental findings.

4.2.1 Stress paths and experimental results

The chemo-mechanical oedometric tests on shales studied in this work were conducted with different stress paths, including mechanical loading at a constant osmotic suction and an increasing osmotic suction at a constant mechanical stress.

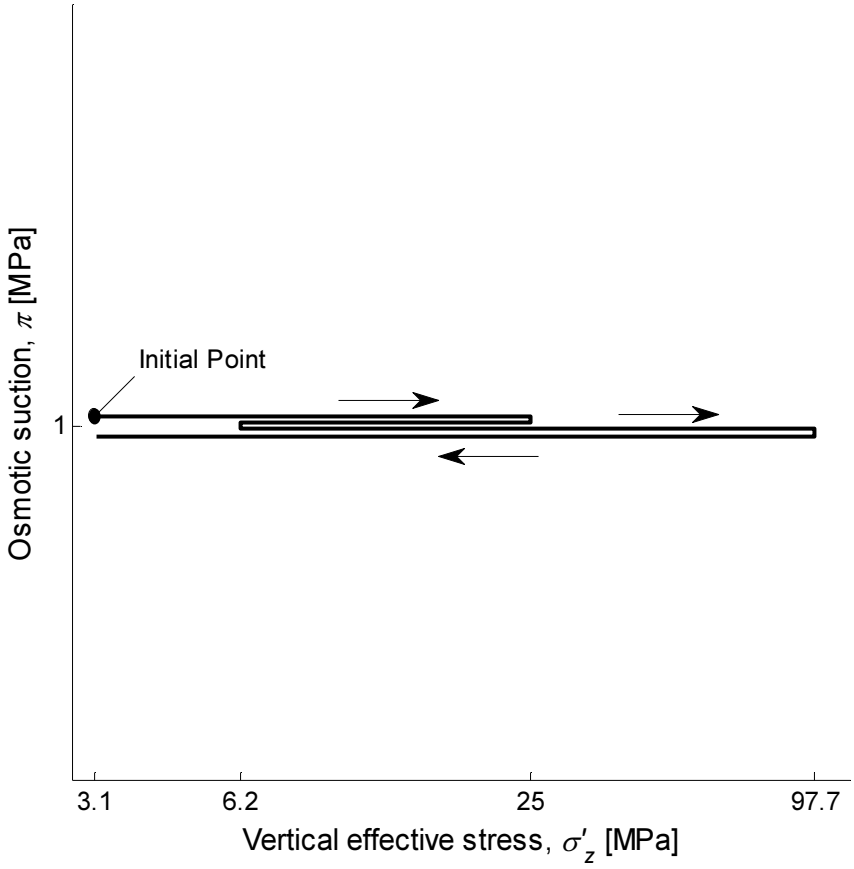

Figure 4.2: Stress Path 1

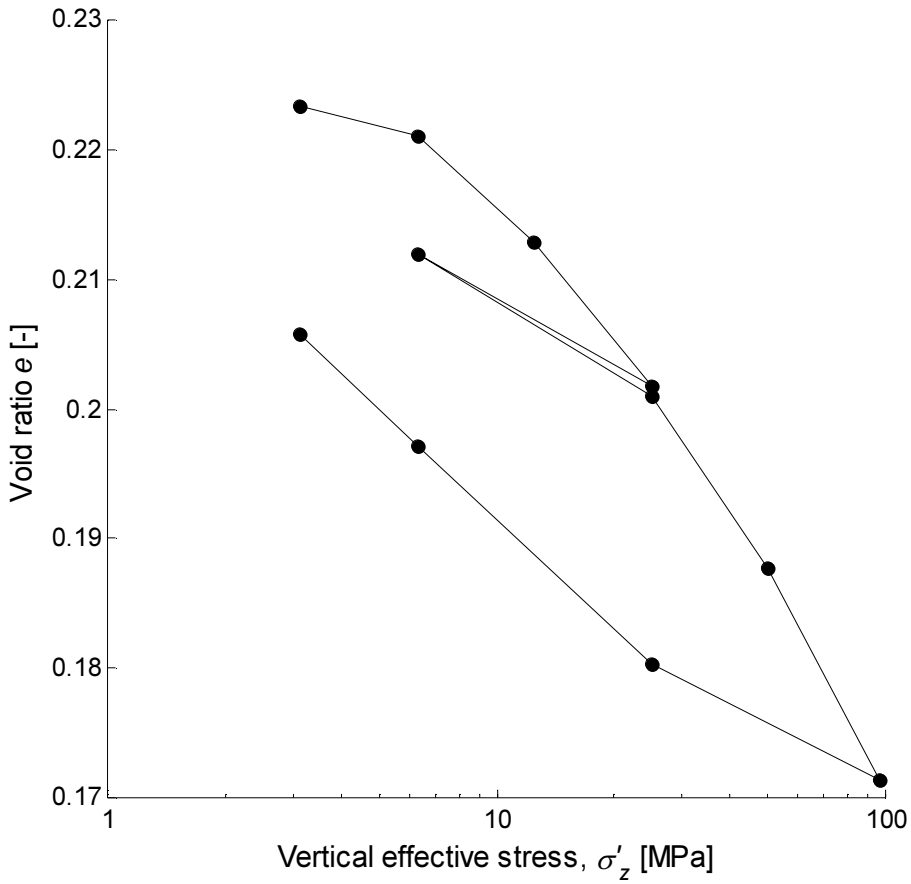

Figure 4.3: Test 1 experimental oedometric curve

The first stress path (fig. 4.2) is composed by a mechanical loading at a constant osmotic suction (1 MPa) with a unloading-reloading appendage. The corresponding experimental results are reported in figure 4.3.

The second stress path is represented in figure 4.4: it is similar to the first one, but with smaller vertical effective stress values. As shown in figure 4.5, it is also characterized by greater void ratio values.

The third stress path (fig 4.6) is composed by an initial mechanical loading at a constant osmotic suction (1 MPa) followed by a reduction of the osmotic suction value until 0.5 MPa. Then the shale sample is subjected to two unloading-reloading cycles ant to a final mechanical unloading.

Figure 4.8 represents the fourth stress path: there is an initial mechanical loading at a constant value of osmotic suction (1 MPa), then an increase of osmotic suction to 15 MPa and, after a unloading-reloading cycle, a final mechanical unloading.

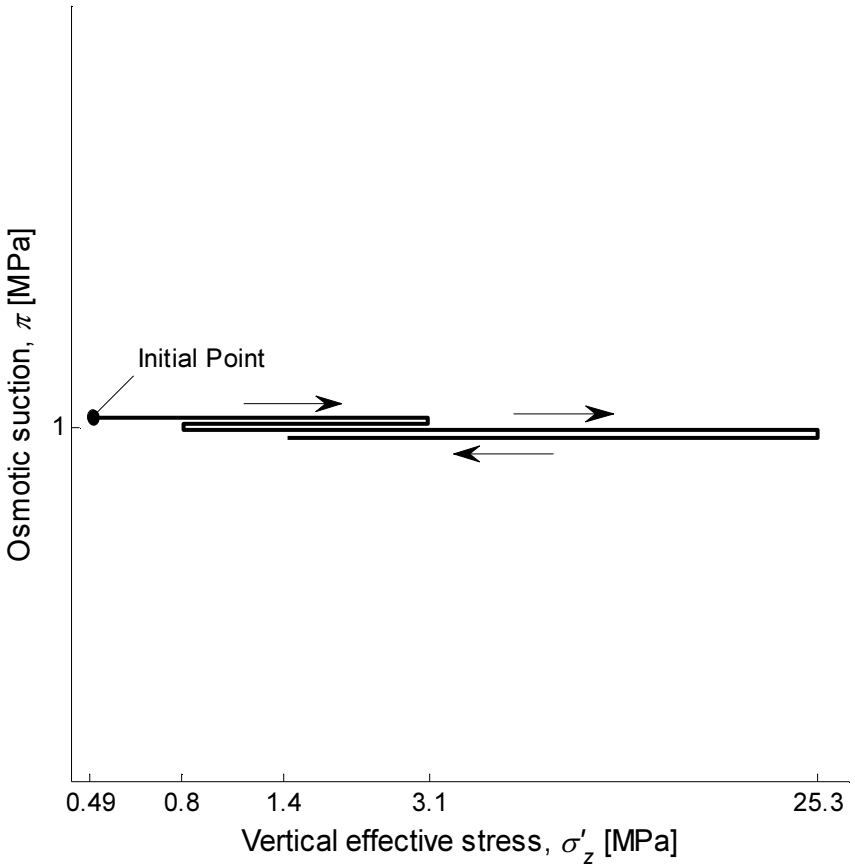

Figure 4.4: Stress Path 2

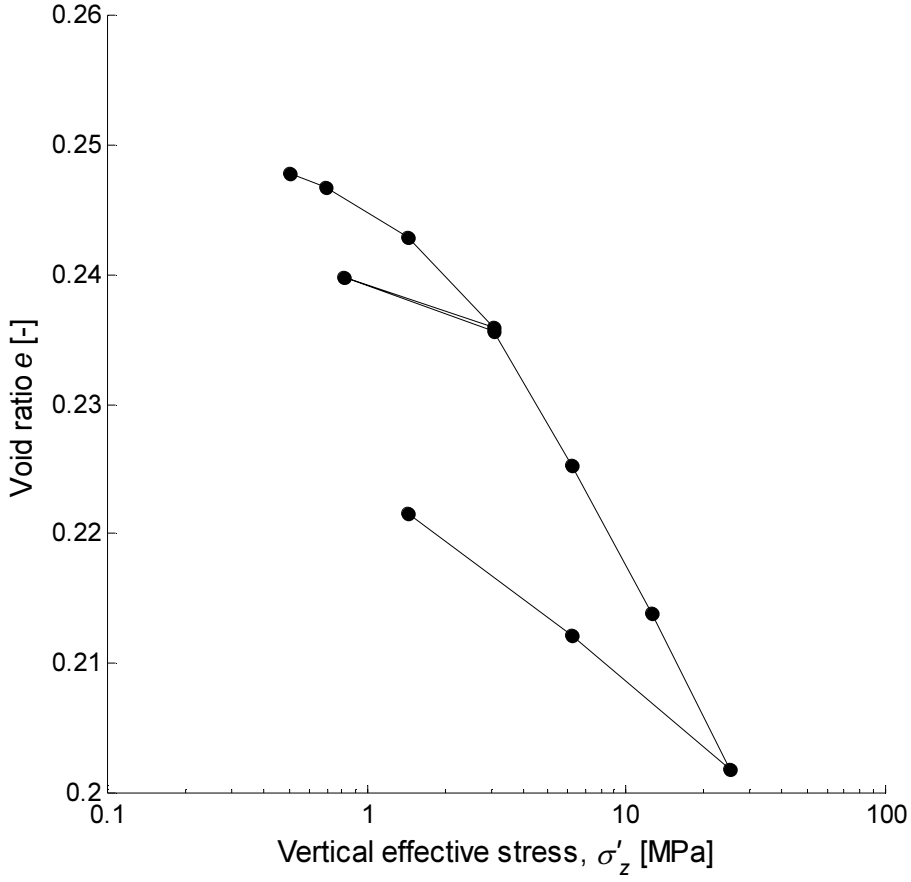

Figure 4.5: Test 2 experimental oedometric curve

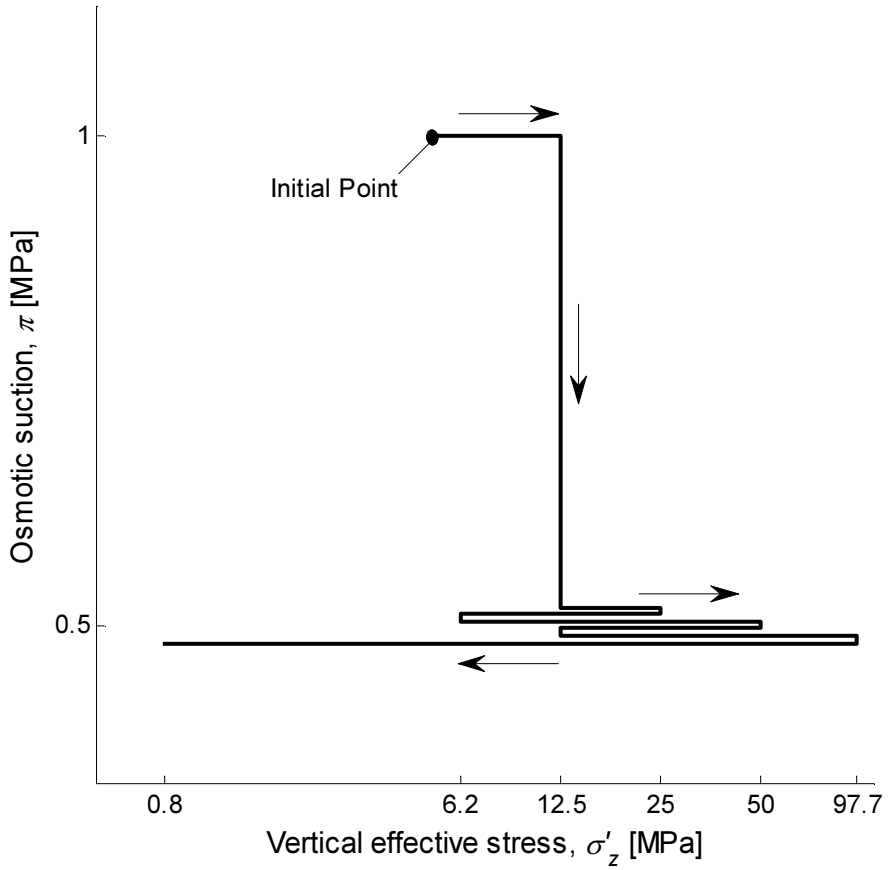

Figure 4.6: Stress Path 3

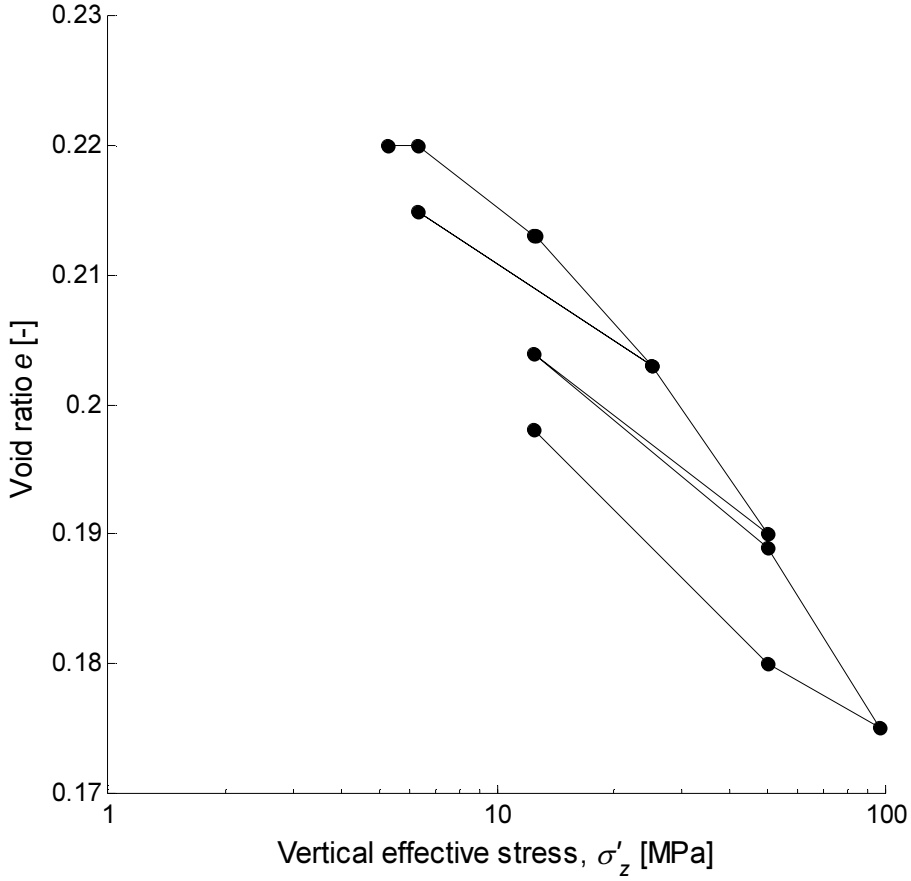

Figure 4.7: Test 3 experimental oedometric curve

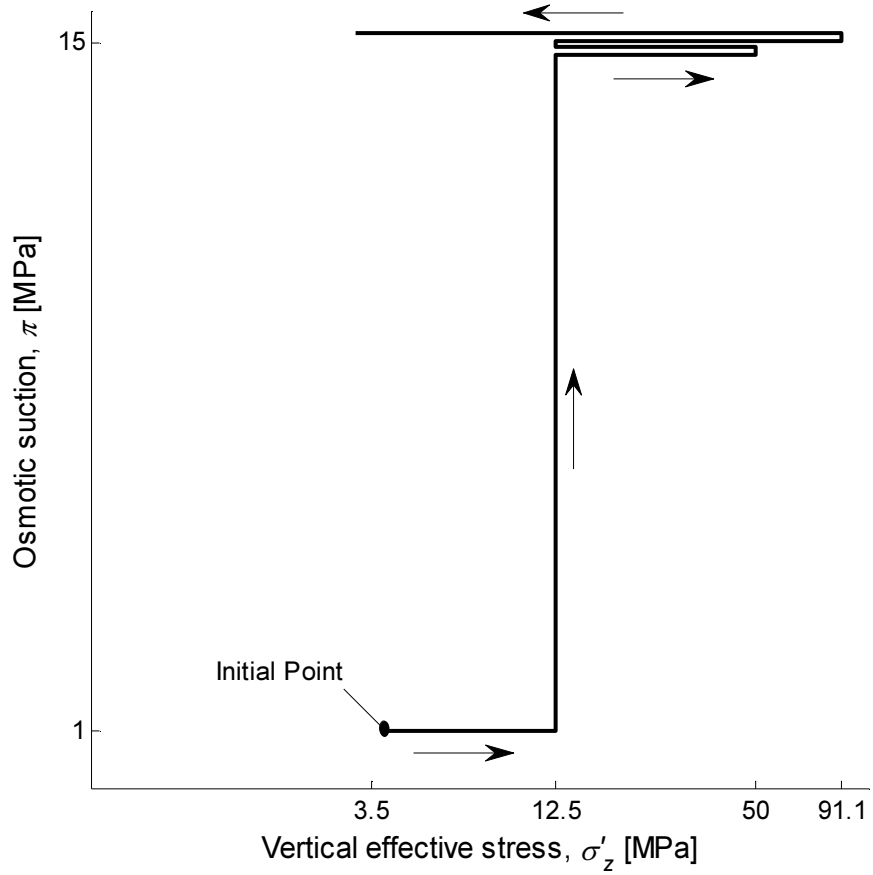

Figure 4.8: Stress Path 4

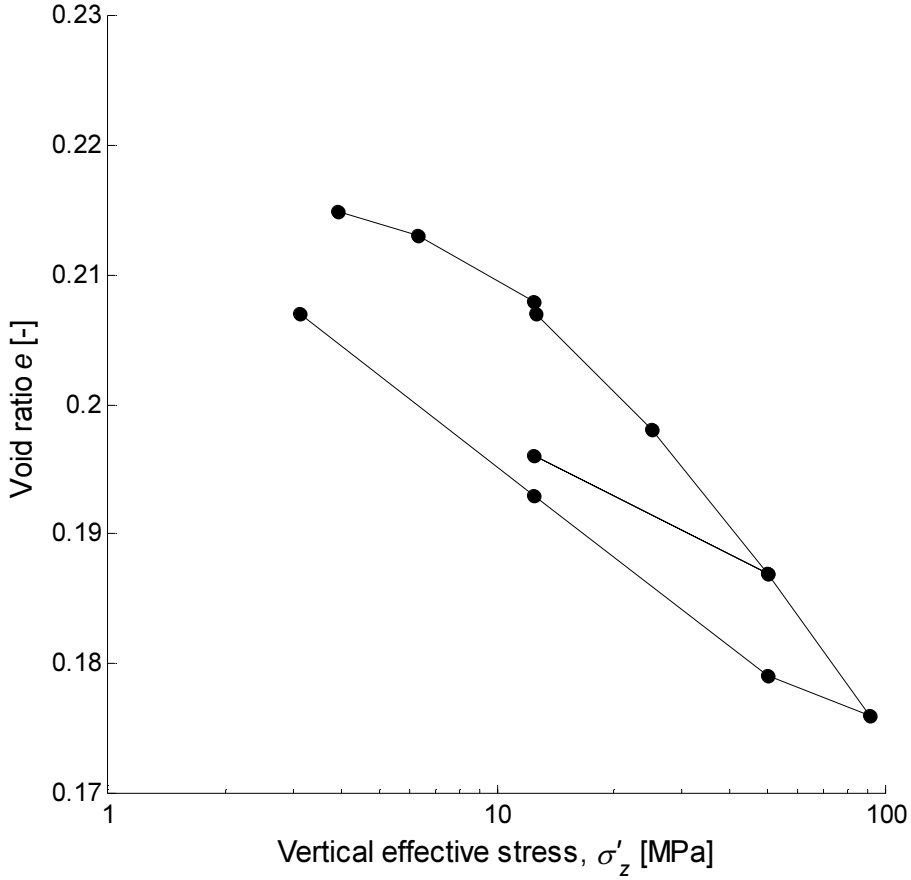

Figure 4.9: Test 4 experimental oedometric curve

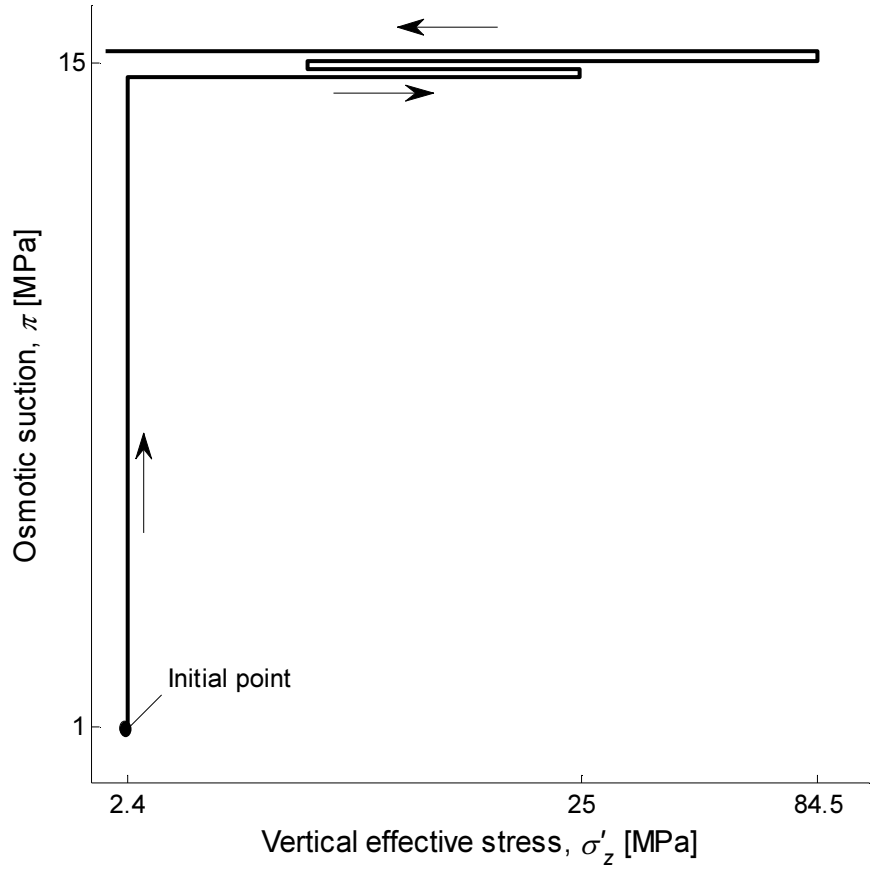

Figure 4.10: Stress Path 5

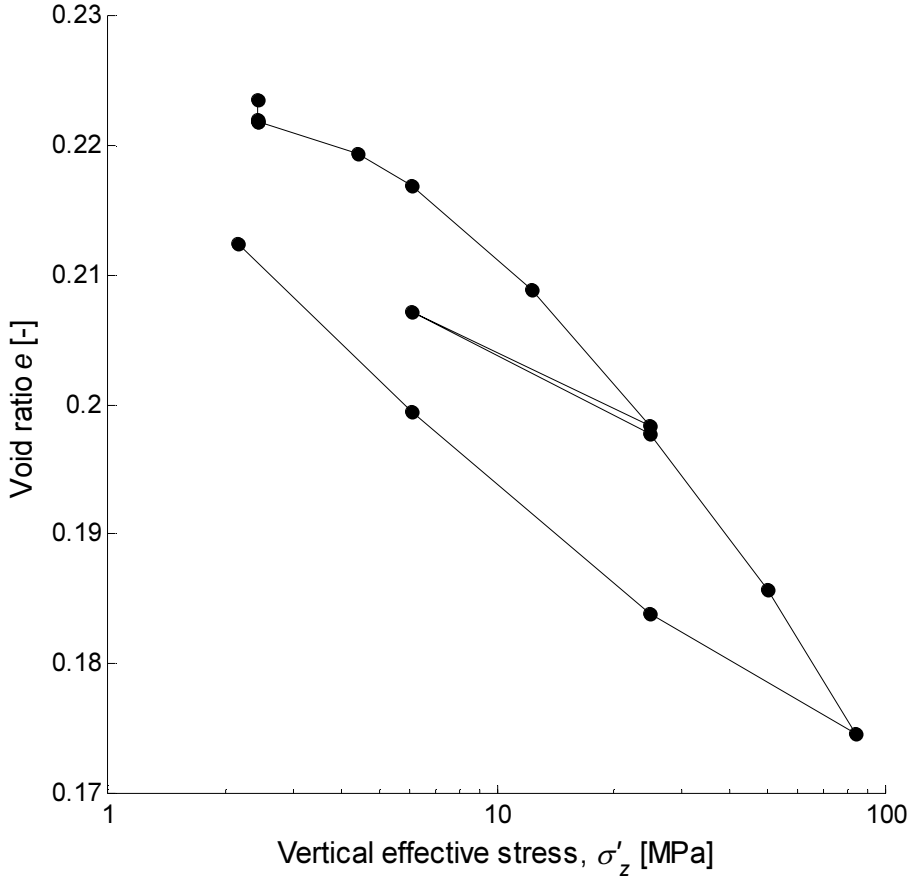

Figure 4.11: Test 5 experimental oedometric curve

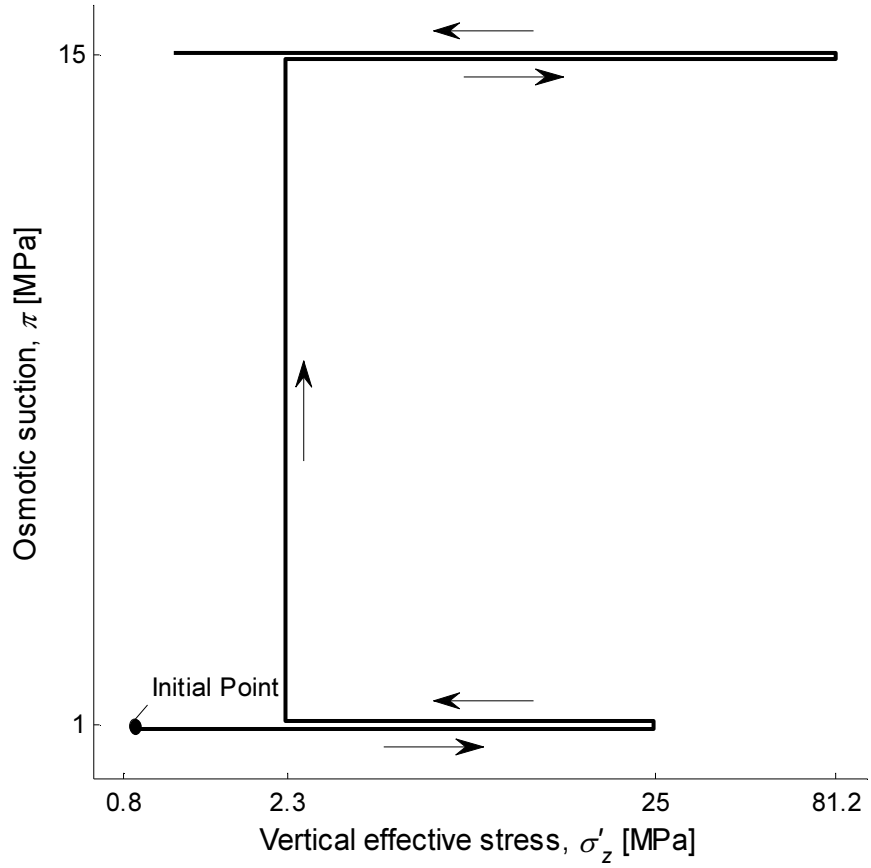

Figure 4.12: Stress Path 6

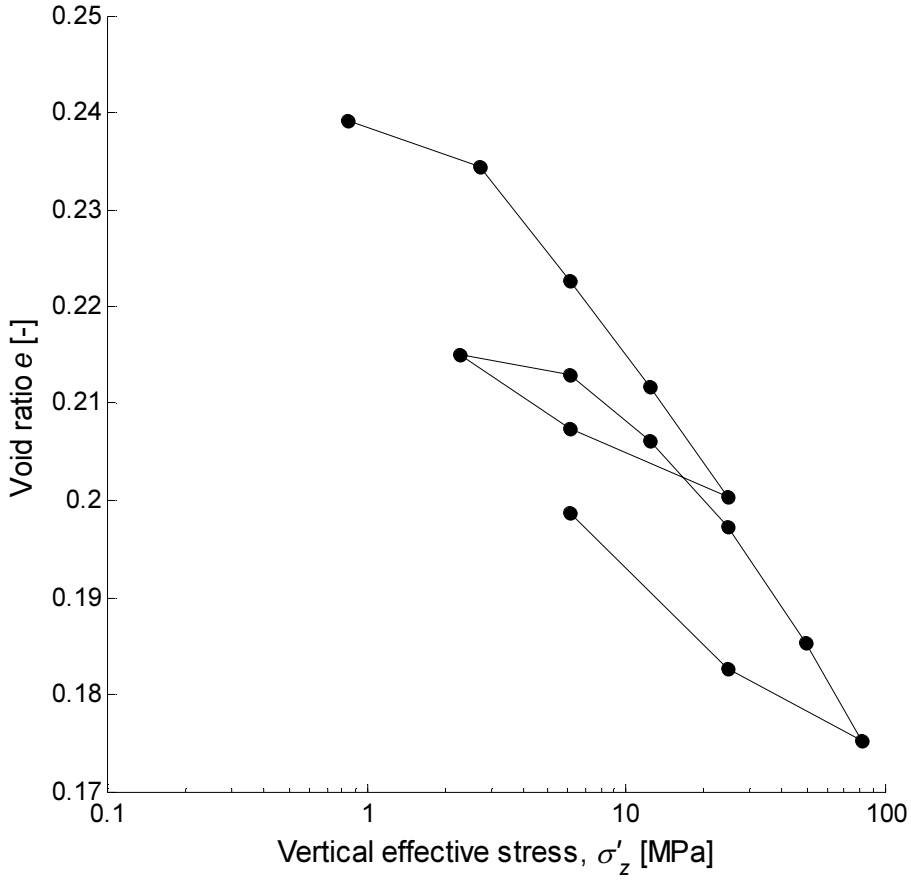

Figure 4.13: Test 6 oedometric curve

The stress path represented in figure 4.10 has an initial variation of osmotic suction at a constant vertical effective stress, followed by a mechanical loading, a unloading-reloading cycle and a final mechanical unloading.
The sixth and last stress path (figure 4.12) is composed by an initial mechanical loading at a osmotic suction of 1 MPa followed by a mechanical unloading, a change in osmotic suction from 1 MPa to 15 MPa, a mechanical loading and a final mechanical unloading at a constant osmotic suction of 15 MPa.

4.2.2 Observations

Some comments can be made starting from the experimental results:

- all the tests show an important behaviour of Opalinus Clay: like shales in general, the so-called *damage* effect characterizes the oedometric curve. This effect is due to an internal reorganization when the sample is subjected to a mechanical stress, and leads to a greater slope of the unloading curve as the void ratio decreases and the deformation increases;
- the unloading-reloading cycles at constant osmotic suction are not observed to involve important quantities of plastic strains;
- a variation in osmotic suction at a constant mechanical stress does not involve important strains in the test 3 and 6, while in the test 4 and 5 a variation of the void ratio of 0.09% and 0.18% respectively is registered;
- the slope of the elasto-plastic part of the oedometric curve does not seem to be influenced by the osmotic suction value;
- test 5 has a particular path in its first steps: there is an initial increase of osmotic suction from 1 MPa to 15 MPa, a following decrease from 15 MPa to 1 MPa and another chemical loading to 15 MPa. The experimental answer to this path is an initial deformation corresponding to the first stress paths and then an approximately constant void ratio.

4.3 Determination of the preconsolidation pressure

A fundamental parameter to determine is the preconsolidation of the samples subjected to the oedometric tests. Two different methods have been used: the *Casagrande's graphic method* and the *Energetic method*.

4.3.1 Casagrande's graphic method

The Casagrande's graphic method is the procedure commonly used in geotechnical applications to determine the preconsolidation pressure. It entails the following steps:

- determination of the point of maximum curvature on the consolidation curve (point M in figure 4.14);
- drawing of a horizontal line from M and of the tangent to the curve at point M;
- drawing of the bisector of the angle between the two lines drawn;
- the intersection of the bisector and the line traced following the last part of the consolidation curve identifies the preconsolidation pressure.

The whole procedure is represented in figure 4.14.

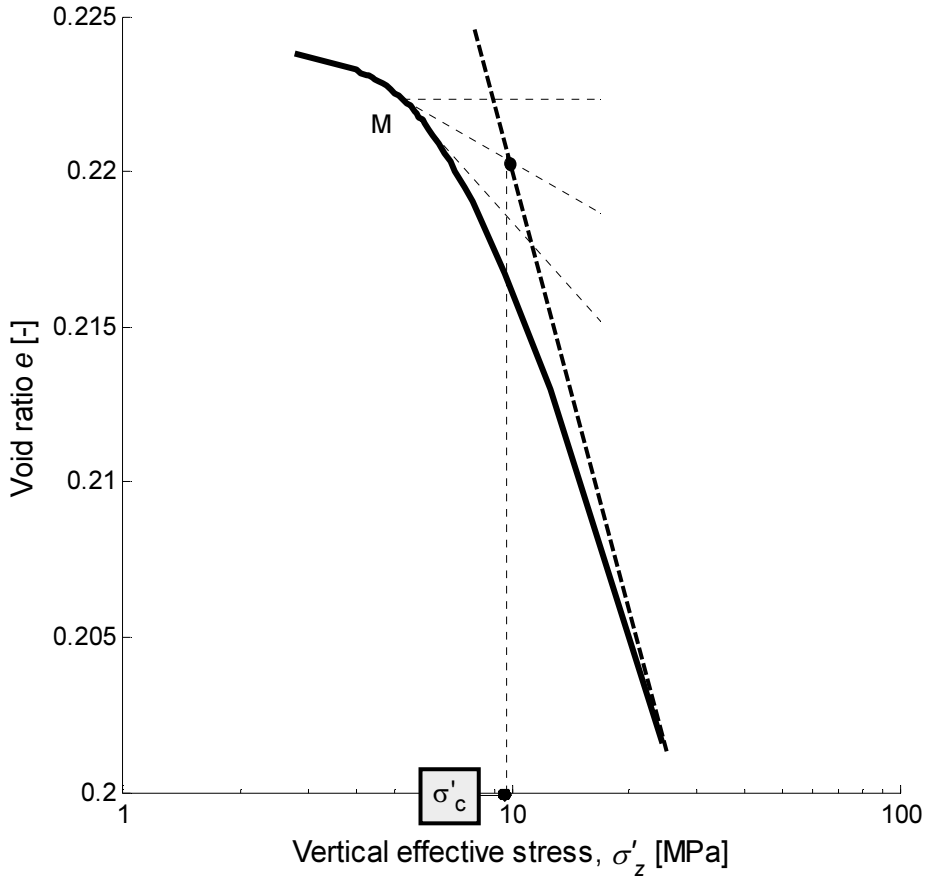

Figure 4.14: Casagrande's graphic method

With this method the preconsolidation pressure is determined together with the corresponding void ratio *e*. Experimental results show that the line traced following the last part of the curve (a sort of experimental Normal Compression Line) is the same for the different tests, being the samples composed by the same material. This line depends only on osmotic suction, and a variation in osmotic suction modifies its position but not its slope. Two different lines were determined: one corresponding to an osmotic suction value of 1 MPa, one of 15 MPa, respectively traced in test 1 (figure 4.15) and test 5 (figure 4.16).

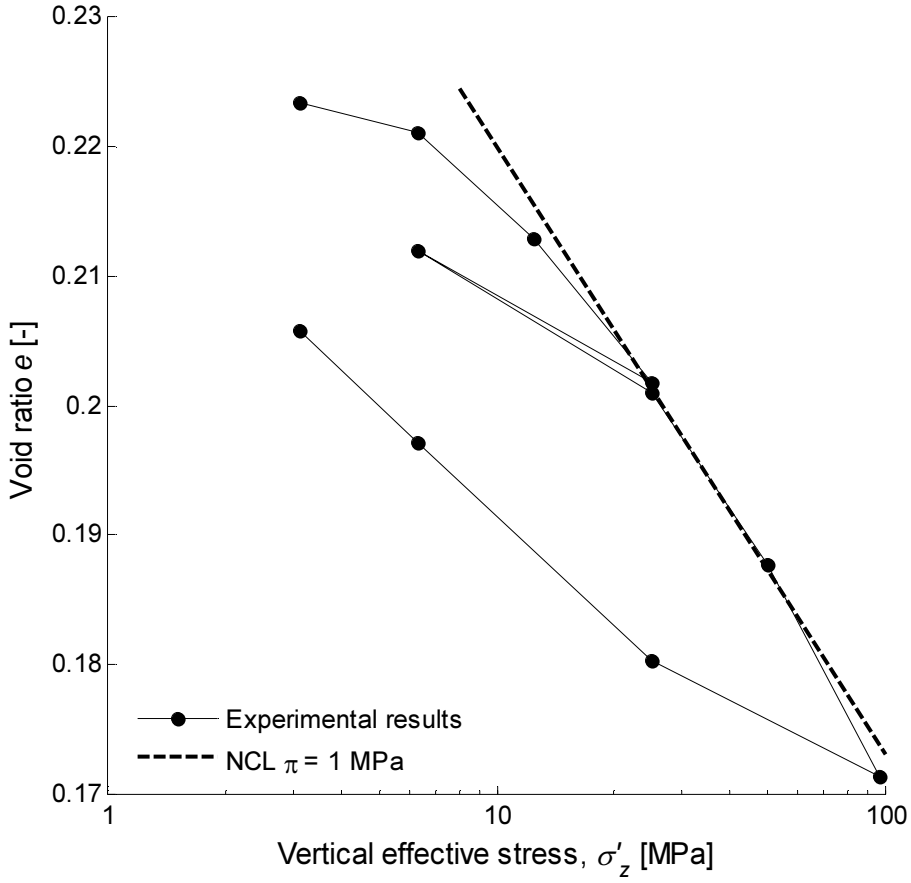

Figure 4.15: Experimental NCL corresponding to π = 1 MPa

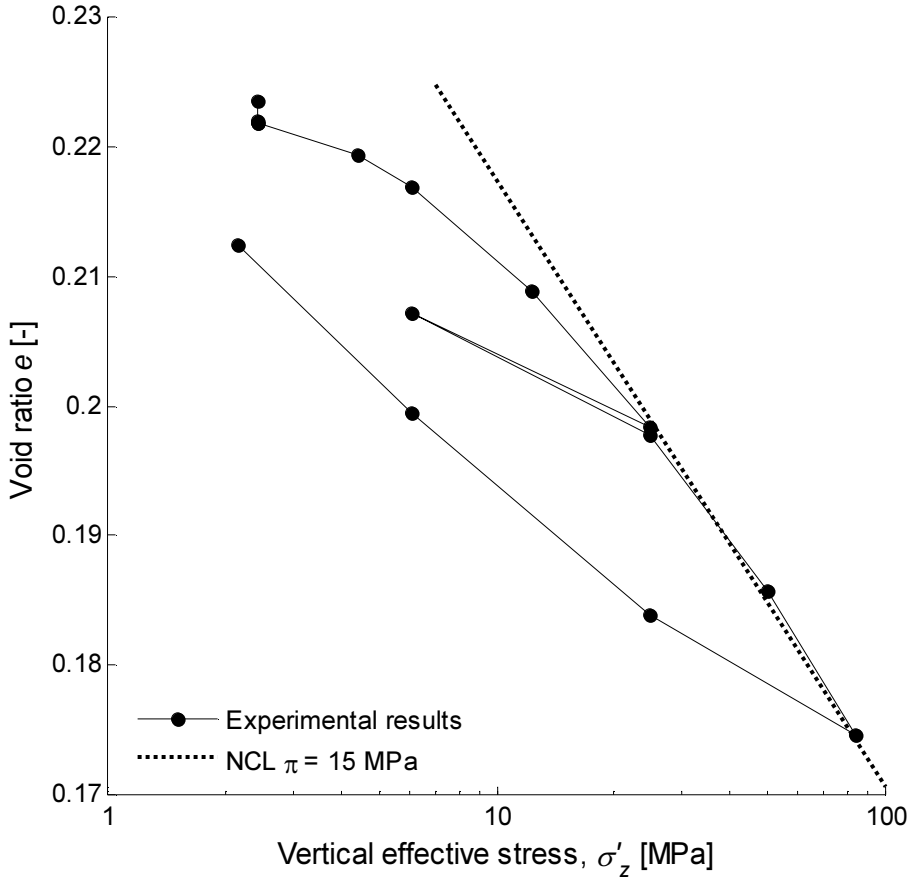

Figure 4.16: Experimental NCL corresponding to π = 15 MPa

4.3.2 Energetic method

An alternative method to calculate the preconsolidation pressure is the energetic method, based on the determination of the energy necessary to deform a sample. In oedometric conditions, this energy can be calculated at any stage from the area underneath the stress-strain curve:

$$W = \int_{\sigma_{v1}}^{\sigma_{v2}} \sigma_v d\varepsilon_v$$

To compute the vertical strain the following equation is used:

$$\varepsilon_v = \frac{\Delta V}{V_0} = \frac{\Delta H}{H_0} = \frac{\Delta e}{1 + e_0}$$

where e_0 is the starting void ratio corresponding to an absence of strains.

The so-calculated cumulative work can be plotted against stress, as showed in figure 4.17: the preconsolidation pressure is determined as the vertical component of the intersection of the tangents to the initial and final part of the curve. The intersection also identifies the corresponding work value, easily convertible in strains and then in void ratio.

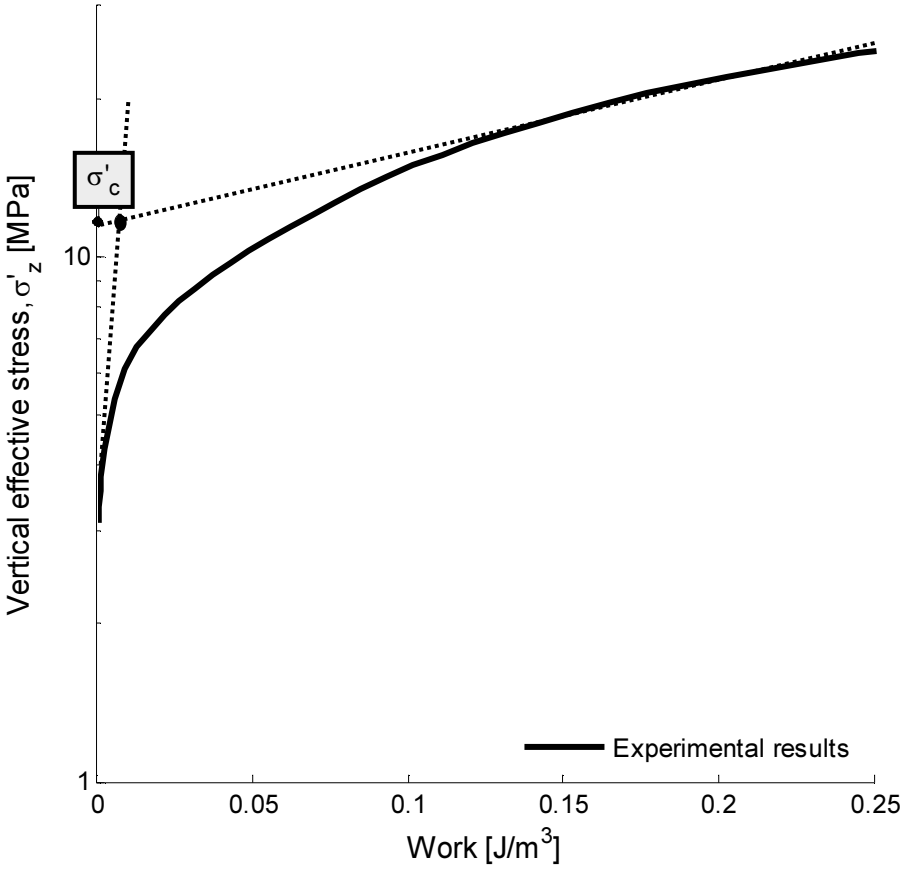

Figure 4.17: Energetic method

4.3.3 Comparison of the results

In the following table 4.1 the results obtained with the two methods are presented. In test 3 the determination of the vertical effective yield stress with the energetic method is not practicable because of the change of osmotic suction in proximity of the beginning of the plasticisation.

Test	σ'c [MPa]		e0	e [-]		π [MPa]
	Casagrande Method	Energetic Method		Casagrande Method	Energetic Method	
1	10.07	11.90	0.223	0.221	0.222	1
2	3.61	2.35	0.248	0.241	0.243	1
3	10.56		0.220	0.219		1
4	14.17	8.97	0.215	0.213	0.213	1
5	10.91	11.11	0.222	0.216	0.218	15
6/ π = 1MPa	6.02	7.98	0.239	0.230	0.235	1
6/ π = 15MPa	14.38	25.80	0.215	0.211	0.211	15

Table 4.1: The two methods results

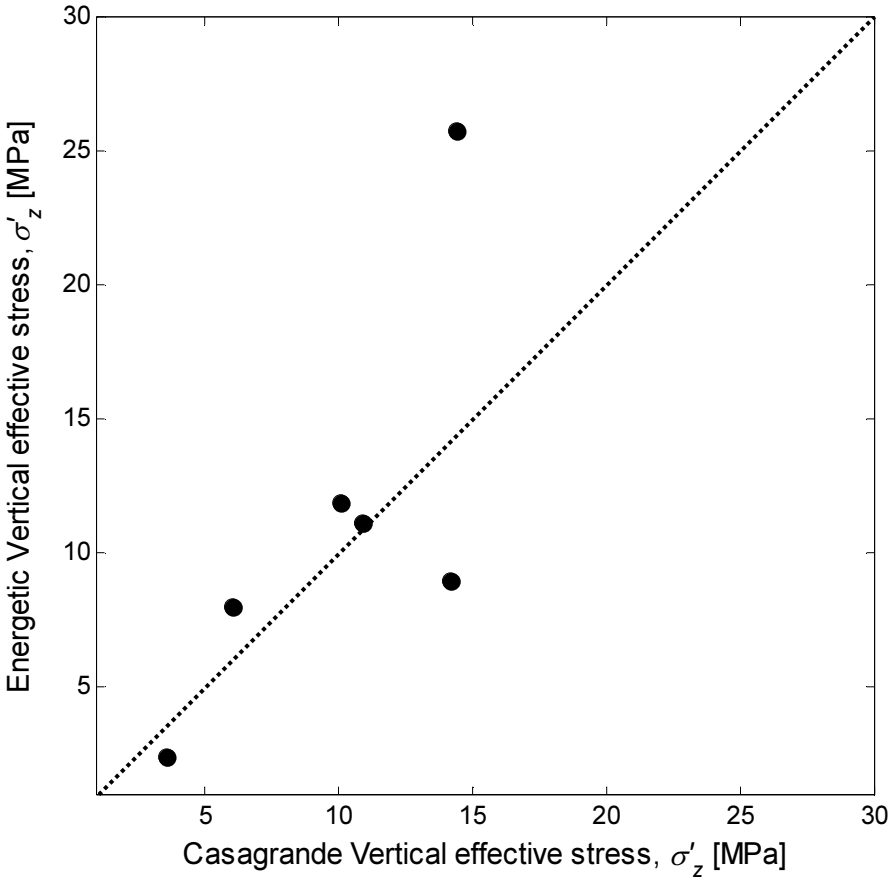

Figure 4.18: Comparison of Casagrande Method and Energetic Method

A visual comparison of the results is reported in figure 4.18: the preconsolidation pressures determined with the two methods are similar except for the one calculated in test 6 after the increase of osmotic suction.

In figure 4.19 the vertical effective yield stress are reported in a semi-logarithmic graph with the corresponding void ratio values. The points determined with Casagrande's graphic method are aligned following the two "experimental" Normal Compression Lines (π = 1 MPa and π = 15 MPa), while the Energetic method points don't possess this feature but have a similar behaviour.

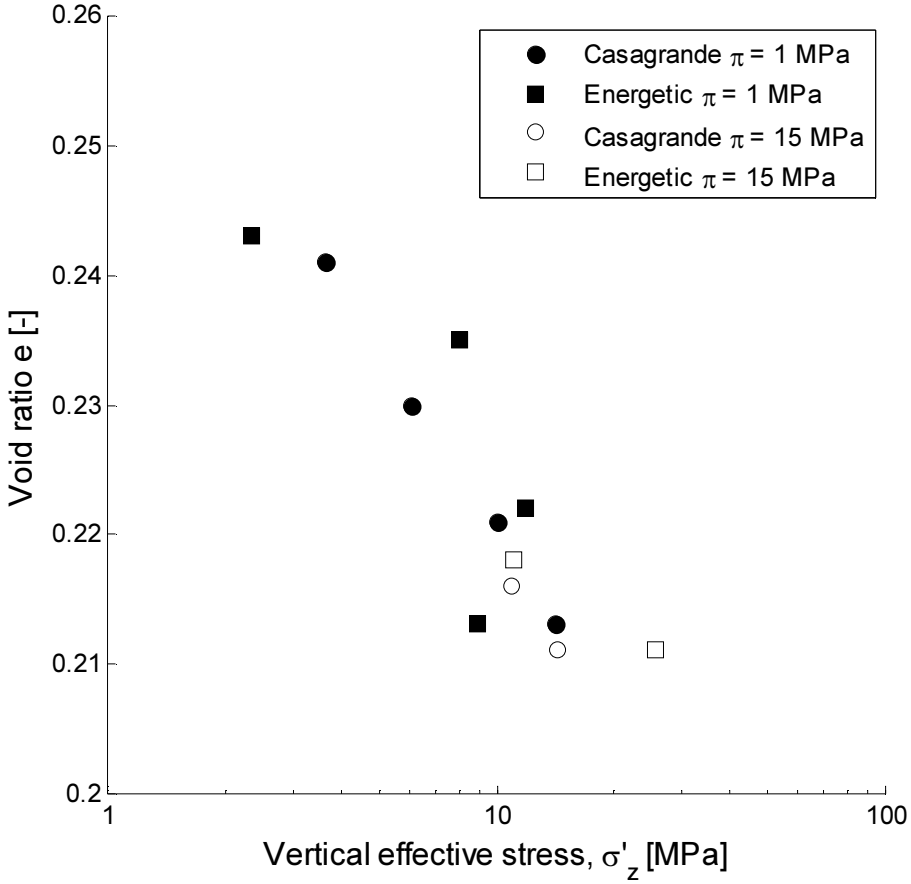

Figure 4.19: Comparison of Casagrande Method and Energetic Method

4.4 Analysis of the experimental results

Other comments can be made starting from the experimental results.

4.4.1 Determination of γ_π

γ_π is the material parameter introduced in the ACMEG model defining the variation of the yield limit with respect to the osmotic suction. In chapter 3 it was introduced in the preconsolidation pressure equation expressed in terms of mean effective yield stress:

$$p'_c = p'_{c0} exp(\beta \varepsilon_v^p) \left(1 - \gamma_\pi \log \frac{\pi}{\pi_0}\right)$$

being p'_{c0} the preconsolidation stress at a reference osmotic suction π_0, β the plastic compressibility, ε_v^p the total plastic volumetric strain, and π the current osmotic suction.

The available experimental data are expressed in terms of vertical effective stress σ'_v (or σ'_z, being z the vertical axis) and not in terms of mean stress p': it is assumed that the functions for the vertical effective yield stress and the mean effective yield stress are of the

same form. Consequently the parameter γ_π can be calculated referring to the following law for the evolution of the yield limit stress with respect to the osmotic suction of pore water:

$$\sigma_c = \left(1 - \gamma_\pi \log \frac{\pi}{\pi_0}\right) \sigma_{c0}$$

being as usual σ_{c0} the vertical yield stress at π_0.

The vertical effective yield stress depends on the void ratio e and on the osmotic suction π: to estimate γ_π it is necessary to refer to a constant void ratio.

The choice is to assume the preconsolidation pressures calculated with Casagrande's graphic method, the classical method used in geotechnical procedures, because of a more regular disposition. As explained in the 4.3.1 paragraph, two different "experimental" Normal Compression Lines corresponding to two different osmotic suction values (π = 1 MPa and π = 15 MPa) have been assumed to develop the method; the lines are experimentally observed to be parallel. An equation can be associated to each one:

$$\text{NCL at } \pi = 1 \text{ MPa:} \quad e = 0.267 - 0.047 \log \sigma'_z$$

$$\text{NCL at } \pi = 15 \text{ MPa:} \quad e = 0.2645 - 0.047 \log \sigma'_z$$

Consequently, assuming a given void ratio, the vertical effective yield stress is immediately determined. For $e = 0.21$ the two equations give:

$$\pi = 1 \text{ MPa: } \sigma'_c = 16.32 \text{ MPa}$$

$$\pi = 15 \text{ MPa: } \sigma'_c = 14.44 \text{ MPa}$$

γ_π can easily be estimated from the equation:

$$\gamma_\pi = \frac{1 - \frac{\sigma'_c}{\sigma_{c0}}}{\log \frac{\pi}{\pi_0}}$$

where σ_{c0} is the vertical effective yield stress corresponding to the chosen reference osmotic suction π_0 of 1 MPa. Substituting the presented values it yields:

$$\gamma_\pi = 0.098$$

The graph reported in figure 4.20 shows the vertical effective yield stress variation with osmotic suction and void ratio; an "artificial" point characterized by a squared marker is added to better illustrate the osmotic suction impact. The black line represents the equation for the evolution of the yield limit stress with respect to the osmotic suction corresponding to $e = 0.216$ and $\gamma_\pi = 0.098$.

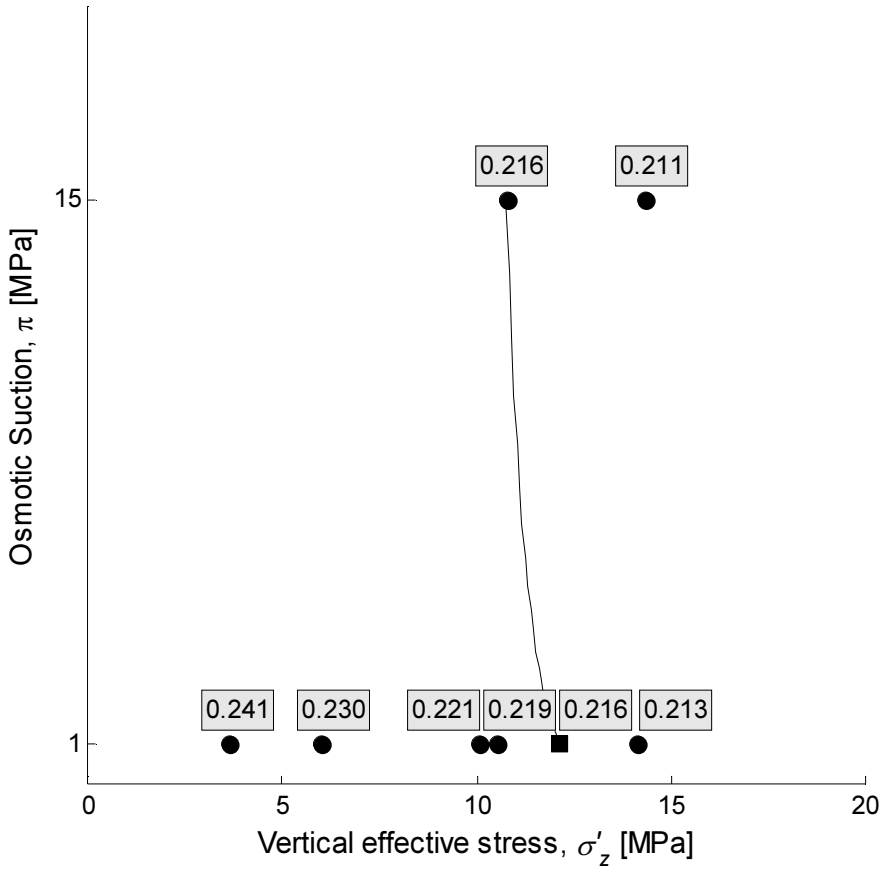

Figure 4.20: Vertical effective yield stress variation with osmotic suction

Test 6, as presented previously, has the peculiarity of a double mechanical loading at two different osmotic suction. Tracing on its oedometric curve the tangents to the elasto-plastic final part, two different Normal Compression Lines can be identify. The corresponding value of γ_π is bigger than 0.098, with a upper limit of 0.2: this characteristic will be considered for the numerical simulation of the six oedometric tests.

4.4.2 Determination of δ and γ_β

Other two parameters, δ and γ_β, can be estimated starting from the experimental results: it is indeed necessary to understand if the different values of osmotic suction influences the slope of the elastic and elasto-plastic strokes of the oedometric curves.

As observed, shales are characterised by the *damage* effect: the slope of the unloading-reloading curve depends on the maximum vertical effective stress achieved. Consequently it is necessary to refer to a constant maximum vertical effective stress $\sigma'_{z,max}$ to compare the slopes of the unloading-reloading curves at different osmotic suction values. This procedure

is possible particularly for two values, $\sigma'_{z,max} = 25$ MPa and $\sigma'_{z,max} = 90$ MPa, which are realized in a sufficient number of tests.

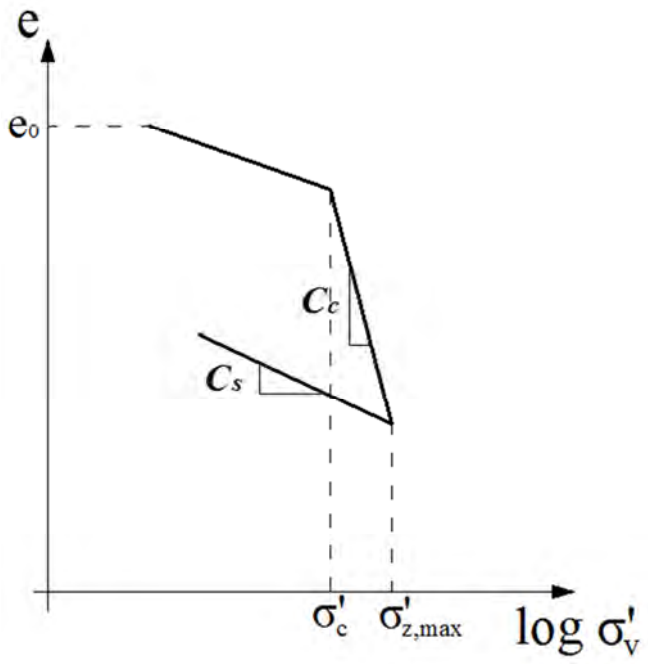

Figure 4.21: Cc and Cs

Form a practical point of view, the goal is to measure the slope C_s as presented in figure 4.21 for a constant $\sigma'_{z,max}$. The results are presented in table 4.2.

$\sigma'_{z,max}$ = 25 MPa			$\sigma'_{z,max}$= 90 MPa		
Test	**π [MPa]**	**Cs**	**Test**	**π [MPa]**	**Cs**
1	1	0.018	1	1	0.023
2	1	0.016	4	15	0.019
5	15	0.015	5	15	0.024
6/π = 1 MPa	1	0.014	6/π = 15 MPa	15	0.022

Table 4.2: Cs values

The following figure 4.22 is a graphical representation of table 4.2: the assumption derived from the experimental data is that there is no dependence of C_s on the osmotic suction π. Particularly the two black lines state the two medium values of the parameter: 0.016 for $\sigma'_{z,max} = 25$ MPa and 0.022 for $\sigma'_{z,max} = 90$ MPa.

C_s is the slope of the oedometric curve in the elastic domain: its value can be linked to the bulk modulus K if some hypothesis which will be presented in the following chapter are verified. The bulk modulus K dependence on osmotic suction in ACMEG-C model is, as previously presented:

$$K_{ref} = K_{ref,0}\left(\frac{\pi}{\pi_0}\right)^{-\delta}$$

Consequently, if no dependence of C_s on osmotic suction is registered, it can be assumed:

$$\delta = 0$$

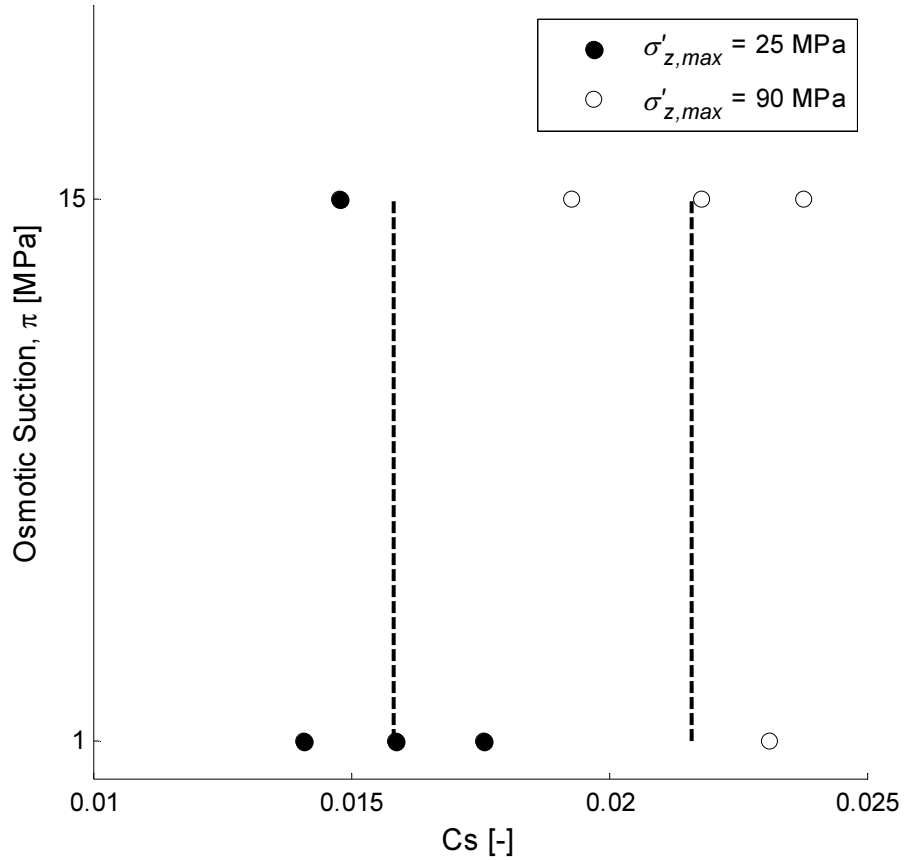

Figure 4.22: C*s* variation with osmotic suction

C_c is the slope of the "experimental" Normal Compression Line, which has been assumed independent from osmotic suction. As C_s is linked to the bulk modulus K, C_c is linked to the plastic modulus β, whose dependence on osmotic suction in ACMEG-C model is as follows:

$$\beta = \beta_0\left(1 + \gamma_\beta \log\frac{\pi}{\pi_0}\right)$$

Being β independent from osmotic suction in this assumption, it can be assumed:

$$\gamma_\beta = 0$$

Consequently in this application osmotic suction has an impact only in the evolution of the preconsolidation pressure and of the elastic domain.

5. Numerical simulations

In this chapter the numerical simulations of the oedometric tests' results will be presented. The determination of the parameters of the model requests adjunctive assumptions and an initial calibration of the model referring to two tests.

5.1 Model parameters

5.1.1 Friction angle assumption and consequences

One of the difference between the experimental results and the numerical model is that the last one is expressed in terms of mean stress *p'* and not in terms of vertical effective stress σ'_z. The input parameters such as the initial stress state and the initial preconsolidation pressure must be converted. In order to answer this point, Jaky's equations for normally consolidated soils (NC) and for overconsolidated soils (OC) are assumed (*J. Jaky, 1948*):

$$K_{0,NC} = 1 - \sin\phi'$$

$$K_{0,OC} = K_{0,NC} \cdot OCR^{\phi'}$$

where OCR is the overconsolidation ratio and ϕ' is the friction angle. The parameter K_0 allows to determine the lateral stress using the following equation:

$$\sigma'_h = K_0 \sigma'_v$$

The mean stress *p'* in oedometric conditions is:

$$p' = \frac{\sigma'_1 + 2\sigma'_3}{3} = \frac{\sigma'_v + 2\sigma'_h}{3}$$

Combining the two equations it yields:

$$p' = \left(\frac{1 + 2K_0}{3}\right)\sigma'_v$$

The fundamental parameter of this theory is the friction angle ϕ': it is assumed

$$\phi' = 25°$$

An identical value is assumed for Opalinus Clay in *"The mechanical behaviour of weak mudstone (Opalinus Clay) at low stresses"* by *A.G.Corkum* and *C.D.Martin* [*Corkum et al.*, 2006]. The consequence is that it can be assumed:

$$K_{0,NC} = 0.577$$

If this theory is assumed, a linear dependence of the mean stress *p'* with respect to the vertical mechanical stress σ'_z is admitted. Therefore with these hypothesis the material parameter γ_π, calculated as

$$\gamma_\pi = \frac{1 - \frac{\sigma'_c}{\sigma_{c0}}}{\log \frac{\pi}{\pi_0}}$$

is the same referring to mean stress instead of the vertical mechanical stress, as previously assumed. If the natural logarithm is used instead of the logarithm to the base 10, the value of γ_π must be divided by ln 10.

Another consequence is that with these assumptions the slopes C_c, C_s are related respectively to the *compression index* λ and to the *swelling index k*. It can be proved that:

$$k = \frac{C_s}{\ln 10}$$

$$\lambda = \frac{C_c}{\ln 10}$$

5.1.2 Parameters required for the model

In this paragraph all the parameters required for the numerical simulation will be presented.

$K_{ref,0}$

$K_{ref,0}$ is the bulk modulus at a reference osmotic suction π_0 (in this case $\pi_0 = 1$MPa). Starting from the Normal Compression Line expression, the assumptions of the last paragraph and the bulk modulus definition, it can be derived:

$$K_{ref,0} = 2.303 \frac{1 + e_0}{C_{s0}} p'_{ref}$$

where e_0 is the starting void ratio corresponding to the undeformed state, C_{s0} is the slope of the oedometric curve in the elastic domain at the reference osmotic suction π_0 (an independence of this value with respect of osmotic suction is assumed) and p'_{ref} is the reference mean stress equal to 1 MPa. A linear dependence of the bulk modulus on the mean stress is admitted with this assumption.

G_{ref}

Combining the oedometric conditions and Jaky's equation, after some substitutions:

$$G_{ref} = \frac{3K_{ref,0}(1 - K_0)}{2 + 4K_0}$$

The reference shear modulus, being dependent on the reference bulk modulus, has a linear dependence on the mean stress.

n^e

This parameter permits the introduction of a non-linear dependence of the bulk modulus and the shear modulus on the mean stress:

$$K = K_{ref}\left(p'/p'_{ref}\right)^{n_e}$$

$$G = G_{ref}\left(p'/p'_{ref}\right)^{n_e}$$

In agreement with the last assumptions:

$$n^e = 1$$

β_0

The plastic modulus is assumed independent from the osmotic suction, so β is constant. The evolution of the mean effective yield stress with the plastic component of the volumetric strain is controlled by this parameter:

$$p'_c = p'_{c0} exp(\beta \varepsilon_v^p)$$

Coherently with the assumptions for the bulk modulus and the shear modulus, it can be determined as:

$$\beta_0 = 2.303 \frac{1 + e_0}{C_c - C_{s0}}$$

where C_c is the compression index.

α

α is an additional parameter introduced in order to catch the various volumetric responses:

$$\frac{d\varepsilon_v^p}{d\varepsilon_d^p} = \alpha \left(M - \frac{q}{p'}\right)$$

a

It is a material parameter which controls the evolution of the degree of mobilization of the deviatoric plastic mechanism r_{dev}:

$$r_{dev} = r_{dev}^{e} + \frac{\varepsilon_d^p}{a + \varepsilon_d^p}$$

$$dr_{dev} = \frac{(1 - {r_{dev}}^2)}{a} d\varepsilon_d^p$$

b

b is a material parameter defining the shape of the deviatoric yield limit:

$$f_{dev} = q - Mp' \left(1 - b \ln \frac{dp'}{{p'}_c}\right) r_{dev} = 0$$

c

c controls the evolution of the degree of mobilization of the isotropic plastic mechanism:

$$r_{iso} = r_{iso}^{e} + \frac{\varepsilon_v^{p,iso}}{c + \varepsilon_v^{p,iso}}$$

$$dr_{iso} = \frac{(1 - {r_{iso}}^2)}{c} d\varepsilon_v^{p,iso}$$

d

d is a material parameter accounting for the ratio between the preconsolidation pressure ${p'}_c$ and the critical pressure ${p'}_{cr}$:

$$d = \frac{{p'}_c}{{p'}_{cr}}$$

d is equal to 2.718 and 2 respectively in the Original Cam-Clay model and in the Modified Cam-Clay model.

ϕ'

The friction angle ϕ' is assumed equal to 25° coherently with previous studies.

r_{iso}^{e}

It is the radius of the isotropic elastic nuclei inside which the strains are fully reversible. Until the plastic mechanism is activated the degree of mobilization of the isotropic plastic mechanism r_{iso} is equal to r_{iso}^{e}.

r_{dev}^{e}

r_{dev}^{e} is the radius of the deviatoric elastic nuclei inside which the strains are fully reversible. Until the plastic deviatoric mechanism is activated the degree of mobilization of the deviatoric plastic mechanism r_{dev} is equal to r_{dev}^{e}.

δ, γ_{β} and γ_{π}

These parameters were assumed coherently with the experimental results as explained in a previous paragraph.

5.1.3 Model parameters assumption

In the following table the parameters assumed for the numerical analysis are presented.

$K_{ref,0}$ [MPa]	390
G_{ref}[MPa]	90
n^{e}	1
ϕ'[Degrees]	25
β_0	68
α	1
a	0.01
b	1
c	0.004
d	2
r_{iso}^{e}	0.2
r_{dev}^{e}	0.5
δ	0
γ_{β}	0
γ_{π}	0.042

Table 5.1: Model parameters

The last three parameters reported in table 5.1 were determined with the experimental analysis, while $K_{ref,0}$, G_{ref} and β_0 were evaluated with the equations presented in the last

paragraph using medium values of e_0, C_{s0} and C_c. These six common parameters are therefore estimated referring to the experimental data.

n^e is equal to 1 coherently with the assumptions for $K_{ref,0}$ and G_{ref}, while $d = 2$ entails that the preconsolidation pressure p'_c is the double of the critical pressure p'_{cr}. Furthermore, $\alpha = b = 1$ implies that the flow rule is associated.

The calibration of the model has been verified with two test: test 1 and test 5. The first one does not present variation in osmotic suction and has been used to improve the simulation of the mechanical behaviour of the material, while test 5 is characterized by the initial collapse, that is the deformation due to a variation of osmotic suction. The fundamental parameters to evaluate with calibration were the two radius of the isotropic and deviatoric elastic nuclei and the material parameters *a* and *c*. Particularly, being the oedometric test characterized by an axial loading, the isotropic mechanism's parameters play the most important role.

In order to explain the chosen value for r_{iso}^e it is necessary to illustrate how the model simulates the deformations consequence of a variation of osmotic suction (the collapse). The last consideration of chapter 4 was that a change in osmotic suction, with the assumptions for this model, has an impact only on the evolution of the preconsolidation pressure and, consequently, of the elastic domain. In other words the model, coherently with the experimental observations, does not contemplate strains caused by a variation of osmotic suction within the elastic domain.

Furthermore, it is fundamental to consider that the position of the Normal Compression Line is unequivocally determined by the mean effective yield stress p'_c of the sample. Therefore, in order to activate the plastic mechanism and make the model predict the collapse, the only parameter which can be adapted is the degree of mobilization of the isotropic plastic mechanism r_{iso}. The radius of the isotropic elastic nuclei r_{iso}^e is assumed small to "anticipate" the activation of the isotropic plastic mechanism f_{iso}, while *c* is little in order to make the convergence of the degree of mobilization of the isotropic plastic mechanism r_{iso} as rapid as possible.

5.2 Modification of the response under unloading-reloading path

In the original ACMEG-C model, during unloading r_{iso} decreases to follow the decrease of effective mean pressure *p'*, while at reloading, r_{iso} is adjusted to keep a constant elastic nuclei (r_{iso}^{e}):

$$r_{iso} = r_{iso}^{e} + \frac{p'_{cyc}}{p'_{c}} + \frac{\varepsilon_{v}^{p,cyc,iso}}{c + \varepsilon_{v}^{p,cyc,iso}}$$

where p'_{cyc} is the evolving mean stress, p'_{c} is the current preconsolidation pressure and $\varepsilon_{v}^{p,cyc,iso}$ is the volumetric plastic strain produced by the isotropic mechanism since the change of direction of the solicitation.

This mechanism was implemented in the numerical analysis to repeat the experimental observations on various typologies of clay. Being small the radius of the isotropic elastic nuclei r_{iso}^{e}, this effect would be even more relevant in this case. However, as observed, for Opalinus Clay the unloading-reloading cycles at constant osmotic suction are observed to involve negligible quantities of plastic strains. In order to make the model more adherent to the experimental observations, the mechanism of reinizialization of the degree of mobilization of the isotropic plastic mechanism r_{iso} is deactivated.

5.3 Numerical simulations

In this paragraph the numerical simulations of the six oedometric tests will be presented and analysed.

5.3.1 About the preconsolidation pressure

The input mean effective yield stress for the simulations p'_{c} is not coincident with the preconsolidation pressure determined starting from the experimental data because of the model formulation. The expression of the isotropic yield limit is:

$$f_{iso} = p' - p'_{c} r_{iso}$$

The isotropic mechanism is activated when $f_{iso} = 0$: hypothesizing a unit value of the degree of mobilization of the isotropic mechanism r_{iso}, it yields:

$$p' = p'_{c}$$

r_{iso} is therefore introduced in the model to "anticipate" the activation of the plastic mechanism and to smooth the angular shape of the passage from the elastic to the elasto-plastic deformation. The consequence is that the input preconsolidation pressure p'_c is the point where the smoothed part of the curve joins the line of elasto-plastic deformation: as previously affirmed, the preconsolidation pressure unequivocally locates the Normal Compression Line. In figure 5.1 two oedometric curves differentiated only by the preconsolidation pressure are represented: the two different Normal Compression Line are easily recognisable.

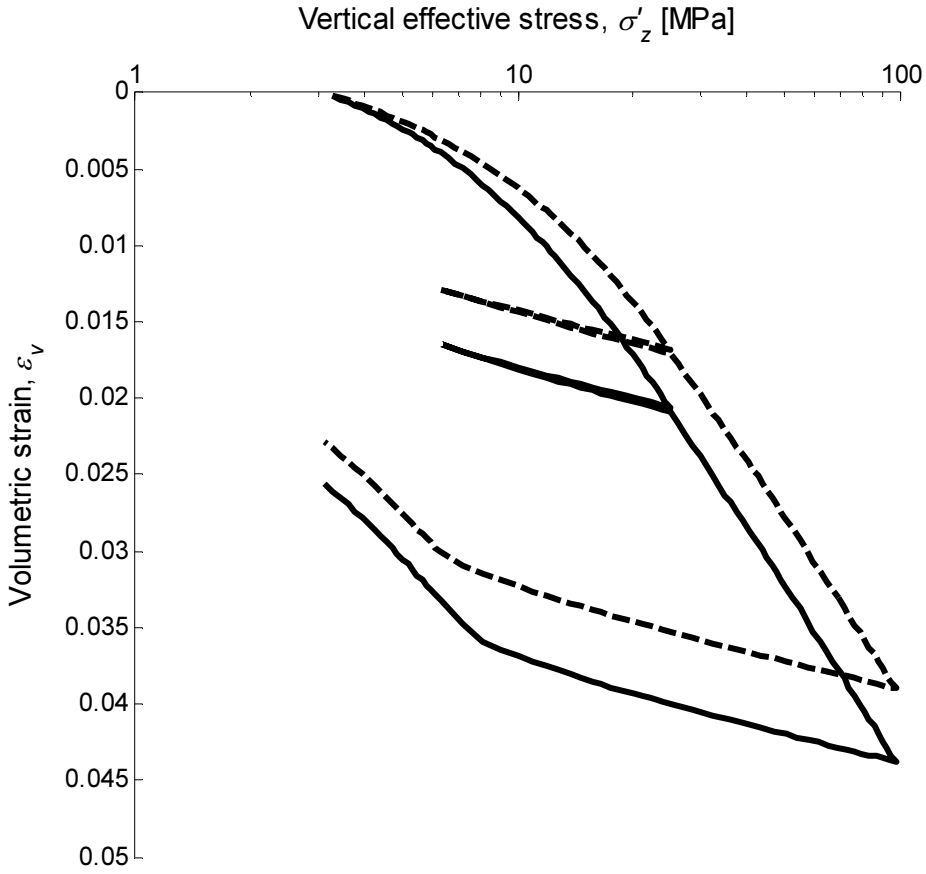

Figure 5.1: Two simulated oedometric curves differenced only by the preconsolidation pressure

It is possible to esteem this value from the experimental data: graphically, it is identified as the point where the oedometric curve is aligned with the experimental Normal Compression Line. The stress component identified with this procedure is named p'_y, obtained from the vertical mean stress σ'_y experimentally revealed converted using Jaky's theory.

Test	p'_y[MPa]
1	10.5
2	4.7
5	10.1
6	11.7

Table 5.2: p'_yvalues

Table 5.2 reports the obtained results: only for four tests this operation is practicable, while the other two tests' stress paths, characterized by a variation of osmotic suction after an initial mechanical loading, do not allow the fulfilment of this calculation. In this case the mean effective yield stress is a variable to evaluate after a calibration.

Being the parameter *d* assumed equal to 2, the final input mean effective yield stress is equal to $\frac{p'_y}{2}$.

Test	p'_c[MPa]
1	4.8
2	1.5
3	5.8
4	8.6
5	4.8
6	2.5

Table 5.3: p'_cvalues

Table 5.3 resumes the input mean effective yield stress p'_c used for the simulations of the six oedometric tests. Test 3 and test 4 values were determined with a calibration, while the others were changed with respect to the experimental results. This variation was limited for test 1, test 2 and test 5 but relevant for test 6, because of the will to make the whole simulation more realistic.

5.3.2 Numerical simulations and analysis

The initial stress conditions of the simulations are:

$$\sigma'_{x,i} = \sigma'_{y,i} = \sigma'_{z,i}$$

This situation corresponds to a unit value of the coefficient K_0 and is the more adherent to the experimental conditions.

Test 1

This test has been used with test 5 to calibrate the model. In figure 5.2 the stress path of the test is reported with the initial and final position of the yield curve determined with the assumed radius of the isotropic elastic nuclei, while the simulation of the oedometric test is represented in figure 5.3. As observed, the simulated strain at the end of the mechanical unloading is quite different from the experimental one because of the damage effect. The difference in the prediction of the maximum volumetric strain is equal to 7%.

Test 2

Test 2 has a stress path similar to test 1 (figure 5.4), being characterized from the same constant osmotic suction of 1 MPa. However, differently from test 1, the initial void ratio is greater and the stress values are smaller. In this case, the difference in the prediction of the maximum volumetric strain is equal to 8%.

Test 3

Test 3 is characterized by a variation in osmotic suction from 1 MPa to 0.5 MPa after an initial mechanical loading (figure 5.6). The two unloading paths reveal a relevant difference between the simulated strain and the experimental strain, while the model well predicts the maximum volumetric deformation (figure 5.7).

Test 4

In this test after, an initial mechanical loading, the stress paths presents a variation in osmotic suction from 1 MPa to 15 MPa which causes a deformation of 75‰ (figure 5.9). The numerical simulation gives a great prediction of this strain, being the difference between the simulated and the experimental value equal only to 3%. An even better prediction regards the maximum volumetric strain (0.6%). In general the simulation of this test is adherent to the experimental results, except for the unloading-reloading paths because of the damage effect.

Test 5

Test 5 has a particular path in its first steps (figure 5.10): an initial increase of osmotic suction from 1 MPa to 15 MPa is followed by decrease from 15 MPa to 1 MPa and by another chemical loading to 15 MPa. The experimental answer to this path is an initial deformation corresponding to the first stress paths and then an approximately constant void ratio. The model has a similar behaviour: the reason is that during the first step there is a

reduction of the preconsolidation pressure and a consequent deformation (the elastic domain's dimensions does not change because of the increase of the degree of mobilization of the isotropic yield limit). Then a change of osmotic suction within the elastic domain does not cause any deformation, as observed. However, the simulated initial collapse is smaller than the experimental one for the 89%: this value could be improved with a greater value of γ_π. The maximum deformation is almost identical to the experimental one.

Test 6

The initial elastic strain of this test is really similar to the measured one, while the elasto-plastic deformations are greater than the experimental values. This oedometric test is characterized by the variation of osmotic suction at the end of the unloading path: after the increase of osmotic suction the yield limit becomes smaller and the start of the elasto-plastic behaviour during reloading is anticipated (figure 5.13). Also in this case the simulation well predicts the maximum observed strain of the oedometric curve (difference equal to 0.8%).

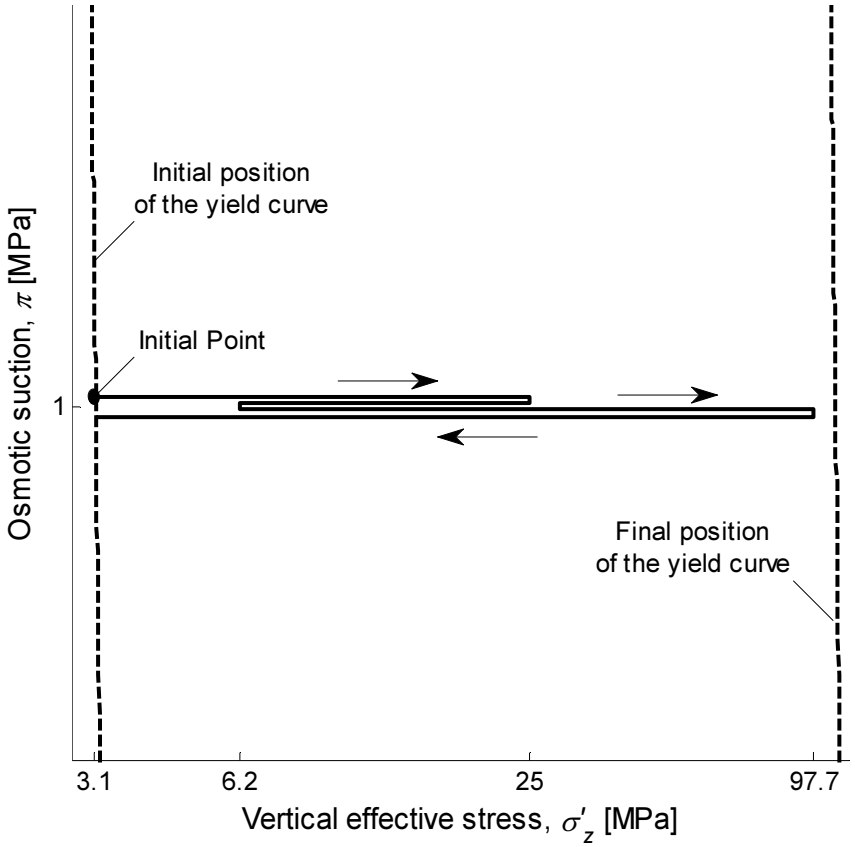

Figure 5.2: Stress Path 1 with yield curves

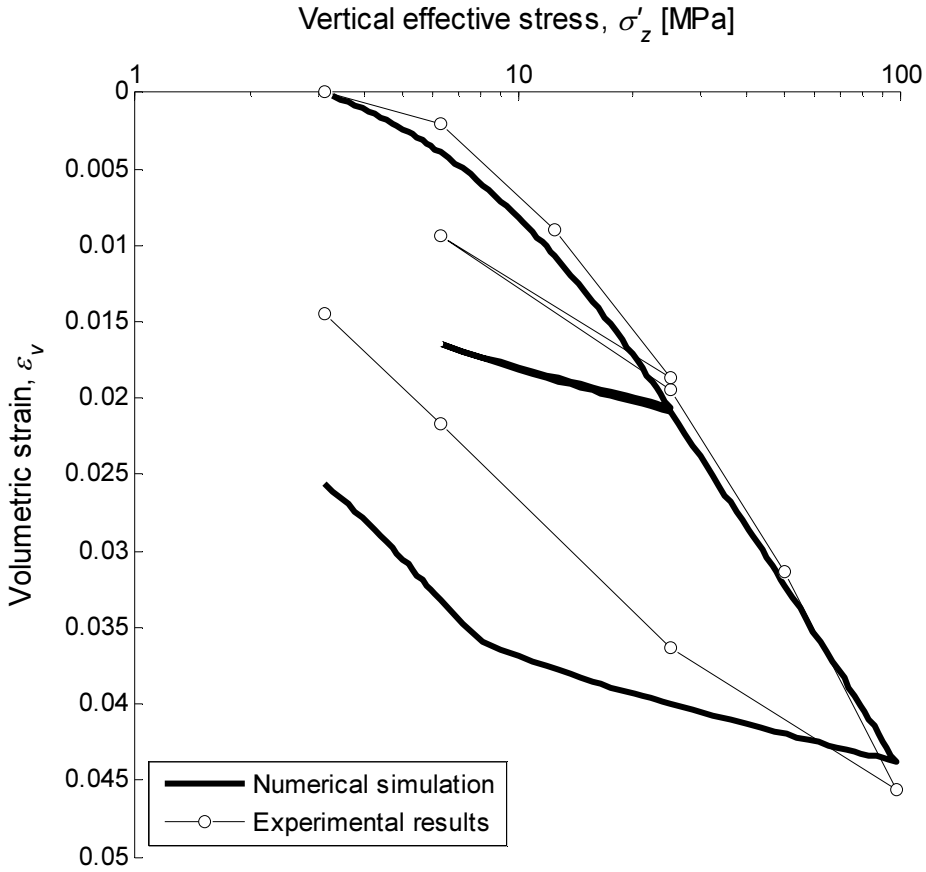

Figure 5.3: Simulation of the oedometric curve of test 1

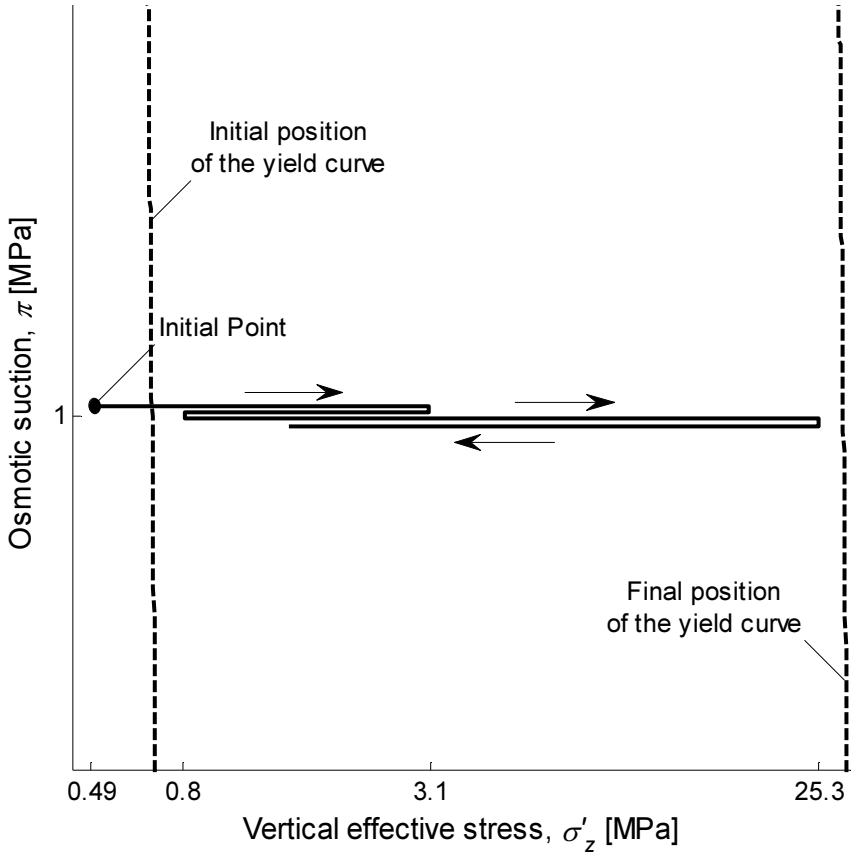

Figure 5.4: Stress Path 2 with yield curves

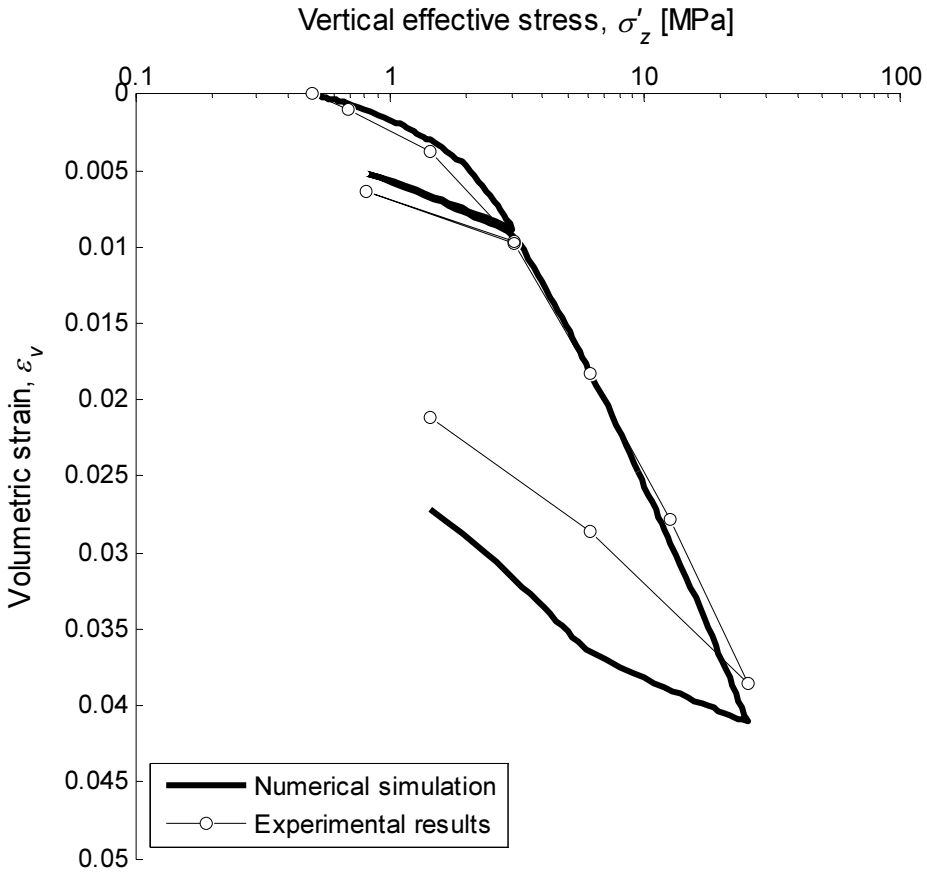

Figure 5.5: Simulation of the oedometric curve of test 2

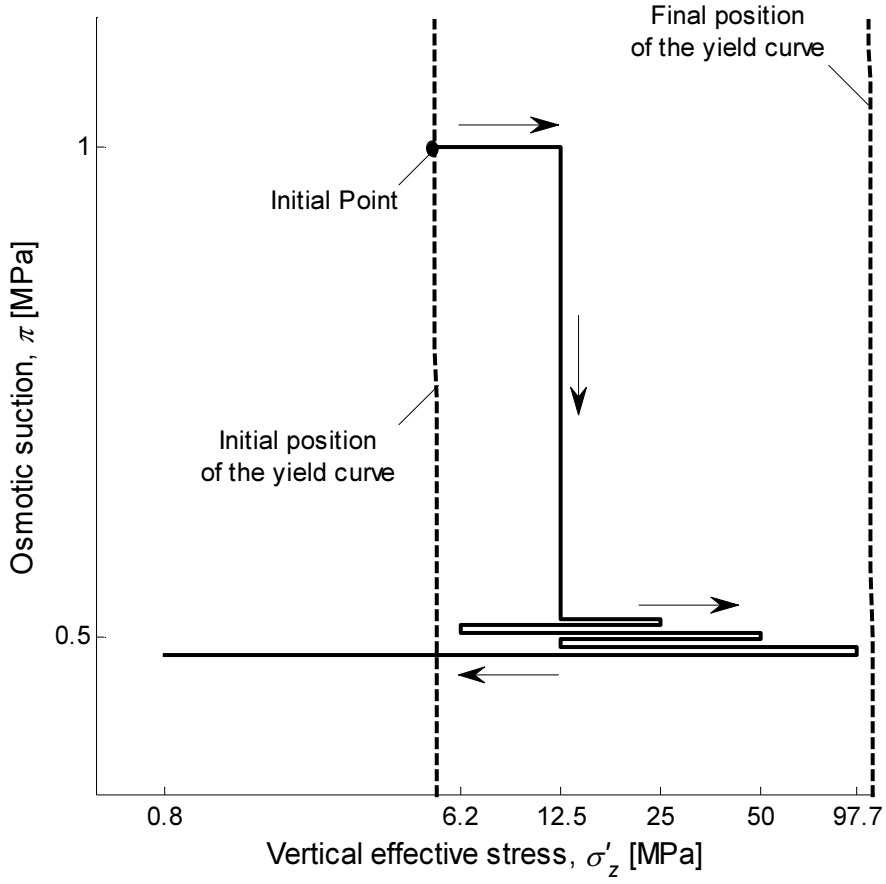

Figure 5.6: Stress Path 3 with yield curves

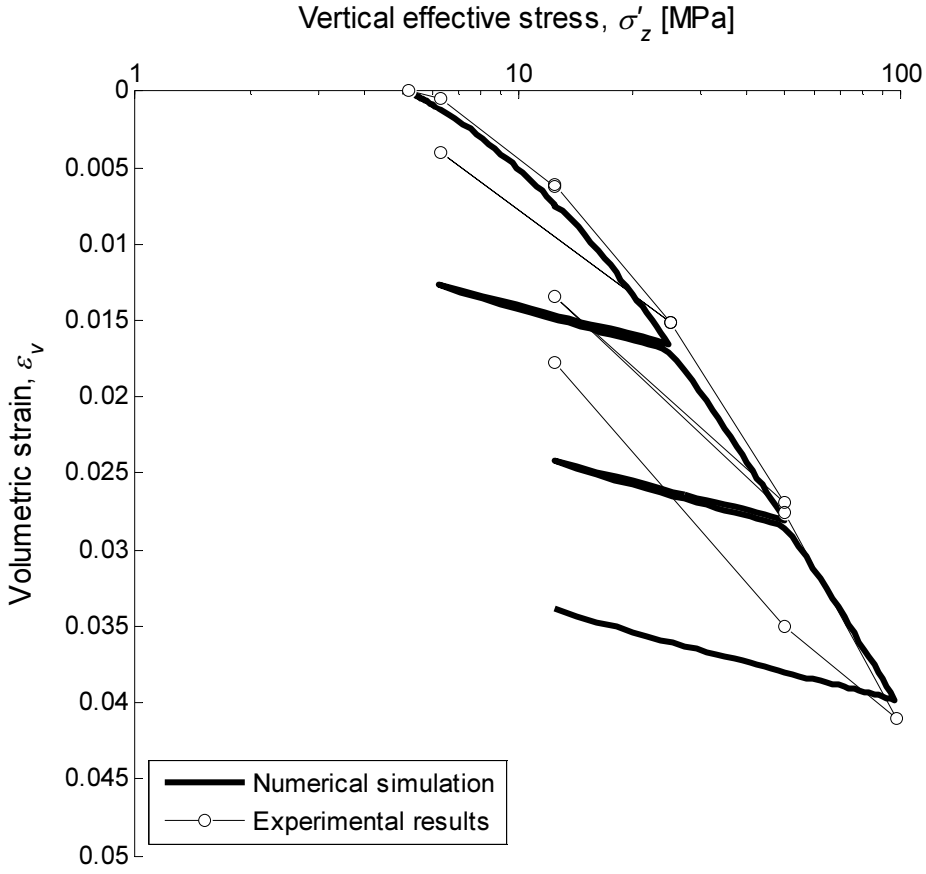

Figure 5.7: Simulation of the oedometric curve of test 3

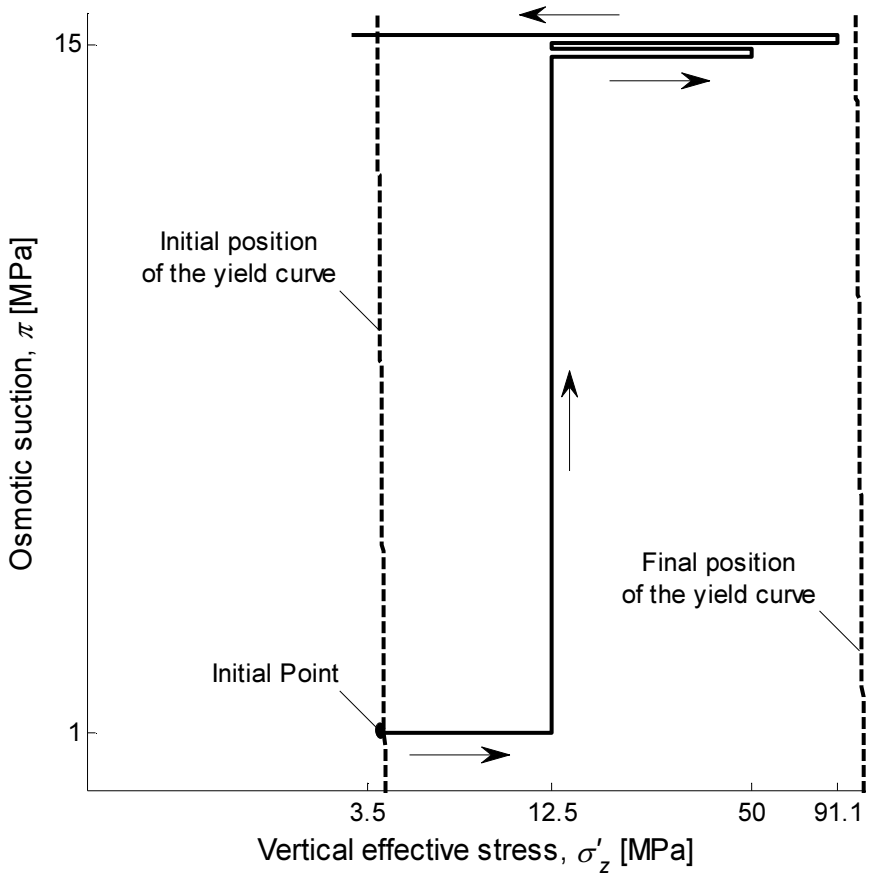

Figure 5.8: Stress Path 4 with yield curves

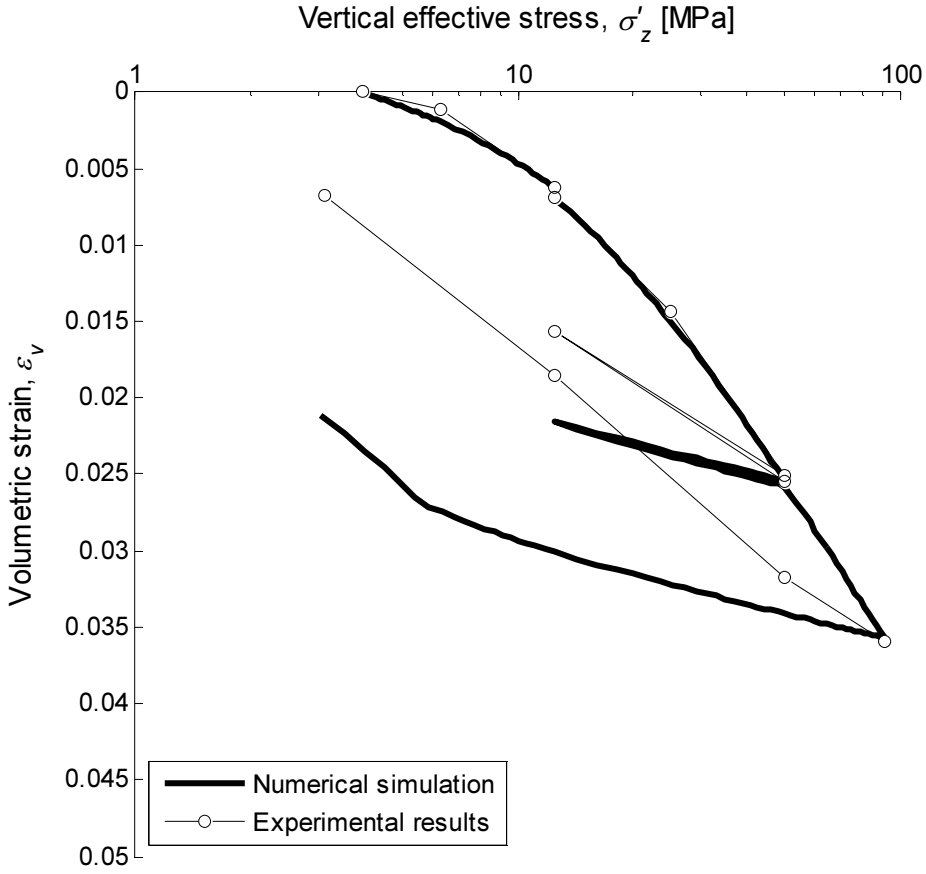

Figure 5.9: Simulation of the oedometric curve of test 4

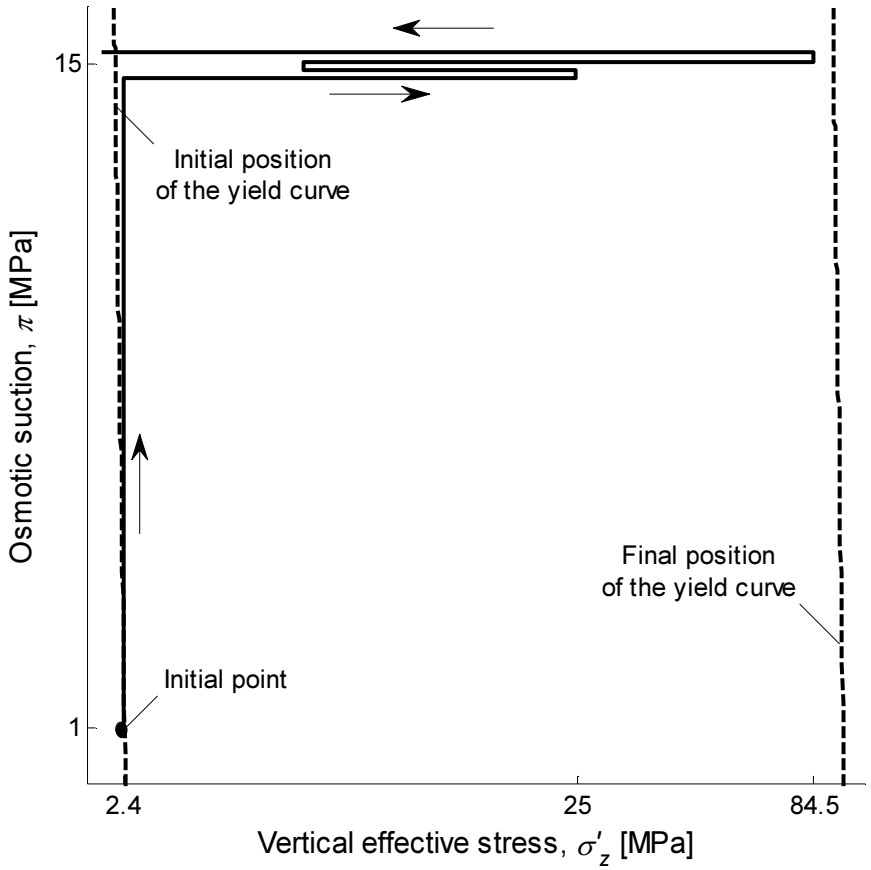

Figure 5.10: Stress Path 5 with yield curves

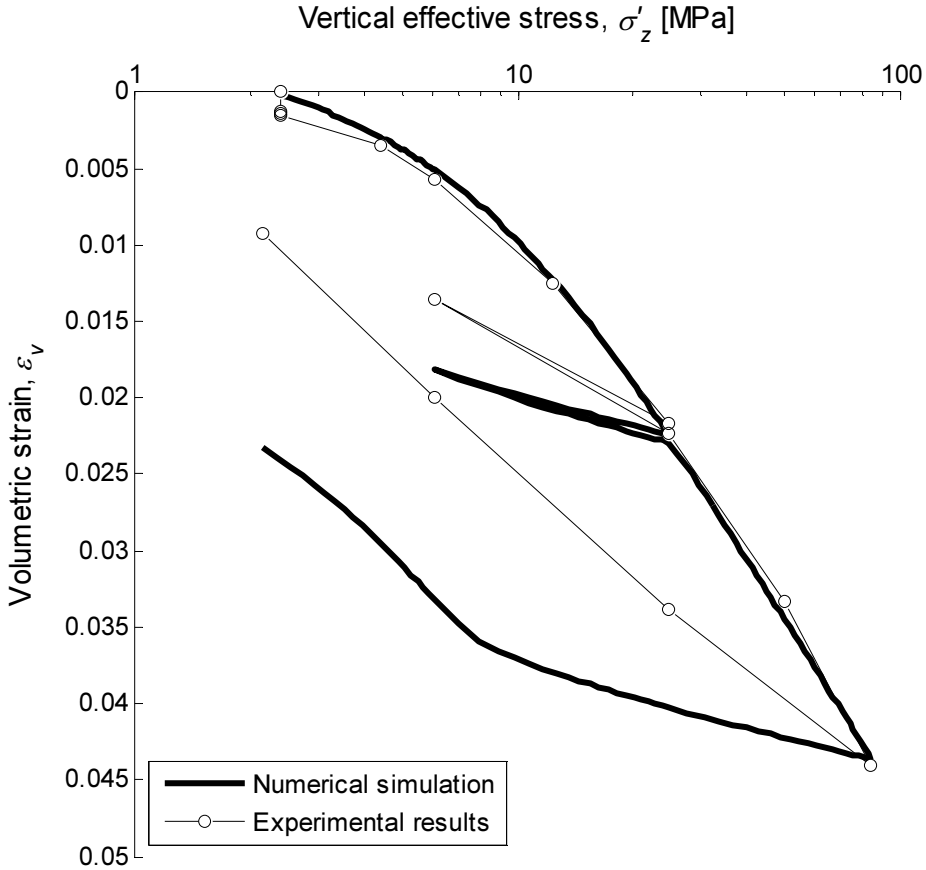

Figure 5.2: Simulation of the oedometric curve of test 5

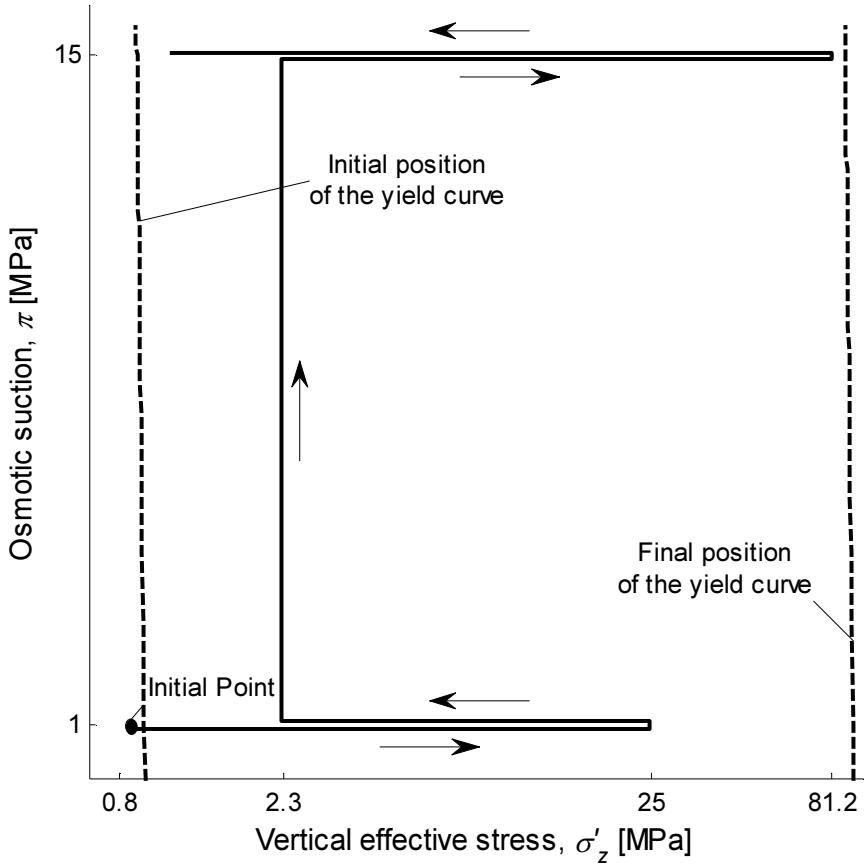

Figure 5.3: Stress Path 6 with yield curves

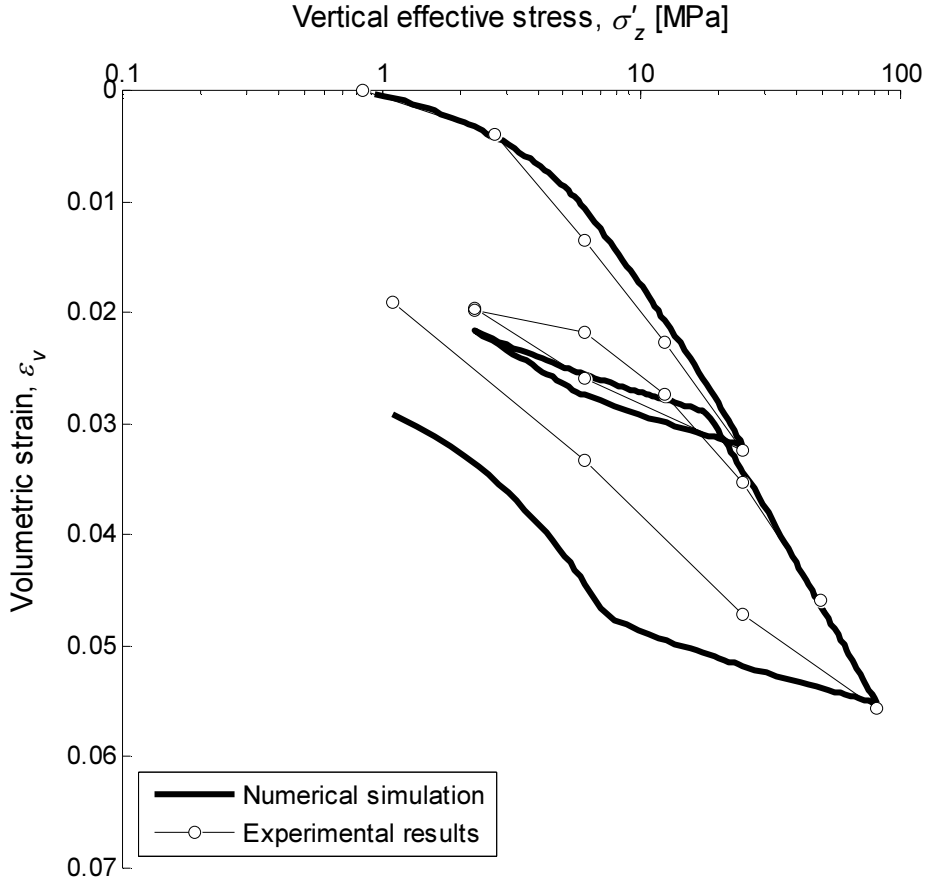

Figure 5.4: Simulation of the oedometric curve of test 6

5.3.3 Observations

Five of the six numerical simulations present a common characteristic: a sudden change of the slope of the final mechanical unloading (for instance fig. 5.11). After an initial elastic behaviour governed by the bulk modulus *K*, whose slope is identical to the former unloading-reloading path, the incline suddenly increases with no apparent explanation. This behaviour is in fact not observed in the experimental data, whose final unloading points are approximately aligned.

The cause of this behaviour is showed in figure 5.14: initially the unloading takes place within the elastic domain but in its final part the deviatoric plastic mechanism is activated. The consequence is a decrease of the dimensions of the elastic domain because of the decrease of the preconsolidation pressure p'_c in order to respect Prager's condition of consistency.

It is necessary to highlight that this particular behaviour is only an artificial consequence of the model's assumption which does not have any correspondence in experimental observations.

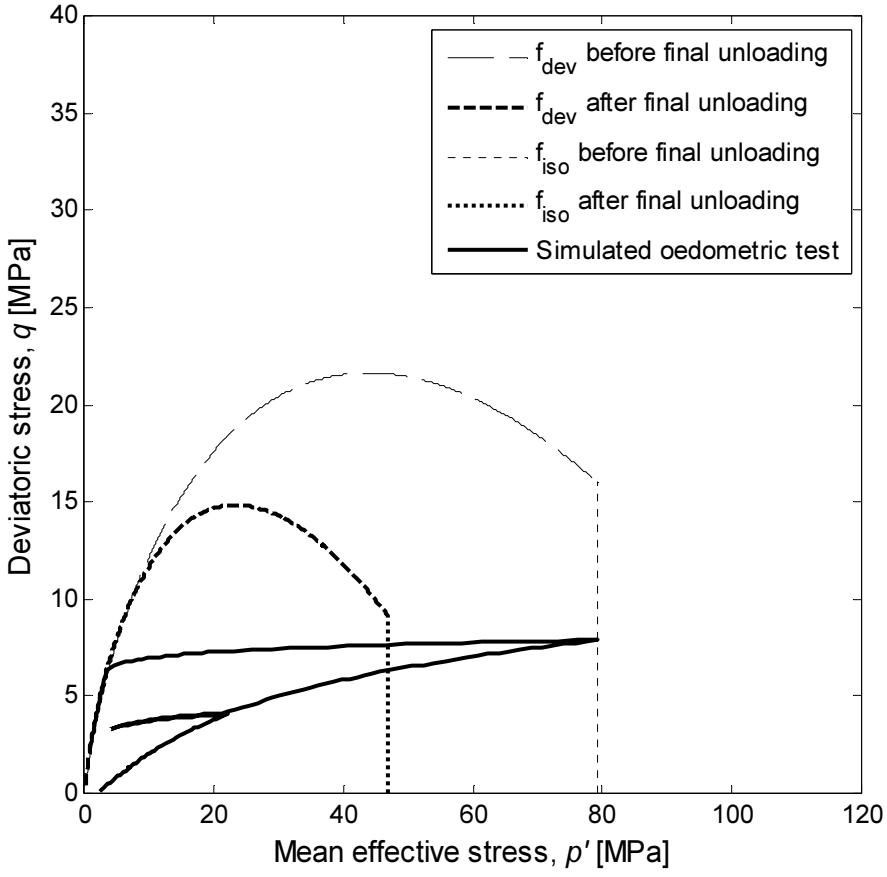

Figure 5.5: Simulated oedometric curve in the p'-q graph

5.4 *Sensitivity analysis*

A sensitivity analysis for the model has been performed with the aim of highlight the different role of the parameters in the simulations of the oedometric curves. This procedure regarded only a fraction of the model's parameters, because of the univocity of the choice of some of them. Moreover, this analysis considers one parameter at a time, even if some parameters are linked each other as, for instance, $K_{ref,0}$ and G_{ref}. For each parameter analysis the most convenient test in terms of impact of the parameter was used and the range of variation was chosen wide enough to provide a visible difference between the simulated results.

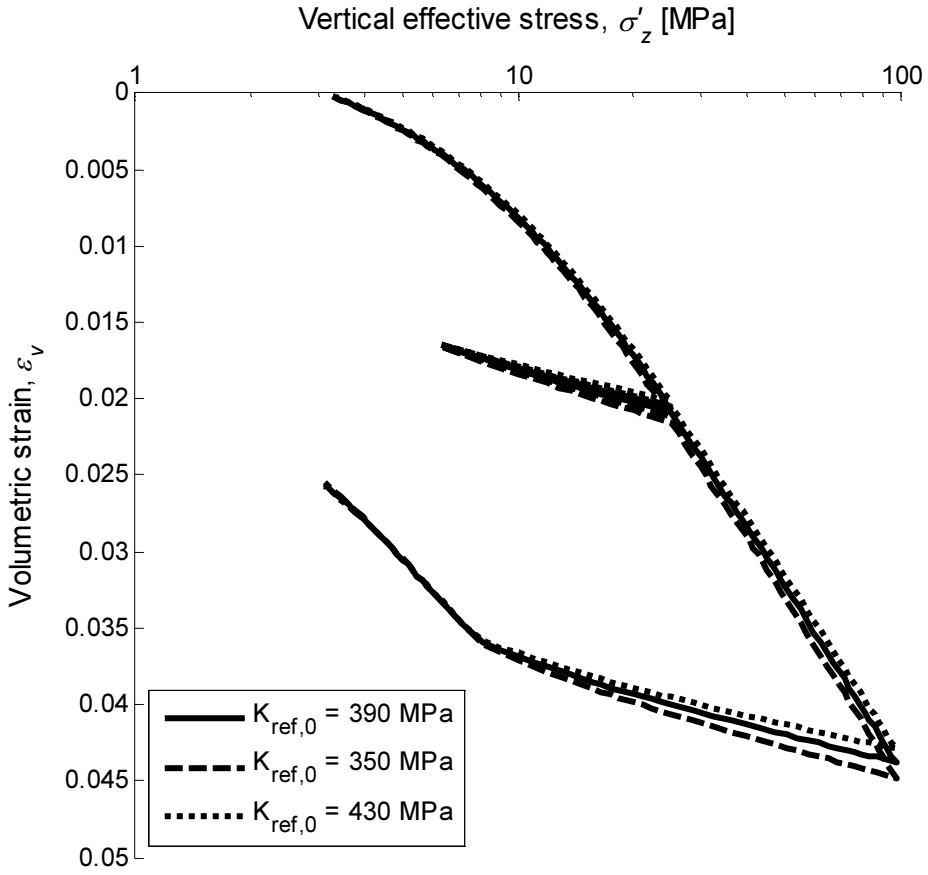

Figure 5.15: Test 1 with different $K_{ref,0}$ values

5.4.1 $K_{ref,0}$

$K_{ref,0}$ is the reference bulk modulus K_{ref} at the reference osmotic suction π_0, equal to 1 MPa in this work. Its influence is related only to the elastic component of the deformation: a different bulk modulus cause greater or smaller initial strains (before the activation of the plastic mechanism) and a transfer of the whole curve. Also the unloading-reloading paths

have different slopes depending on K_{ref} value. In figure 5.15, being short the initial elastic deformation, a change of this parameter has limited consequences on the simulation results.

5.4.2 G_{ref}

A variation of the reference shear modulus is not expected to have important consequences on the simulated results: this parameter controls only the deviatoric strains, which are not relevant in these tests. This deduction is confirmed by figure 5.16: only the final part of the simulated oedometric curve is influenced by a variation of the shear modulus.

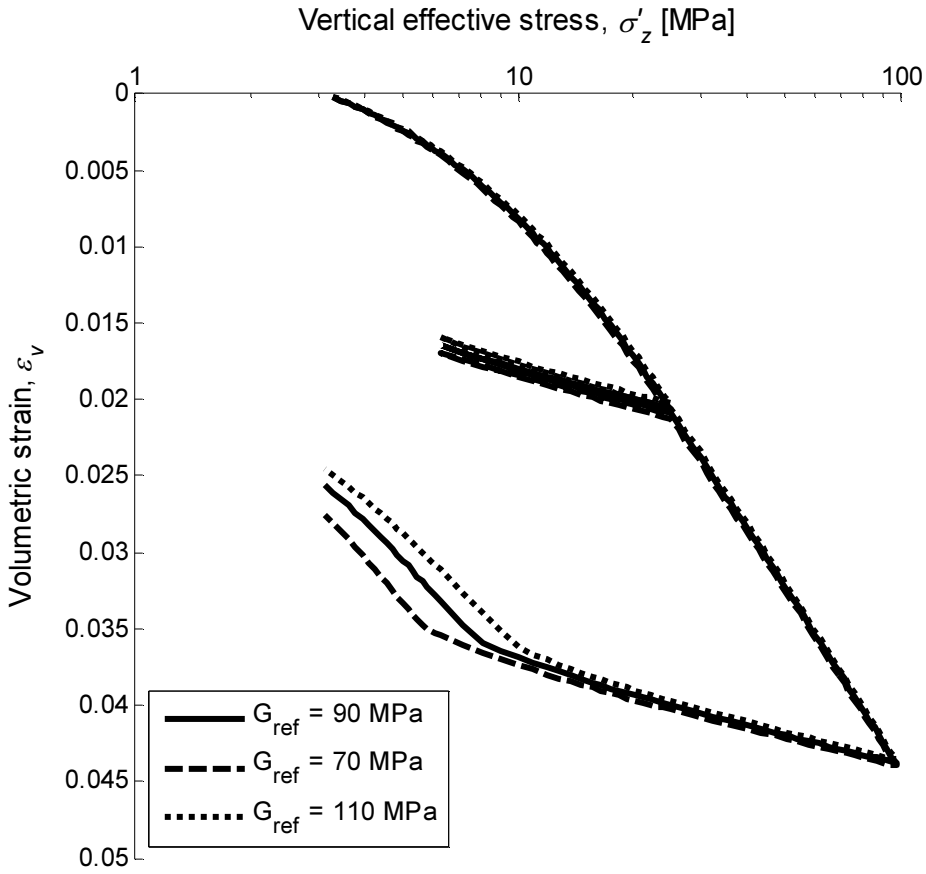

Figure 5.16: Test 1 with different G_{ref} values

5.4.3 β_0

The plastic stiffness modulus β is assumed constant in this work and therefore equal to its value at the reference osmotic suction π_0. β is the inverse of the slope of the linear function $\varepsilon_v^p - \ln p'_c$ (figure 3.2) and its influence regards the elasto-plastic strains of the simulation: the consequence of a greater plastic stiffness modulus is a more stiff behaviour of the material (figure 5.17).

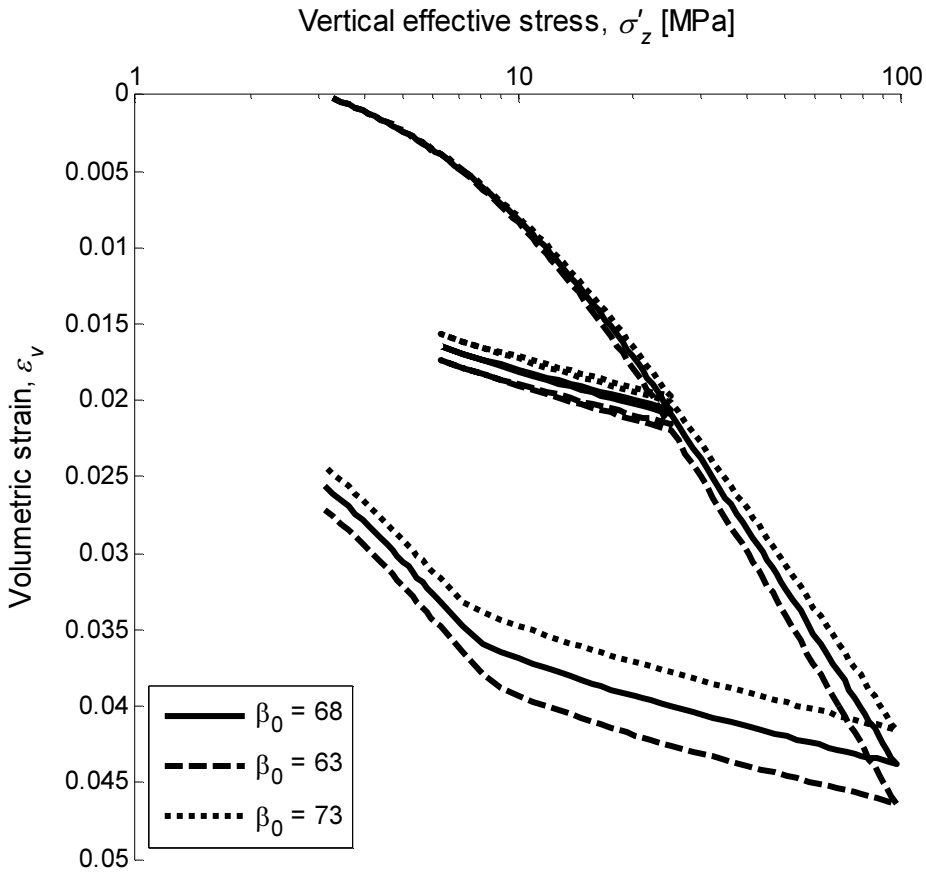

Figure 5.17: Test 1 with different β_0 values

5.4.4 ϕ

The influence of the friction angle is limited, because this term intervenes only in the critical state parameter M and consequently in the deviatoric mechanism f_{dev}, which is activated only at the end of the final unloading as explained in 5.3.3 (figure 5.18).

5.4.5 a

This parameter is not expected to play an important role in the simulation, controlling the evolution of the degree of mobilization of the deviatoric plastic mechanism r_{dev}:

$$dr_{dev} = \frac{(1 - {r_{dev}}^2)}{a} d\varepsilon_d^p$$

The influence regards only the end of the final unloading, as shown in figure 5.19.

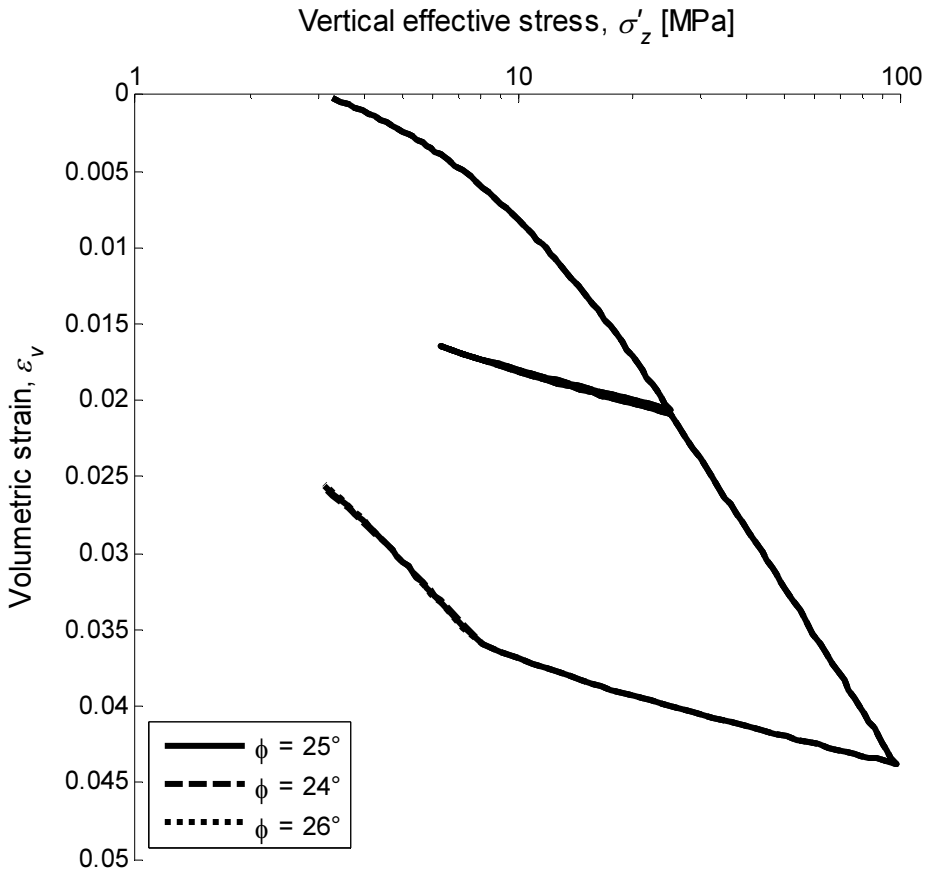

Figure 5.18: Test 1 with different ϕ values

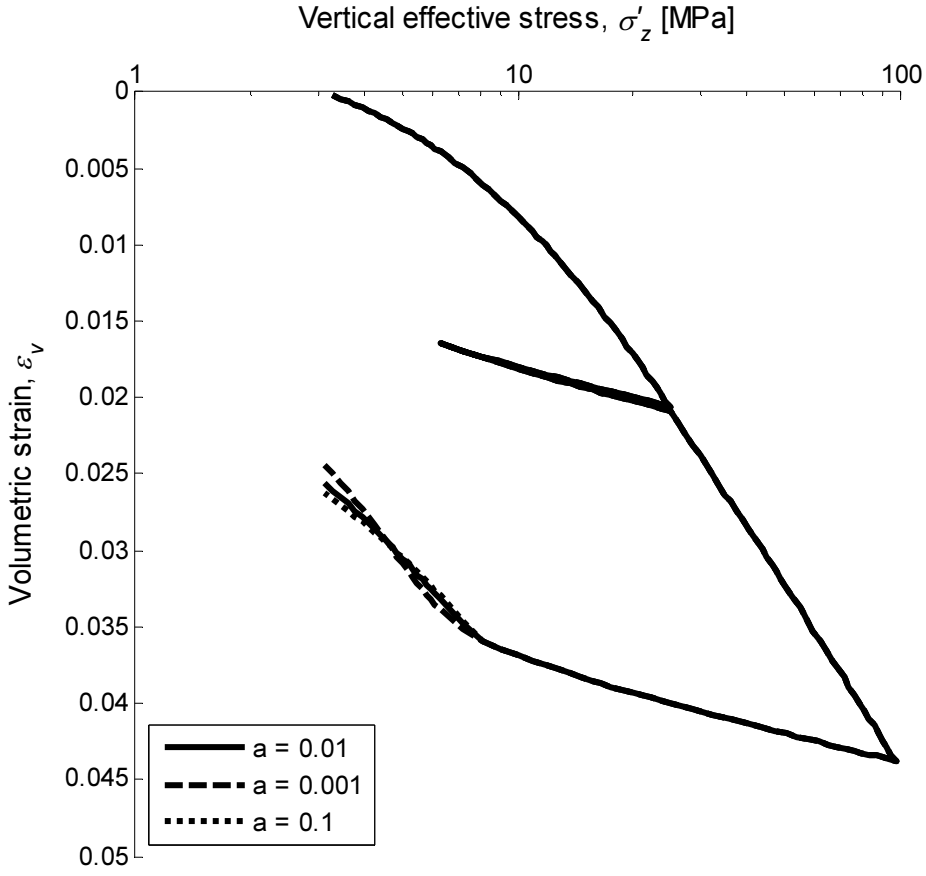

Figure 5.19: Test 1 with different *a* values

5.4.6 *b*

b defines the shape of the deviatoric yield limit (figure 3.6):

$$f_{dev} = q - Mp'\left(1 - b\ln\frac{dp'}{p'_c}\right)r_{dev} = 0$$

As shown in figure 5.20, its influence is very limited.

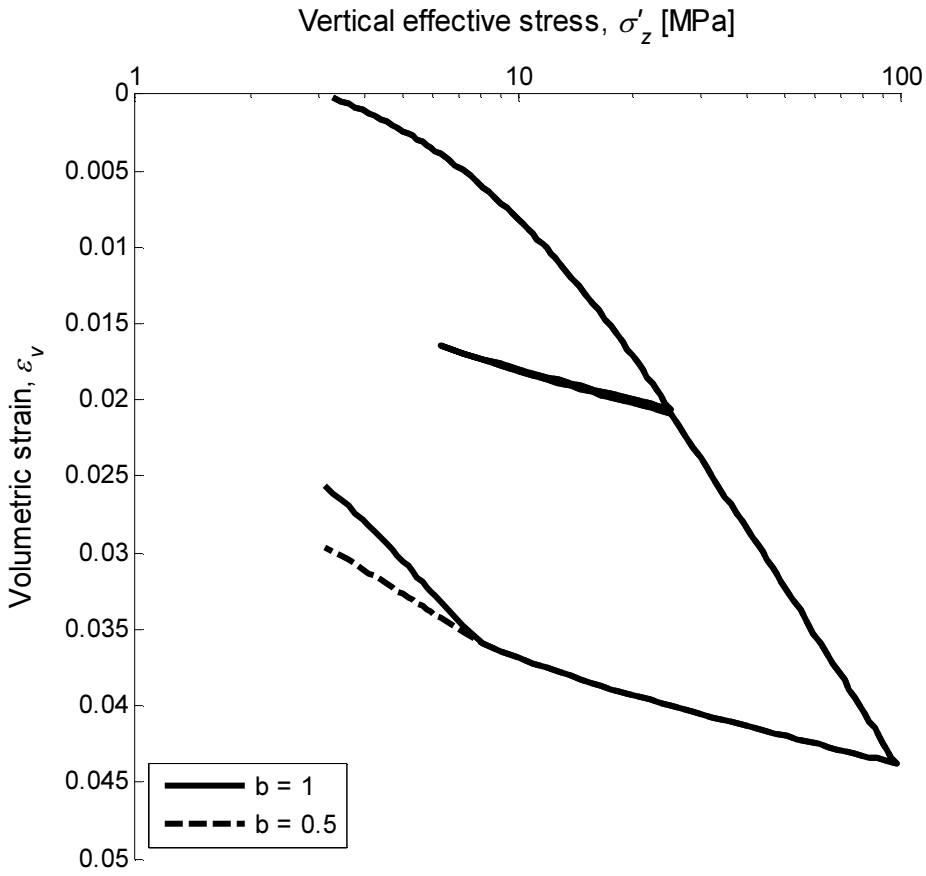

Figure 5.20: Test 1 with different *b* values

5.4.7 *c*

A sensitivity analysis has been conducted to understand the impact of the parameter *c* on the simulation results. As shown in figure 5.21, the evaluation of *c* has a great importance for the numerical analysis: an increase of this parameter leads to a less stiff behaviour of the material and to greater deformations. The cause is comprehensible looking at the following equation:

$$dr_{iso} = \frac{(1 - {r_{iso}}^2)}{c} d\varepsilon_v^{p,iso}$$

A greater *c* value entails a smaller increment of the degree of the plastification of the isotropic yield limit for a given volumetric isotropic plastic increment. The consequences of a lower value of r_{iso} are greater plastic strains for a given vertical effective stress value.

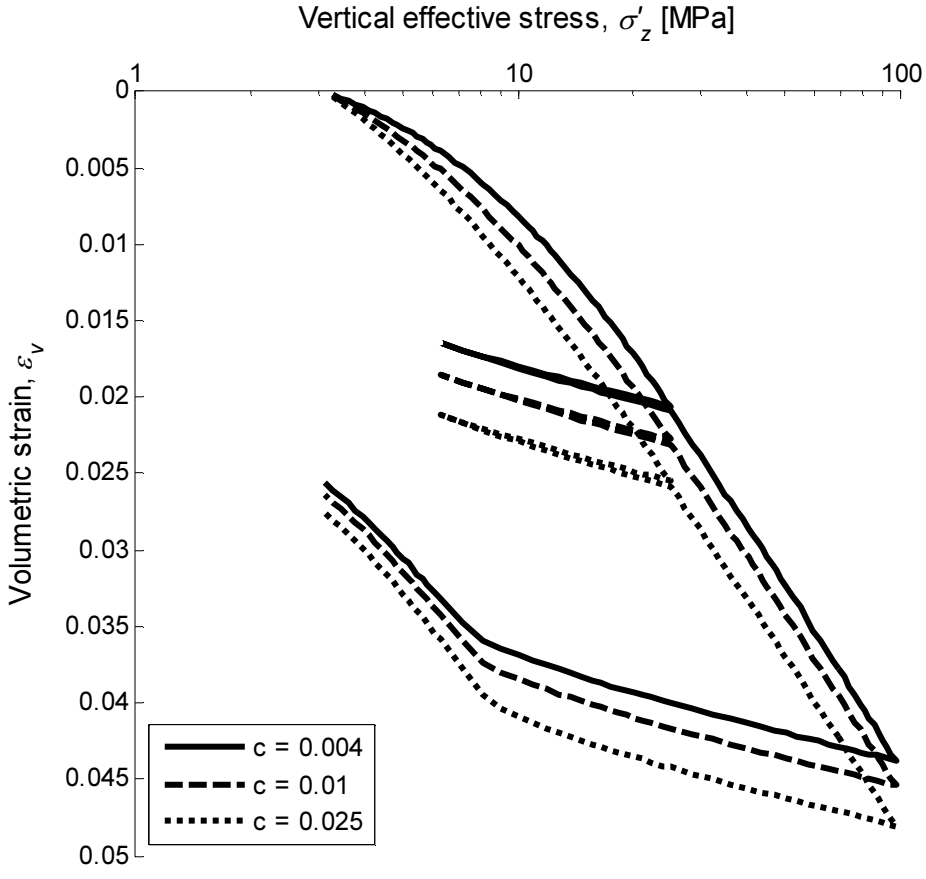

Figure 5.21: Test 1 simulations with different *c* values

5.4.9 r_{iso}^{e}

r_{iso}^{e} is the radius of the isotropic elastic nuclei inside which the strains are fully reversible. Until the plastic mechanism is activated the degree of mobilization of the isotropic plastic mechanism is equal to r_{iso}^{e}:

$$r_{iso} = r_{iso}^{e} + \frac{\varepsilon_v^{p,iso}}{c + \varepsilon_v^{p,iso}}$$

A smaller value of r_{iso}^{e} rounds the shape of the passage from the elastic to the elasto-plastic part of the oedometric curve "anticipating" the activation of the degree of mobilization of the isotropic plastic mechanism (figure 5.22).

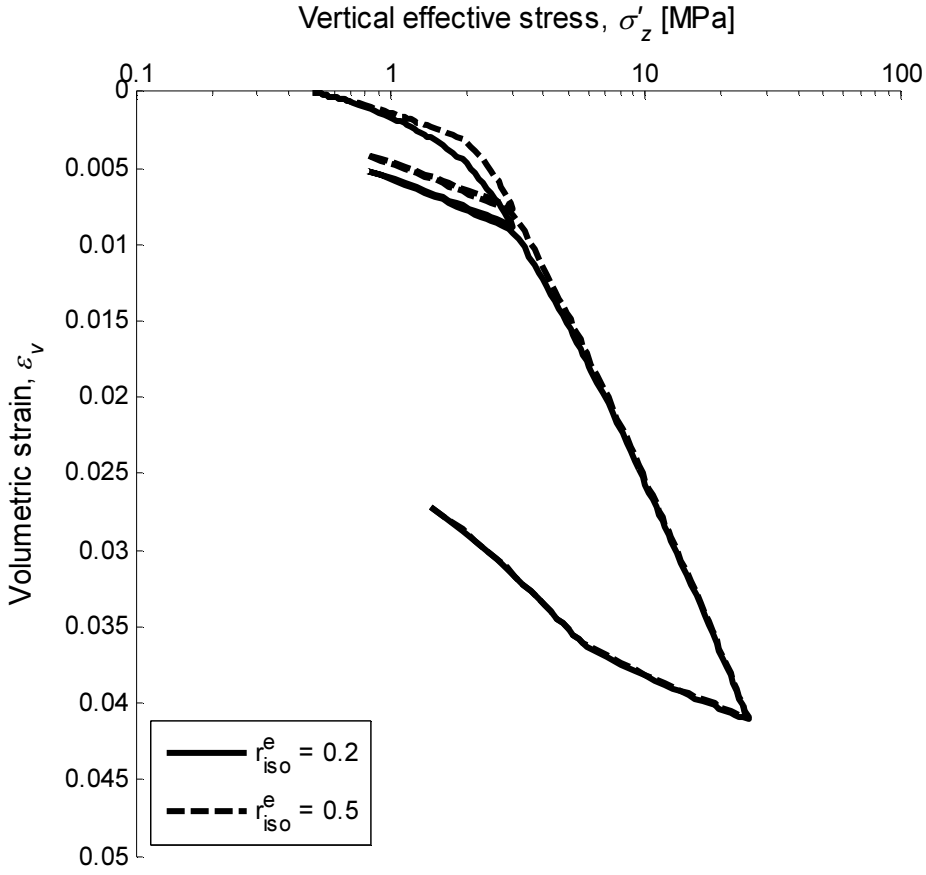

Figure 5.22: Test 2 simulations with different r_{iso}^{e} values

5.4.8 r^e_{dev}

r^e_{dev} is the radius of the deviatoric elastic nuclei inside which the strains are fully reversible. Until the plastic deviatoric mechanism is activated the degree of mobilization of the deviatoric plastic mechanism r_{dev} is equal to r^e_{dev}:

$$r_{dev} = r^e_{dev} + \frac{\varepsilon^p_d}{a + \varepsilon^p_d}$$

r^e_{dev} is not expected to play an important role in the simulation, being related to the deviatoric plastic mechanism which is activated only at the end of the final unloading. This statement is confirmed by figure 5.23.

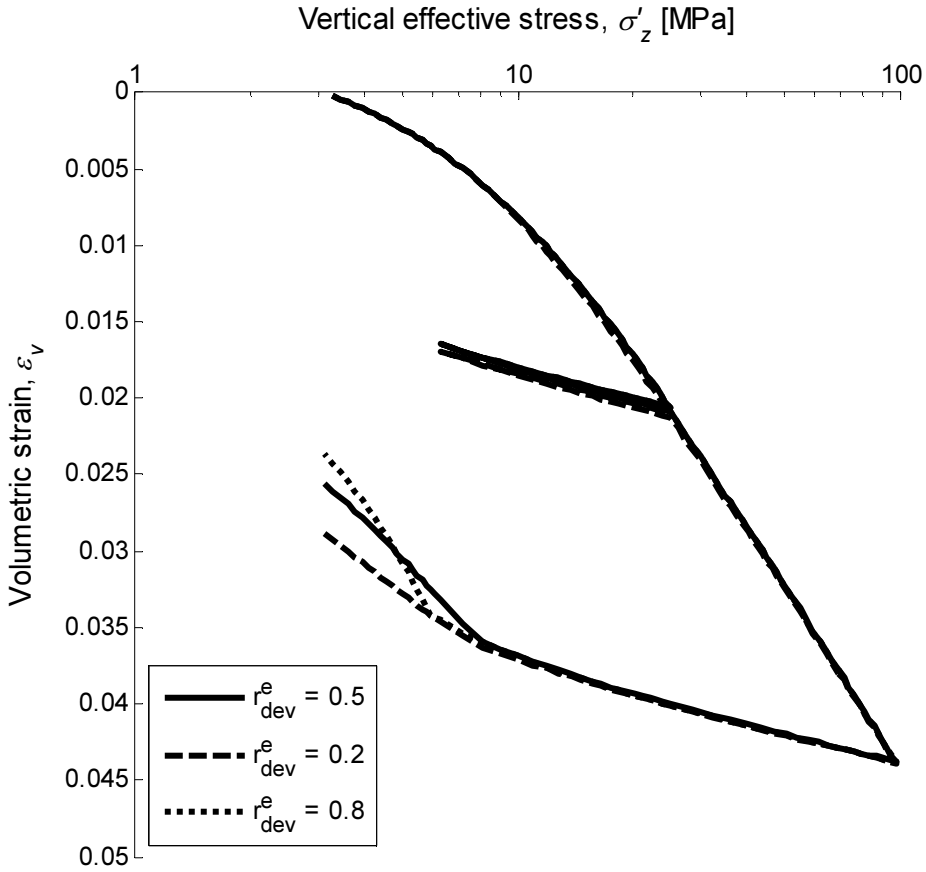

Figure 5.23: Test 1 simulations with different r^e_{dev} values

5.4.2 γ_π

γ_π, being the only parameter of the model which takes in account a variation of osmotic suction, plays a fundamental role in the efficiency of the simulation. As affirmed in the previous paragraphs, its value is not unequivocally defined: a value of 0.042 was assumed for the numerical simulations, but experimental data allow to assume a greater value, with a maximum of around 0.1.

In figure 5.24 and 5.25, which represent test 4 and test 5, a value equal to 0.1 was assumed without a change of the other parameters of the model. The aim is to understand the impact of a variation of this value in the simulated results, and the two tests characterized by a deformation due to a variation of osmotic suction were chosen. The consequences of this new assumption are greater strains in correspondence of the collapse and a different position of the Normal Compression Line: being higher γ_π value, a greater reduction of the preconsolidation pressure takes place with the same variation of osmotic suction. In figure 5.26 test 6 simulation with the two different γ_π values is reported: the last statement is confirmed, and a greater move of the Normal Compression Line is verified.

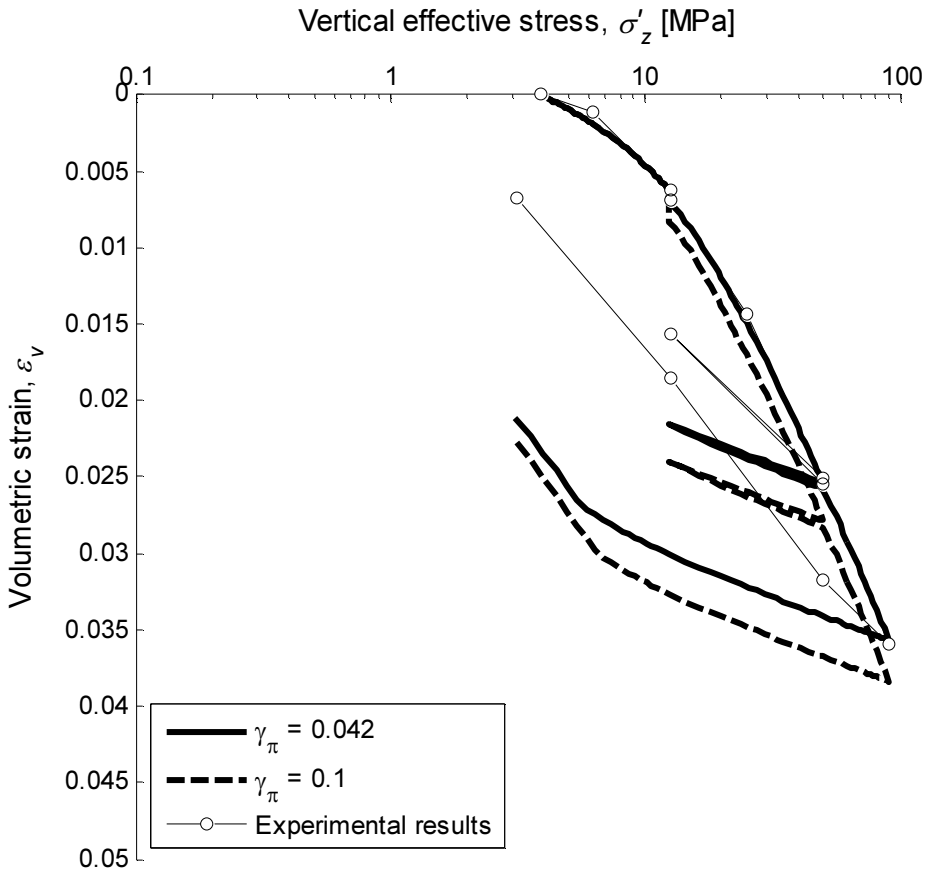

Figure 5.24: Test 4 with different γ_π values

The following tables 5.4 and 5.5 report the simulated collapse strains corresponding to the two different γ_π values and the experimental results for test 4 and test 5. The smaller value of the parameter allows a more precise prediction of this phenomenon.

Test 4 collapse			
	Experimental	γ_π	
		0.1	0.04
$\Delta\varepsilon$(‰)	0.76	1.62	0.73
Δ%		-114.4	3.5

Table 5.4: Test 4 experimental and simulated collapse

Test 5 collapse			
	Experimental	γ_π	
		0.1	0.04
$\Delta\varepsilon$(‰)	1.47	0.4	0.16
Δ%		72.8	89

Table 5.5: Test 5 experimental and simulated collapse

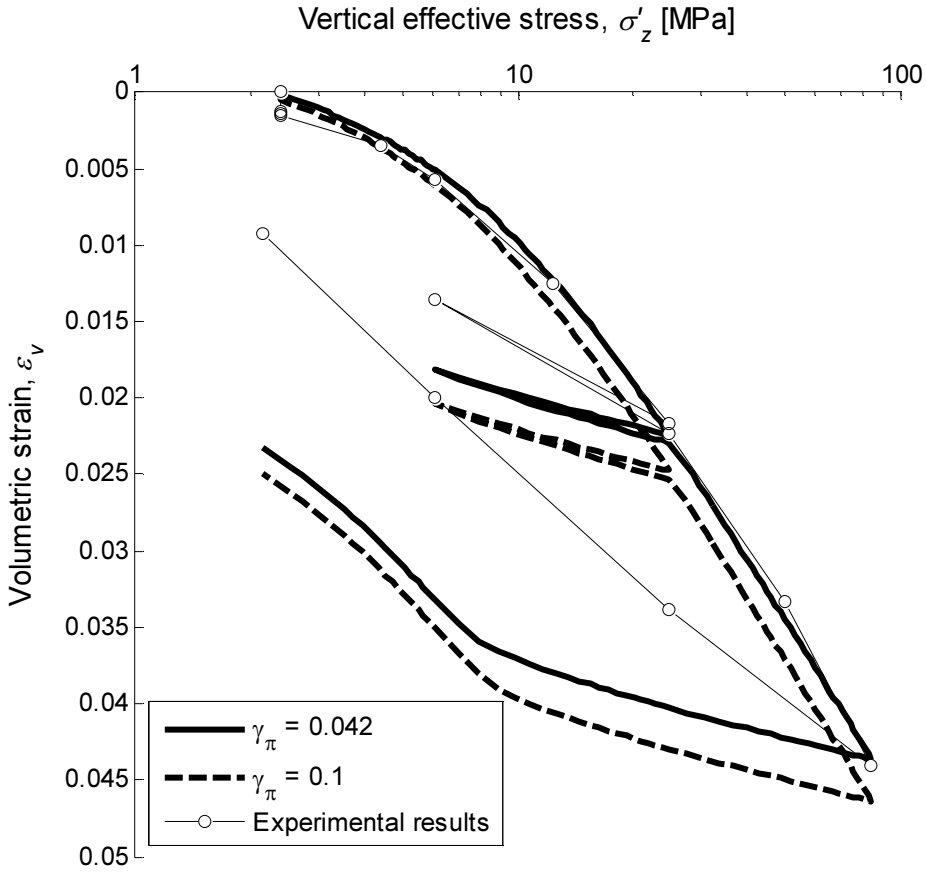

Figure 5.25: Test 5 with different γ_π values

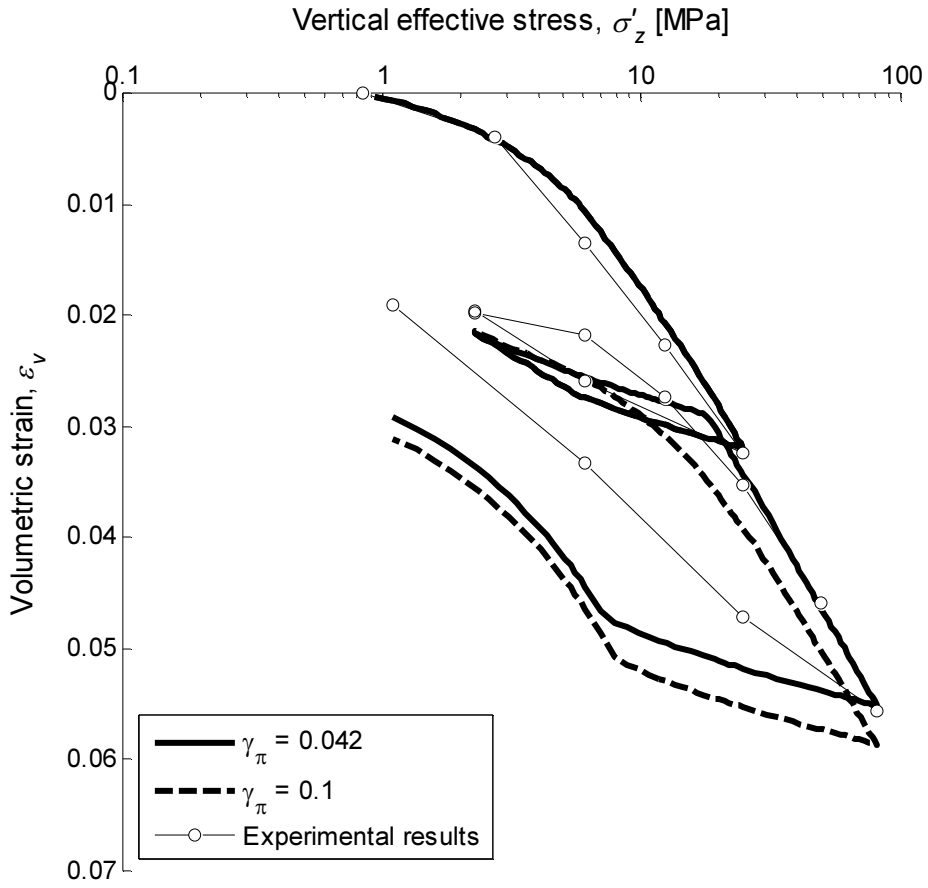

Figure 5.26: Test 6 with different γ_π values

6. Conclusions

The aim of this thesis is to understand if the ACMEG-C constitutive model, developed for a non-swelling illite, is suitable also for shales, and particularly if it is able to reproduce the different behaviour of the material due to the different chemical composition of the pore liquid. A set of experimental tests with different stress paths, including mechanical loading at a constant osmotic suction and a chemical loading at a constant mechanical stress, were performed in EPFL LMS structures to provide an experimental evidence on the this topic.
The experimental findings were analysed in order to determine the characteristics of the material (Opalinus Clay); the preconsolidation pressure was evaluated with two different methods, Casagrande's graphic method and the Energetic method, the first one traditionally used in geotechnical applications and the second one possessing a physical background. Casagrande's graphic method was preferred for the greater regularity of its results.
The successive step was the study of the influence of osmotic suction in the material's behaviour: the experimental findings elaboration led to the conclusion that osmotic suction has an impact on the preconsolidation pressure. The behaviour during unloading-reloading and the slope of the Normal Compression Line are in fact observed independent from osmotic suction. A logarithmic dependence of the preconsolidation pressure on osmotic suction is assumed and the material parameter which governs this relation is determined.
The ACMEG-C constitutive model is based on the ACMEG constitutive model and it was presented in "*An experimental and constitutive investigation on the chemo-mechanical behaviour of a clay*" *(P. Witteveen, A. Ferrari and L. Laloui, Géotechnique, 2013)*. This model is able to take in account changes in the osmotic suction as well as the plastic deformation induced by that changes and the evolution of the elastic and plastic material parameters. The mechanical behaviour was calibrated with two oedometric tests and was then applied to the whole set of tests. In all cases the simulated results corresponds well with the experimental ones: the elasto-plastic behaviour of the material and the changes induced by a variation of osmotic suction are well reproduced by the model. Only the simulation of the unloading-reloading paths is quite different from the experimental findings because of the damage effect, which typically occurs in shales.

This lack does not reduce the great ability of the model to reproduce the chemo-mechanical behaviour of Opalinus Clay.

Successive improvements could be made with other experimental tests on the same material to confirm the assumption for this study and to eventually improve the model. The particular behaviour of this material during mechanical unloading-reloading is not taken in account by the model, and a future improvement should consider this characteristic.

Bibliography

Websites:

http://www.britannica.com/EBchecked/topic/538082/shale

http://geology.com/rocks/shale.shtml

http://www.claysandminerals.com/materials/shales

http://geotecnica.dicea.unifi.it/

http://www.ing.unitn.it/~labgtec/corso_geotecnica/Dispense_Tarantino/

Scientific publications:

Y.N. Abousleiman, S.K. Hoang, M.H. Tran. Mechanical characterization of small shale samples subjected to fluid exposure using the inclined direct shear testing device. *International Journal of Rock Mechanics and Mining Sciences*, 47(3): 355-367, 2010

M. Bonini, D. Debernardi, M. Barla, G. Barla. The Mechanical Behaviour of Clay Shales and Implications on the Design of Tunnels. *Rock Mechanics and Rock Engineering*, 42(2): 361-388, 2007

A.P. Bunger, J. Sarout, J. Kear, C. Delle Piane, E. Detournay, M. Josh, D.N. Dewhurst. Experimental chemoporoelastic characterization of shale using millimeter-scale specimens. *Journal of Petroleum Science and Engineering*, 118: 40-51, 2014

A. Carpinteri. Scienza delle costruzioni 1. Pitagora Editrice Bologna, 1992

X. Chen, C.P. Tan, C.M. Haberfield. Numerical evaluation of the deformation behaviour of thick-walled hollow cylinders of shale. *International Journal of Rock Mechanics and Mining Sciences*, 37(6): 947-961, 2000

A.G. Corkum, C.D. Martin. The mechanical behaviour of weak mudstone (Opalinus Clay) at low stresses. *International Journal of Rock Mechanics and Mining Sciences*, 44(2): 196-209, 2007

J. Eichenberger. Geomechanical modelling of rainfall-induced landslides in partially saturated slopes. PhD thesis, EPFL, 2012

S.R. Etminan, F. Javadpour, B.B. Maini, Z. Chen. Measurement of gas storage processes in shale and of the molecular diffusion coefficient in kerogen. *International Journal of Coal Geology*, 123: 10-19, 2014

V. Favero, A. Ferrari, L. Laloui. Experimental investigation of the thermo-mechanical behaviour of shales. *American Rock Mechanics Association*, 2014

B. François. Thermo-Plasticity of Fine-Grained Soils at Various Saturation States: Application to Nuclear Waste Disposal. PhD thesis, EPFL, 2008

A. Ghassemi, Q. Tao, A. Diek. Influence of coupled chemo-poro-thermoelastic processes on pore pressure and stress distributions around a wellbore in swelling shale. *Journal of Petroleum Science and Engineering*, 67(1-2): 57-64, 2009

W. Gräsle. Multistep triaxial strength tests: Investigating strength parameters and pore pressure effects on Opalinus Clay. *Physics and Chemistry of the Earth, Parts A/B/C*, 36(17-18): 1898-1904, 2011

S. Hsu, P.P. Nelson. Characterization of Eagle Ford Shale. *Engineering Geology*, 67(1-2): 169-183, 2002

M. Josh, L. Esteban, C. Delle Piane, J. Sarout, D.N. Dewhurst, M.B. Clennell. Laboratory characterisation of shale properties. *Journal of Petroleum Science and Engineering*, 88-89: 107-124, 2012

M. Lal, SPE, BP Amoco. Shale Stability. Drilling Fluid Interaction and Shale Strength. *SPE Latin American and Caribbean Petroleum Engineering Conference*, Venezuela, 21–23 April 1999

J. Sarout, E.Detournay. Chemoporoelastic analysis and experimental validation of the pore pressure transmission test for reactive shales. *International Journal of Rock Mechanics and Mining Sciences*, 48(5): 759-772, 2011

L. Schmitt, T. Forsans F.J. Santarelli. Shale Testing and Capillary Phenomena. *International Journal of Rock Mechanics and Mining Sciences & Geomechanics Abstracts,* 31(5): 411-427, 1994

Q. Wang, Z. Yingcao, G. Wang, H. Jiang, Y. Liu. A fluid-solid-chemistry coupling model for shale wellbore stability. *Petroleum exploration and development*, 39(4): 508-513, 2012

P. Witteveen, A. Ferrari and L. Laloui. An experimental and constitutive investigation on the chemo-mechanical behaviour of a clay. *Géotechnique*, 63(3): 244-255, 2013

Acknowledgements

I would like to thank all the staff of the *Laboratoire de Mécanique des Sols* of the *École Polytechnique Fédérale de Lausanne* for their fundamental contribution to this Master Thesis. Particularly, I would like to acknowledge Prof. Lyesse Laloui for giving me this amazing opportunity, Dr. Alessio Ferrari for his advices and his constant support and Ing. Valentina Favero for her precious help.

Vorrei poi ringraziare il Prof. Lorenzo Sanavia per la fiducia e la costante disponibilità.

Vorrei inoltre ringraziare i miei genitori, Domenico e Carla, e mia sorella Francesca per l'incondizionato e insostituibile supporto durante tutto il mio cammino universitario.

Un doveroso ringraziamento va infine a tutti gli amici che mi hanno accompagnato in questi anni: ognuno di voi ha lasciato un segno in maniera diversa e unica, e non posso che esservi grato per questo.